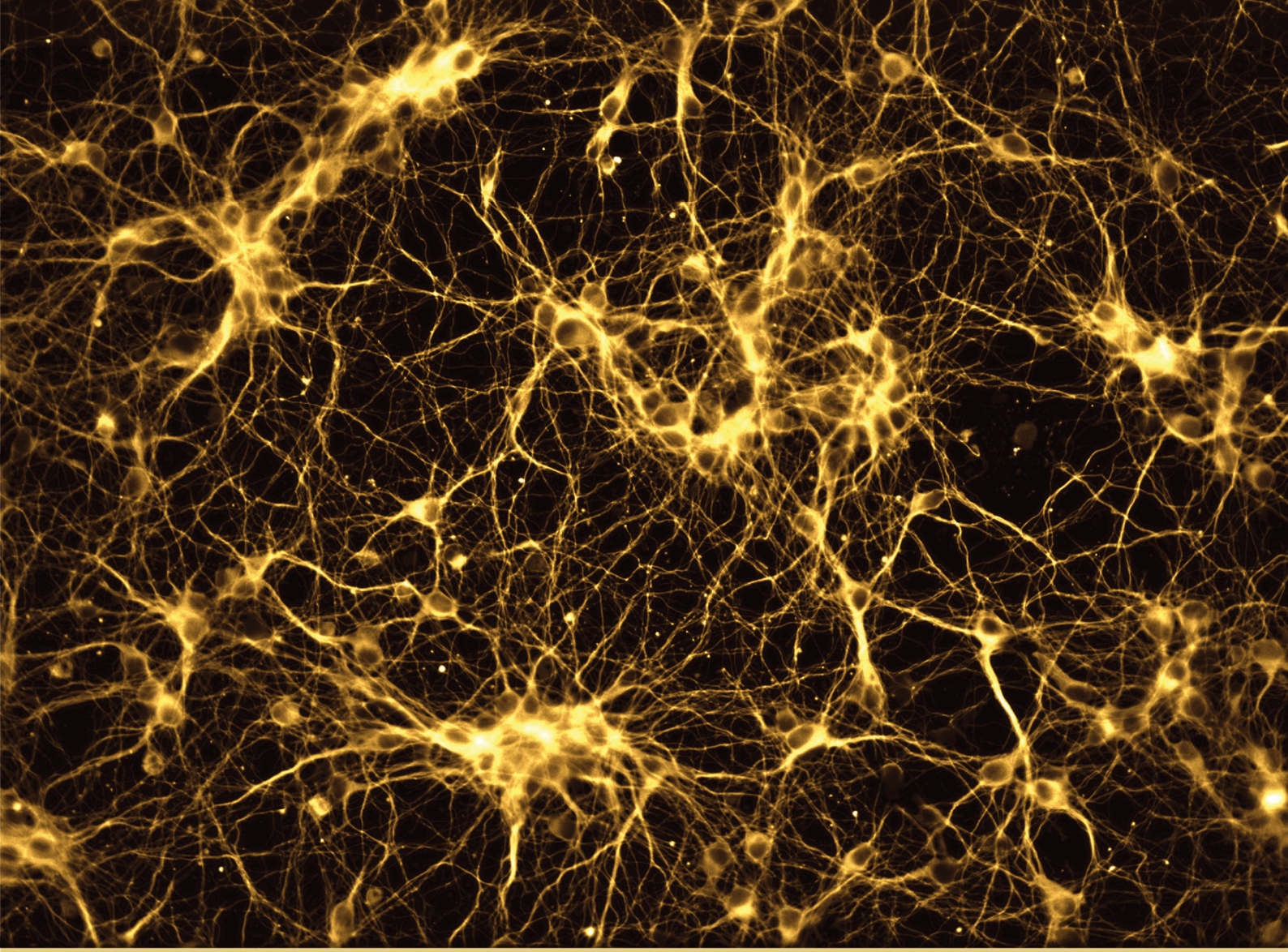

Sofia Marques Ribeiro Carlton

METABOLIC CONTROL OF NEURONAL ACTIVITY BY FUEL SUBSTRATE SWITCHING: A ROLE FOR BAD

Tese de doutoramento em Biologia Experimental e Biomedicina, Ramo de Neurociências e Doença, orientada pela Professora Doutora Nika N. Danial e pelo Professor Doutor Carlos Palmeira e apresentada ao Instituto de Investigação Interdisciplinar da Universidade de Coimbra (IIIUC)

Agosto de 2016

· U C ·

UNIVERSIDADE DE COIMBRA

• U C •

METABOLIC CONTROL OF NEURONAL ACTIVITY BY FUEL SUBSTRATE SWITCHING: A ROLE FOR BAD

Sofia Marques Ribeiro Carlton

Agosto de 2016

Tese de Doutoramento apresentada ao Instituto de Investigação Interdisciplinar da Universidade de Coimbra (IIIUC), para cumprimento dos requisitos necessários à obtenção do grau de Doutor em Biologia Experimental e Biomedicina, Ramo de Neurociências e Doença, realizada sob a orientação científica da Professora Doutora Nika N. Danial (Department of Cancer Biology, Dana-Farber Cancer Institute and Department of Cell Biology, Harvard Medical School) e do Professor Doutor Carlos Palmeira (Departamento de Ciências da Vida, Faculdade de Ciências e Tecnologia da Universidade de Coimbra). Este trabalho foi desenvolvido no Dana-Farber Cancer Institute, Boston, EUA, em colaboração com o Centro de Neurociências e Biologia Celular da Universidade de Coimbra.

PhD thesis presented to the Institute for Interdisciplinary Research of the University of Coimbra (IIIUC) in partial fulfilment of the requirements for the degree of Doctor of Philosophy in Experimental Biology and Biomedicine in the subject of Neuroscience and Disease, under the supervision of Doctor Nika N. Danial (Department of Cancer Biology, Dana-Farber Cancer Institute and Department of Cell Biology, Harvard Medical School) and Doctor Carlos Palmeira (Department of Life Sciences, Faculty of Sciences and Technology, University of Coimbra). The studies here described were carried out at the Dana-Farber Cancer Institute, Boston, USA, in collaboration with the Center for Neuroscience and Cell Biology at the University of Coimbra.

The study presented in this dissertation was supported by a PhD Fellowship from the Portuguese Foundation for Science and Technology, FCT (SFRH/BD/51200/2010), awarded by the PhD Programme in Experimental Biology and Biomedicine (PDBEB).

Ao meu Pai,
o meu eterno herói,
a minha constante fonte de inspiração.
In memoriam Carlos Ribeiro (1962-2015)

ACKNOWLEDGMENTS

Five years ago, I packed my life into two suitcases and embarked on a journey across the ocean. I came to Boston in pursuit of knowledge and scientific expertise. What I discovered here was much more than that. I was blessed to share this PhD journey with truly remarkable people to whom I would like to express my deepest gratitude.

I first thank my supervisor, Dr. Nika N. Danial, for believing in a youthful student from Portugal. Shortly after my interview in Nika's lab, I wrote to her, "I feel quite lucky because I really think that I found the place, the type of science and the mentor that I went looking for." I knew it then, and I know it now that I had the greatest mentor one could ask for. Nika's unwavering support and encouragement have brought the best out of me. Words cannot describe how much I learned from her, but I will certainly carry in me her lessons and wisdom for the rest of my life.

Agradeço ao Professor Carlos Palmeira pela orientação e todo o apoio nesta jornada, pela confiança que depositou em mim e no meu trabalho, e por estar sempre disponível. O seu apoio foi fundamental neste precurso. Agradeço ainda ao Programa Doutoral em Biologia Experimental e Biomedicina (PDBEB) e ao Professor João Ramalho-Santos pela oportunidade que me proporcionaram e pelo voto de confiança na minha vinda para Boston.

I am incredibly grateful for all the help, support and friendship I have received from the present and past members of the Danial lab. I especially thank Alfredo Giménez-Cassina for taking me under his wing and being the best bench mentor I could have had. If I were to write about all that I have learned under his tutelage, I would easily run out of space. I thank Luisa Garcia-Haro for being a superb teammate and a great collaborator on this project. Her help and encouragement over the years have meant a lot to me. It has also been an absolute joy to work with Mari-Carmen Fernandez-Aguera and Dong Wook Choi, recent lab members that have joined the project and continue to teach me new things every day. Their enthusiasm for science has been contagious. I would also like to acknowledge our animal technician, Meghan Tedoldi. The technical assistance I have received from her has been instrumental for the success of this work. I thank Liz, Calie, Pei, Lindsay, Ana, Illana, Erik, Sanda, Ben, Elaura,

Klaudia and Marina for making the Danial lab such a great place to work. Last but not least, my gratitude also goes to our terrific research administrator, Jollanda Lako, for her tireless attention to details and administrative paperwork, for her kind and friendly spirit and sunny demeanor that always make me smile.

Over the past years, I have had the privilege of working with an incredible team of collaborators. In particular, I am grateful to our long term collaborator Dr. Gary Yellen and his lab members. I have learned a great deal about the brain and neuronal excitability from our scientific discussions. Their contributions and support throughout the project have been invaluable. Gary has also been a great mentor and his endless enthusiasm for science has been an inspiration to me.

I owe the beginning of my passion for mass spectrometry and metabolomics to Dr. Alan Saghatelian and Tejia Zhang. They taught me everything I know about LC-MS, and made our initial metabolomics endeavors possible. My special thanks also go to Drs. Russel Jones and Daina Avizonis for our productive and exciting collaboration. They have been vital for the metabolomics studies described in this thesis and kindly hosted me during my visit to McGill. I cannot thank Daina enough for all the time, effort, and care she dedicated to teaching me GC-MS data analysis and overseeing my work. She brought my passion for the field of metabolomics to a whole new level. She has also been a great mentor. I am also indebted to Luc Choinière in their team for the endless stream of sample analyses he performed on the GC-MS instrument.

I am truly thankful to Mark Jedrychowski in Dr. Steve Gygi's lab here at HMS for all the hard work and insight on the quantitative proteomics studies described in this thesis. Our progress in protein interaction studies would not have been possible without his help.

I am grateful for the wonderful friends I met in Boston, who have made this city feel like home to me. From my Portuguese buddies, my international friends, and Randy's friends, I have received nothing but kindness, friendship, and support. I thank Buzzy, my ESL teacher, for helping me improve my English and for teaching me so many things about American history and culture. What started as a Thursday evening English class grew into a beautiful friendship that I truly cherish. À Inês em especial, agradeço por ter dado toda uma outra vida ao CLS,

pelos almoços, lanches, conversas interminaveis e passeis por Boston. Obrigada pela amizade especial que criámos e que tornou os meus dias muito mais sorridentes.

Ao Rodrigo, agradeço por estar sempre presente, por ser um exemplo e inspiração para mim, e por me lembrar que aquilo que não nos mata torna-nos mais fortes. A amizade que nos une é bem maior que este oceano que nos separa. Às minha meninas, Ana Lúcia, Joana Batista, Joana Cerveira, Mafada e Marguerita, agradeço a amizade, a força e apoio constantes. A minha vida não teria a mesma alegria sem vocês. Agradeço ainda à Carla e à Maria Joana por terem tornado o primeiro ano de doutoramento num ano inesquecivel e pela amizade que desde aí perdura. Obrigada também aos amigos de Leiria pelas amizades que já vão em quase 20 anos. Mesmo à distância, o vosso apoio e carinho cá se fazem sentir.

I am grateful for having Randy's family as part of my family. Their love and support have been a blessing in my life.

Este doutoramento não teria sido possível sem o amor, carinho e dedicação da minha família. Por detrás destas páginas estão muitos anos de sacrifícios e luta constante, estão os pilares onde assenta a minha vida, os meus três mosqueteiros. Um por todos e todos por um sempre foi o lema da nossa família. À Dina, agradeço por ser a melhor irmã do mundo. Não há palavras para descrever aquilo que nos une. É com muito orgulho que te tenho visto crescer ao longo dos anos. Obrigada pelo apoio incondicional, sobretudo nos momentos mais dificeis deste precurso. À mãe, agradeço por cuidar tão bem de mim, por me ter preparado para a vida, e por me ter ensinado os principios e valores que me têm permitido acançar os meus objectivos. Obrigada por seres a minha fã número um e por toda a força que me dás. Ao pai, agradeço por me ter ensinado tantas lições de vida, por me apoiar tão profundamente, e por sempre acreditar que eu poderia voar mais alto. Trago em mim tanto de ti.

My beloved husband Randy was undoubtedly the biggest discovery of my PhD. As many of the greatest discoveries in history, it happened serendipitously, and it changed my world forever. His love, kindness, and care know no boundaries. He is a true inspiration to me. He has shared with me the greatest joys and the hardest losses of my life, and he always stood firmly by my side. This work belongs to him as much as it belongs to me. I could not have done it without his love and unconditional support.

ABSTRACT

Fuel metabolism is important not only for providing energy to neurons and astrocytes in the brain, but also as a key regulator of neuronal activity. A remarkable example of how metabolism can alter brain activity is the strong resistance to epileptic seizures displayed by mice with deletion or alteration of BAD, a BCL-2 family protein that imparts reciprocal effects on glucose and ketone body metabolism independent of its ability to regulate apoptosis. BAD modifications lead to reduced mitochondrial oxidation of glucose and concomitantly enhance ketone body oxidation in neural cells. The metabolic shift upon BAD modification, increased propensity to consume ketone bodies in face of diminished glucose metabolism, recapitulates the actual change in fuel consumption by the brain in fasting or on ketogenic diet, a high fat, low carbohydrate diet that has been successfully used to treat epileptic seizures. However, these BAD-dependent changes occur in the absence of dietary manipulation, providing a new molecular and cellular handle on the metabolic control of neuronal activity. Compared with systemic effects of dietary alterations, the seizure resistance in BAD mutant mice appears likely to arise from alterations in brain cell metabolism rather than systemic changes. This provides an opportunity to test and define the metabolic contributions to regulation of neuronal activity at the molecular level in a way that has not been easy with dietary manipulations due to their systemic effects.

How does BAD alter the metabolism of glucose and ketone bodies, and how are these changes in fuel substrate metabolism related to neurotransmission? The answers to these questions will help define a metabolic signature for the BAD-dependent glucose-to-ketone-body fuel switch and provide valuable insights into the metabolic state associated with seizure protection. To answer these questions, we undertook an integrative and multidisciplinary approach comprised of targeted metabolomics analyses using ^{13}C-glucose and ketone body tracers, quantitative proteomics and biochemical studies. We have found that diminished glucose oxidation in BAD mutant neurons maps to a defect in the lower arm of the glycolytic pathway that consequently diminishes TCA cycle activity. Our studies also show that diminished TCA cycle activity in response to glucose is linked to reduced availability of

glucose-derived pyruvate rather than a more generalized defect in mitochondrial entry or handling of pyruvate. In comparison, ketone bodies led to significantly higher increase in TCA cycle flux in BAD mutant neurons. Remarkably, this appears to be associated with higher availability of metabolic precursors for the synthesis of the inhibitory neurotransmitter γ-aminobutyric acid (GABA) as well as an actual increase in GABA pools. These data provide new information about potential changes in neurotransmission that might be directly derived from altered fuel utilization in BAD mutant neurons. In an effort to delve deeper into the biochemical underpinning of BAD's effect on fuel utilization, we sought to identify the BAD-interacting partners in the brain. Our initial multipronged approach to protein-protein interactions has revealed that BAD is present in higher molecular weight complexes the components of which are under current investigation.

Overall, the studies described herein begin to provide an integrated molecular view at the level of metabolite fluxes and biochemical interactions that underlie BAD-dependent reciprocal utilization of glucose and ketone bodies in the brain and their influence on neuronal excitability as it relates to seizure responses. In the fullness of time, this work may have broader implications and utility for identifying and predicting other genetic and pharmacologic manipulations of metabolism that may similarly induce a glucose-to-ketone-body fuel switch and protect against seizures.

RESUMO

O metabolismo energético é importante não só para fornecer energia a neurónios e astrócitos no cérebro, mas funciona também como um regulador fundamental da actividade neuronal. Um exemplo notável de como o metabolismo pode alterar a actividade cerebral é a profunda resistência a convulsões epilépticas apresentada por ratinhos com uma deleção ou alteração da BAD, uma proteína da família BCL-2 que possui efeitos recíprocos no metabolismo da glucose e corpos cetónicos, independentemente da sua capacidade de regular a apoptose. As modificações na BAD levam a uma reduzida oxidação mitocondrial e, consequentemente, a um aumento da oxidação de corpos cetónicos em células neuronais. Este desvio metabólico resultante de modificações da BAD, que aumenta a propensão para o consumo de corpos cetónicos devido à diminuição do metabolismo da glucose, mimetiza as alterações que ocorrem no consumo energético pelo cérebro em jejum, ou quando sujeito a dietas cetogénicas. Estas dietas, ricas em gorduras e com baixo teor de hidratos de carbono, têm sido utilizadas de forma eficaz no tratamento de convulsões epilépticas. Contudo, estas alterações dependentes da BAD ocorrem independentemente de manipulações da dieta, evidenciando um novo papel molecular e celular desta proteína no controlo metabólico da actividade neuronal. Em comparação com os efeitos sistémicos de alterações nutricionais, a resistência a convulsões em ratinhos mutantes para a BAD parece ser consequência de alterações específicas ao nível do metabolismo celular no cérebro, e não de alterações sistémicas. Estas observações constitutem uma oportunidade para testar e definir as contribuições metabólicas para a regulação da actividade neuronal ao nível molecular, de uma forma que não foi até agora possível com manipulações nutricionais, devido aos efeitos sistémicos que estas causam.

As questões que se impõem são: como é que a BAD altera o metabolismo da glucose e corpos cetónicos e como é que estas alterações nos substratos do metabolismo energético se relacionam com a neurotransmissão? As respostas a estas perguntas vão permitir definir uma assinatura metabólica para a mudança de substrato energético de glucose para corpo cetónico dependente da BAD e reunir factos determinantes no que diz respeito ao estado

metabólico associado à protecção contra convulsões. Para responder às questões acima mencionadas adoptámos uma estratégia integrativa e multidisciplinar que envolve análises de metabolómica direccionadas, utilizando dois marcadores de ^{13}C-glucose e corpos cetónicos, proteómica quantitativa e estudos bioquímicos. Observou-se que a diminuição da oxidação da glucose em neurónios mutantes para a BAD aponta para uma falha nas etapas finais da via glicolítica que, consequentemente, diminui a actividade do ciclo dos TCA. Estes estudos também demonstram que uma diminuição da actividade do ciclo dos TCA, em resposta à glucose, está relacionada com uma diminuição no piruvato derivado de glucose, ao invés de um defeito generalizado na transferência ou oxidação do piruvato na mitocôndria. Em comparação, os corpos cetónicos levaram a um aumento significativo do fluxo do ciclo dos TCA, em neurónios mutantes para a BAD. Este fenómeno parece estar associado a um aumento nos níveis de percursores metabólicos para a síntese do neurotransmissor inibitório ácido γ-aminobutírico (GABA), bem como um aumento das reservas de GABA. Os resultados aqui apresentados mostram as potenciais alterações na neurotransmissão que podem ser consequência directa de uma alteração da utilização de substratos metabólicos pelos neurónios mutantes para a BAD. De modo a analizar detalhadamente o mecanismo bioquímico por detrás dos efeitos da BAD na utilização de substratos metabólicos, propusemo-nos a identificar parceiros de interacção da BAD no cérebro. Numa primeira e ampla abordagem a interacções proteicas, concluiu-se que a BAD está presente em complexos de alto peso molecular cujos componentes específicos estão a ser investigados.

Em geral, os estudos aqui descritos são o ponto de partida para obter uma visão molecular integrada dos fluxos metabólicos e interacções biológicas que estão subjacentes à utilização recíproca de glucose e corpos cetónicos dependentes da BAD no cérebro e do seu efeito na excitabilidade neuronal e covulsões epilepticas. No futuro, este trabalho poderá ter amplas implicações e ser de extrema utilidade para a identificação e desenvolvimento de outras manipulações genéticas e farmacológicas do metabolismo que, de forma semelhante, podem induzir uma alteração de glucose para corpo cetónico e assim proteger contra convulsões.

TABLE OF CONTENTS

LIST OF FIGURES AND TABLES

FIGURES

TABLES

SUPPLEMENTARY FIGURES

LIST OF ABBREVIATIONS

2PG – 2-phosphoglycerate

3PG – 3-phosphoglycerate

ADP – adenosine diphosphate

ALD – aldolase

ALT – alanine aminotransferase

ANOVA – analysis of variance

AraC – cytosine arabinoside

AST – aspartate aminotransferase

ATP – adenosine triphosphate

BAD – B cell lymphoma 2-associated agonist of cell death

BBB – blood brain barrier

BCL-w – B cell lymphoma-2-like protein 2

BCL-X_L – B cell lymphoma-extra large

BDH – β-hydroxybutyrate dehydrogenase

CoA – coenzyme A

DHAP – dihydroxyacetone phosphate

DIV – days in vitro

E – embryonic day

ENO – enolase

ETC – electron transport chain

F1,6BP – fructose-1,6-bisphosphate

F6P – fructose-6-phosphate

FAD – flavin adenine dinucleotide

$FADH_2$ – flavin adenine dinucleotide (reduced)

FAs – fatty acids

G6P – glucose-6-phosphate

G6PDH – glucose-6-phosphate dehydrogenase

GABA – γ-amino-butyric acid

GABA-T – GABA-transaminase

GAD – glutamate decarboxylase

GAP – glyceraldehyde 3-phosphate

GAPDH – glyceraldehyde 3-phosphate dehydrogenase

GC-MS – gas chromatography mass spectrometry

GFAP – glial fibrillary acidic protein

GFAT – glutamine-fructose-6-phosphate transaminase

GK – glucokinase

GLS – glutaminase

GPDH – glycerol-3-phosphate dehydrogenase

GPI – glucose-6-phosphate isomerase

GPS – glycerol-phosphate shuttle

GS – glutamine synthetase

GSH – glutathione (reduced)

HK – hexokinanase

IDH – isocitrate dehydrogenase

K_{ATP} – ATP-sensitive potassium channels

KBs – ketone bodies

KD – ketogenic diet

LC-MS – liquid chromatography mass spectrometry

LC-MS/MS – tandem liquid chromatography mass spectrometry

LDH – lactate dehydrogenase

MAS – malate-aspartate shuttle

MDH – malate dehydrogenase

MDV – mass distribution vector

ME – malic enzyme

MID – mass isotopomer distribution

NAD^+ – nicotinamide adenine dinucleotide (oxidized)

NADH – nicotinamide adenine dinucleotide (reduced)

$NADP^+$: nicotinamide adenine dinucleotide phosphate (oxidized)

NADPH: nicotinamide adenine dinucleotide phosphate (reduced)

OAA – oxaloacetate

OCS – octanoyl-CoA synthetase

OXPHOS – oxidative phosphorylation

PAG – phosphate-activated glutaminase

PC – pyruvate carboxylase

PDH – pyruvate dehydrogenase

PEP – phosphoenolpyruvate

PFK – phospho-fructokinase

PGAM – phosphoglycerate mutase

PGK – phosphoglycerate kinase

PHGDH – phosphoglycerate dehydrogenase

PKM – pyruvate kinase

PLL – poly-L-lysine

ROS – reactive oxygen species

SCOT – succinyl-CoA:3-ketoacid CoA transferase

SDH – succinate dehydrogenase

SEC – size exclusion chromatography

SEM – standard error of the mean

SSA – succinate semi aldehyde

SSADH – succinate semi aldehyde dehydrogenase

TCA cycle – tricarboxylic acid cycle

TIC – total ion count

TMT – tandem mass tags

TPI – triose-phosphate isomerase

WT – wild type

α-KG – α-ketoglutarate

LIST OF PUBLICATIONS

Ribeiro, S.M., Gimenez-Cassina, A., and Danial, N.N. (2015). Measurement of mitochondrial oxygen consumption rates in mouse primary neurons and astrocytes. Methods Mol Biol 1241, 59-69.

Stanley, I.A.*, **Ribeiro, S.M.***, Gimenez-Cassina, A., Norberg, E., and Danial, N.N. (2014). Changing appetites: the adaptive advantages of fuel choice. Trends Cell Biol 24, 118-127.

*co-first authors

The work described in this dissertation is in preparation for publication.

CHAPTER 1

Introduction

1.1 Fuel choice in the brain and its adaptive advantages

Different cell states have specific anabolic and catabolic needs that can be met by processing distinct fuel substrates such as glucose, amino acids, ketone bodies (KBs), and fatty acids (FAs) (Figure 1.1). Fuel substrates not only fulfill specific energy and biosynthetic needs, but also enable programmatic adaptations to stress conditions, beyond compensating for changes in nutrient availability (Stanley et al., 2014). Although glucose is the predominant fuel utilized by the brain, neural cells can metabolize alternative fuel substrates such as lactate, ketone bodies, certain fatty acids and amino acids, particularly in conditions of low glucose availability (Mergenthaler et al., 2013; Zielke et al., 2009). Understanding the mechanisms of fuel choice in the brain is of particular relevance, given its high energetic demands and key functions.

At the cellular and molecular level, fuel utilization can directly affect multiple processes in the brain ranging from developmental cell fate decisions and axonal transport to neurotransmission. For example, in neuronal stem cells (NSCs), a switch from glycolytic to mitochondrial oxidative metabolism underlies the transition from quiescence to proliferation or multi-lineage differentiation (Agostini et al., 2016; Cavallucci et al., 2016; Rafalski and Brunet, 2011). On the other hand, the energy demand for fast axonal transport of cargos is fulfilled by ATP generated locally via the glycolytic enzyme glyceraldehyde 3-phosphate dehydrogenase (GAPDH) (Figure 1.1), which co-localizes with motile vesicles (Zala et al., 2013). Gluco-regulatory mechanisms also modulate mitochondrial motility along axons, a process tightly integrated with synaptic transmission. Specifically, high concentrations of glucose and the attendant increase in flux through the hexosamine biosynthetic pathway (Figure 1.1) lead to *O*-GlcNAcylation of mitochondrial motor/adaptor complex protein Milton, inhibiting mitochondrial motility (Pekkurnaz et al., 2014).

The aforementioned processes are but examples of fuel-dependent regulatory mechanisms that occur under normal physiology. Fuel metabolism can also have profound effects on adaptive responses to stress (Stanley et al., 2014). For example, increased diversion of glucose metabolism to the pentose phosphate pathway (Figure 1.1) was recently shown to be protective against brain ischemic injury through increases in redox balance and

reductive power for neuronal anti-oxidant responses (Quaegebeur et al., 2016). Another clear example of the connection between fuel choice and altered neuronal stress responses is the anti-seizure effects of diets that reduce glucose consumption and promote ketone body metabolism (Lutas and Yellen, 2013).

The purpose of this introductory chapter is to highlight the specific contributions of different fuels to neuronal function, especially neurotransmission, in both normal physiology and pathologic states. We have deliberately avoided an exhaustive account of metabolism in the brain, and limited the description to metabolic details as they relate to the current state of knowledge on coupling of carbon substrate metabolism to neurotransmission. We then focus on glucose *versus* ketone body utilization in the brain in connection with neuronal excitability as exemplified by the anti-seizure effects of ketogenic diets, as well as the recently discovered glucose-to-ketone-body fuel switch triggered by the protein BAD, which produces seizure resistance independently of dietary treatment.

Figure 1.1 Schematic of select fuel utilization pathways in the brain

For fatty acids, only the octanoate oxidation pathway is shown in light of published evidence that it is a physiologically relevant fuel in the brain (Ebert et al., 2003).

Abbreviations: 2PG: 2-phosphoglycerate; 3PG: 3-phosphoglycerate; ADP: adenosine diphosphate; ATP: adenosine triphosphate; BDH: β-hydroxybutyrate dehydrogenase; ETC: electron transport chain; F1,6BP: fructose-1,6-bisphosphate; F6P: fructose-6-phosphate; FADH2: flavin adenine dinucleotide (reduced); G6P: glucose-6-phosphate; G6PDH: glucose-6-phosphate dehydrogenase; GAP: glyceraldehyde 3-phosphate; GFAT: glutamine-fructose-6-phosphate transaminase; GLS: glutaminase; LDH: lactate dehydrogenase; NAD+: nicotinamide adenine dinucleotide (oxidized); NADH: nicotinamide adenine dinucleotide (reduced); NADPH: nicotinamide adenine dinucleotide phosphate; OAA: oxaloacetate; OCS: octanoyl-CoA synthetase; OXPHOS: oxidative phosphorylation; PEP: phosphoenolpyruvate.

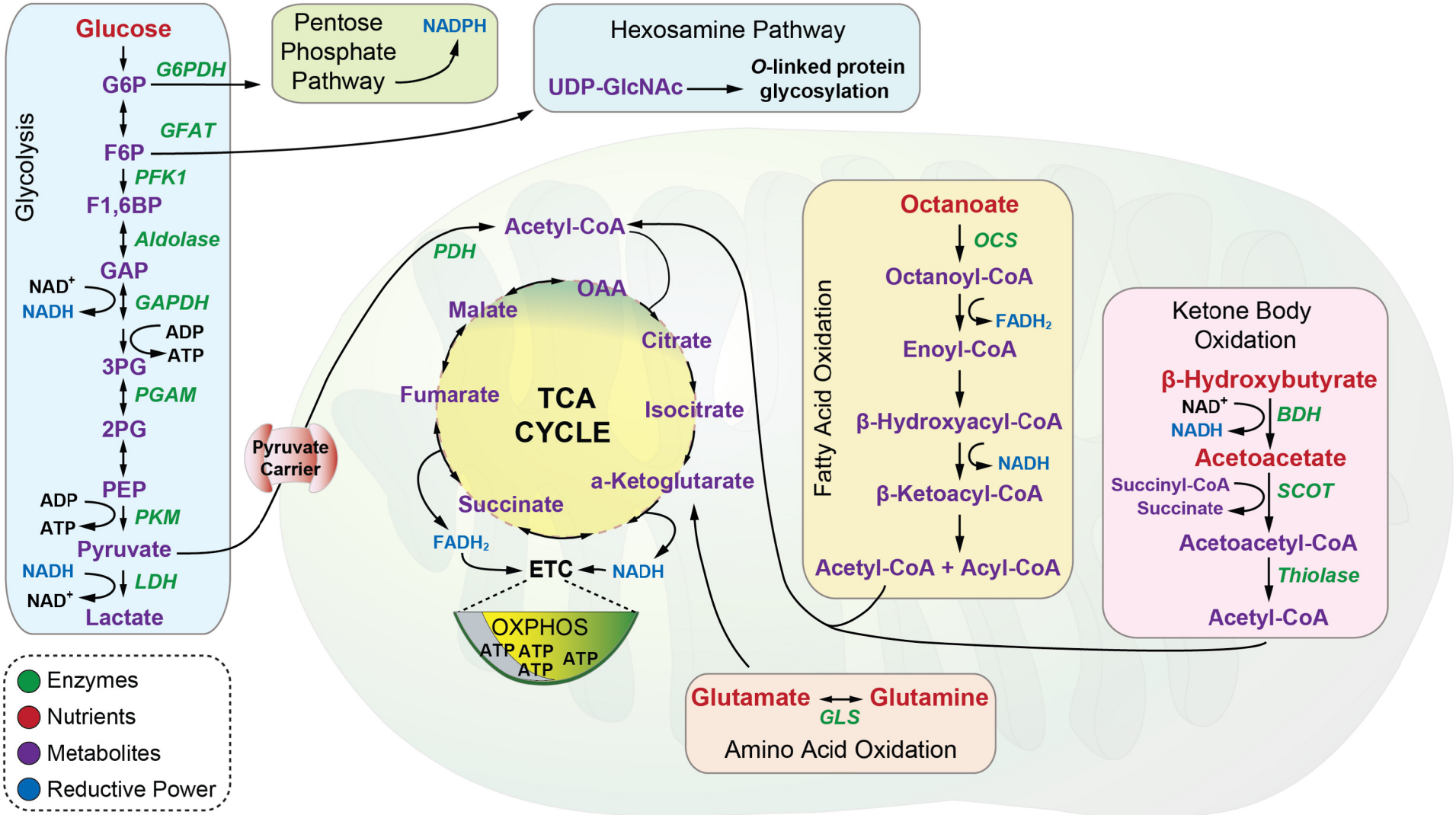
Glucose
G6P
G6PDH
F6P
GFAT
F1,6BP
PFK1
Aldolase
GAP
NAD+
NADH
GAPDH
ADP
ATP
3PG
PGAM
2PG
PEP
ADP
ATP
PKM
Pyruvate
NADH
NAD+
LDH
Lactate
Glycolysis
Pentose Phosphate Pathway
NADPH
Hexosamine Pathway
UDP-GlcNAc
O-linked protein glycosylation
Pyruvate Carrier
PDH
Acetyl-CoA
OAA
Malate
Citrate
Fumarate
TCA CYCLE
Isocitrate
a-Ketoglutarate
Succinate
FADH2
ETC
NADH
OXPHOS
ATP ATP ATP ATP
Octanoate
OCS
Octanoyl-CoA
FADH2
Enoyl-CoA
β-Hydroxyacyl-CoA
NADH
β-Ketoacyl-CoA
Acetyl-CoA + Acyl-CoA
Fatty Acid Oxidation
Ketone Body Oxidation
β-Hydroxybutyrate
NAD+
NADH
BDH
Acetoacetate
Succinyl-CoA
Succinate
SCOT
Acetoacetyl-CoA
Thiolase
Acetyl-CoA
Glutamate
GLS
Glutamine
Amino Acid Oxidation
Enzymes
Nutrients
Metabolites
Reductive Power

Figure 1.1

1.2 Metabolic control of neurotransmission

Glucose as the preferred fuel in the brain

Glucose is the primary source of energy in the adult brain. While the brain constitutes only 2% of the total body weight, it accounts for 20% of the resting glucose-derived energy consumption (Mergenthaler et al., 2013). Glucose metabolism fuels ATP production, which provides the energy required to sustain complex neuronal activities, including the generation of action potentials, synaptic transmission, maintenance of ion gradients across the plasma membrane, and neuronal resting potentials (Belanger et al., 2011; Lutas and Yellen, 2013). In addition, glucose metabolism generates key biosynthetic intermediates for the synthesis of neurotransmitters (Mergenthaler et al., 2013).

Glucose crosses the blood-brain barrier (BBB) and enters the brain through facilitated transport by glucose transporters. In astrocytes, oligodendrocytes and microglia, this is predominantly mediated by glucose transporter (GLUT) 1, whereas GLUT3, which has a higher affinity and transport activity than GLUT1, mediates glucose uptake in neurons (Belanger et al., 2011; Simpson et al., 2007). The kinetic properties of GLUT3 ensure that glucose is continuously available to neurons even in the face of fluctuating blood glucose levels (Maher et al., 1996). Under resting conditions, the majority of glucose metabolism in the brain is oxidative so that the majority of glucose is fully oxidized to CO_2. However, when specific brain regions are stimulated, cerebral blood flow and glucose uptake increase significantly and glucose metabolism becomes predominantly glycolytic. This is evident from decreased glucose oxidation and a shift to lactate production (Dienel, 2012). As detailed below, the extent to which neurons or astrocytes upregulate glycolytic metabolism upon activation of neural networks, as well as and their contribution to lactate production and utilization have been the subject of intense investigation and debate.

Activity-dependent remodeling of substrate utilization in neurons and astrocytes

During glutamatergic neurotransmission, the extracellular concentration of glutamate, the main excitatory neurotransmitter, quickly rises from ~1-10 µM to 100 µM-1 mM. Such high

levels of glutamate are toxic to neurons and need to be promptly removed from the synaptic cleft. Astrocytes residing in close proximity to the synapse avidly take up glutamate using the excitatory amino acid transporters (EAAT1-2) and convert it to glutamine via astrocyte-specific glutamine synthetase (GS) (reaction 1 in Figure 1.2). Glutamine is in turn released and taken up by neurons and converted to glutamate via phosphate-activated glutaminase (PAG) (reaction 2 in Figure 1.2). This neurotransmitter recycling process is classically known as the glutamate-glutamine cycle (represented by the green arrows in Figure 1.2) (Belanger et al., 2011; Walls et al., 2015). The uptake and recycling of glutamate consumes two molecules of ATP; one to eliminate the Na^+ ions co-transported with every molecule of glutamate, and another for GS-dependent conversion of glutamate to glutamine (Belanger et al., 2011; McKenna, 2013).

How do astrocytes overcome the energetic cost of glutamate recycling upon glutamatergic neurotransmission? The astrocyte-to-neuron lactate shuttle (ANLS) hypothesis postulates that astrocytes fulfill this energy demand by increasing glucose uptake and glycolysis, which generates ATP as well as lactate through the action of lactate dehydrogenase (LDH) (reaction 3 in Figure 1.2). Lactate secreted by astrocytes is taken up and oxidized by neurons for ATP production (Belanger et al., 2011; Magistretti and Pellerin, 1999; Pellerin and Magistretti, 2004). This hypothesis is supported by experimental observations that reduced expression of astrocyte-specific glutamate transporters severely diminishes the activity-dependent rise in glucose metabolism (Cholet et al., 2001; Herard et al., 2005; Voutsinos-Porche et al., 2003). However, the ANLS hypothesis is challenged by other studies showing that lactate can be utilized by both neurons and astrocytes and that during brain activation, glucose is a necessary substrate for neurons (Bak et al., 2006; Patel et al., 2014; Zielke et al., 2007). These studies take into account the concentrations and kinetic properties of glucose and lactate transporters in neurons and astrocytes to support the idea that activity-dependent increases in glucose uptake and metabolism are primarily driven by neuronal metabolic needs (Chih et al., 2001; DiNuzzo et al., 2010; Gandhi et al., 2009; Lundgaard et al., 2015; Mangia et al., 2009; Simpson et al., 2007).

Metabolic control of glutamatergic and GABAergic transmission

Beyond activity-stimulated glucose and lactate metabolism, regulated synthesis and degradation of neurotransmitters glutamate and γ-amino-butyric acid (GABA) constitute an important metabolic control point in neurotransmission (Figure 1.2) (Duarte et al., 2015; Kreft et al., 2012; Sonnewald, 2014; Walls et al., 2015). Glutamate synthesis in glutamatergic neurons can be fueled either through the oxidation of glucose or lactate or through the glutamate-glutamine cycle between neurons and astrocytes described above (Figure 1.2). In addition to converting glutamate to glutamine, astrocytes oxidize part of the glutamate taken up from the synapse to compensate for the high energetic cost of its recycling (Hertz and Hertz, 2003; McKenna, 2012; Sonnewald et al., 1993). In astrocytes, glutamate enters the tricarboxylic acid (TCA) cycle via its conversion to α-ketoglutarate by aspartate aminotransferase (AST) (reaction 4 in Figure 1.2), and can be partially or completely oxidized to generate ATP. As the TCA cycle cannot fully oxidize 4- and 5-carbon compounds such as malate (Owen et al., 2002), glutamate oxidation requires the conversion of malate to pyruvate by malic enzyme (ME) (reaction 5 in Figure 1.2) and the re-entry of pyruvate in the TCA cycle in the form of acetyl-CoA via the pyruvate dehydrogenase (PDH) reaction (reaction 6 in Figure 1.2) (Hertz and Rodrigues, 2014; McKenna, 2013).

The main inhibitory neurotransmitter GABA is synthesized via glutamate decarboxylase (GAD) in the cytosol of GABAergic neurons (reaction 7 in Figure 1.2). The combined actions of mitochondrial and cytosolic AST enzymes supply cytosolic glutamate for the GAD reaction. Mitochondrial AST transaminates the TCA cycle-derived glutamate to α-ketoglutarate, which shuttles to the cytosol and is used by cytosolic AST to produce glutamate (reaction 4 in Figure 1.2) (Schousboe et al., 2013). GABA is degraded by GABA-transaminase (GABA-T) (reaction 8 in Figure 1.2), which converts GABA to succinate-semialdehyde (SSA). SSA enters the TCA cycle as succinate by the action of succinate-semialdehyde dehydrogenase (SSADH) (reaction 9 in Figure 1.2) (Schousboe et al., 2013). GAD, GABA-T and SSADH constitute the GABA shunt (see inset in Figure 1.2), collectively providing a metabolic loop for GABA synthesis and degradation. The GABA shunt ultimately integrates the metabolism of glutamate and GABA with the TCA cycle. The physiologic relevance of the

GABA shunt is also underscored by pathologic conditions associated with loss of GAD and SSADH functions, which include uncontrolled neuronal activity and epileptic seizures (Chowdhury et al., 2007; Cortez et al., 2004; Rowley et al., 2012).

De novo synthesis of glutamate and GABA lead to efflux of α-ketoglutarate from the TCA cycle, which needs to be replenished by anaplerotic reactions such as the one catalyzed by pyruvate carboxylase (PC) (reaction 10 in Figure 1.2) (Schousboe et al., 2013). PC expression and activity are predominantly attributed to astrocytes, whereas neurons are believed to have minimal PC expression and undetectable PC activity (Morken et al., 2014; Serres et al., 2008; Waagepetersen et al., 2002; Waagepetersen et al., 2001; Yu et al., 1983). However, this idea has been challenged by *in vitro* and *in vivo* studies showing PC activity in neurons as measured by the appearance of ^{14}C-labeled glutamate from ^{14}C-pyruvate or $NaH^{14}CO_3$, both of which are PC substrates (Hassel and Brathe, 2000a, b). These studies highlight a potentially underappreciated role for neuronal PC-dependent anaplerosis during neurotransmitter synthesis that warrants future investigation.

Figure 1.2 Metabolic control of glutamatergic and GABAergic transmission

Abbreviations: α-KG: α-ketoglutarate; AST: aspartate aminotransferase; EAAT1-2: excitatory amino acid transporter 1 or 2; GABA-T: γ-amino-butyric acid transaminase; GABA: γ-amino-butyric acid; GAD: glutamate decarboxylase; GS: glutamine synthetase; LDH, lactate dehydrogenase; ME: malic enzyme; OAA: oxaloacetate; PAG: phosphate activated glutaminase; PC: pyruvate carboxylase; PDH: pyruvate dehydrogenase; SSA: succinate-semialdehyde; SSADH: succinate-semialdehyde dehydrogenase; TCA cycle: tricarboxylic acid cycle.

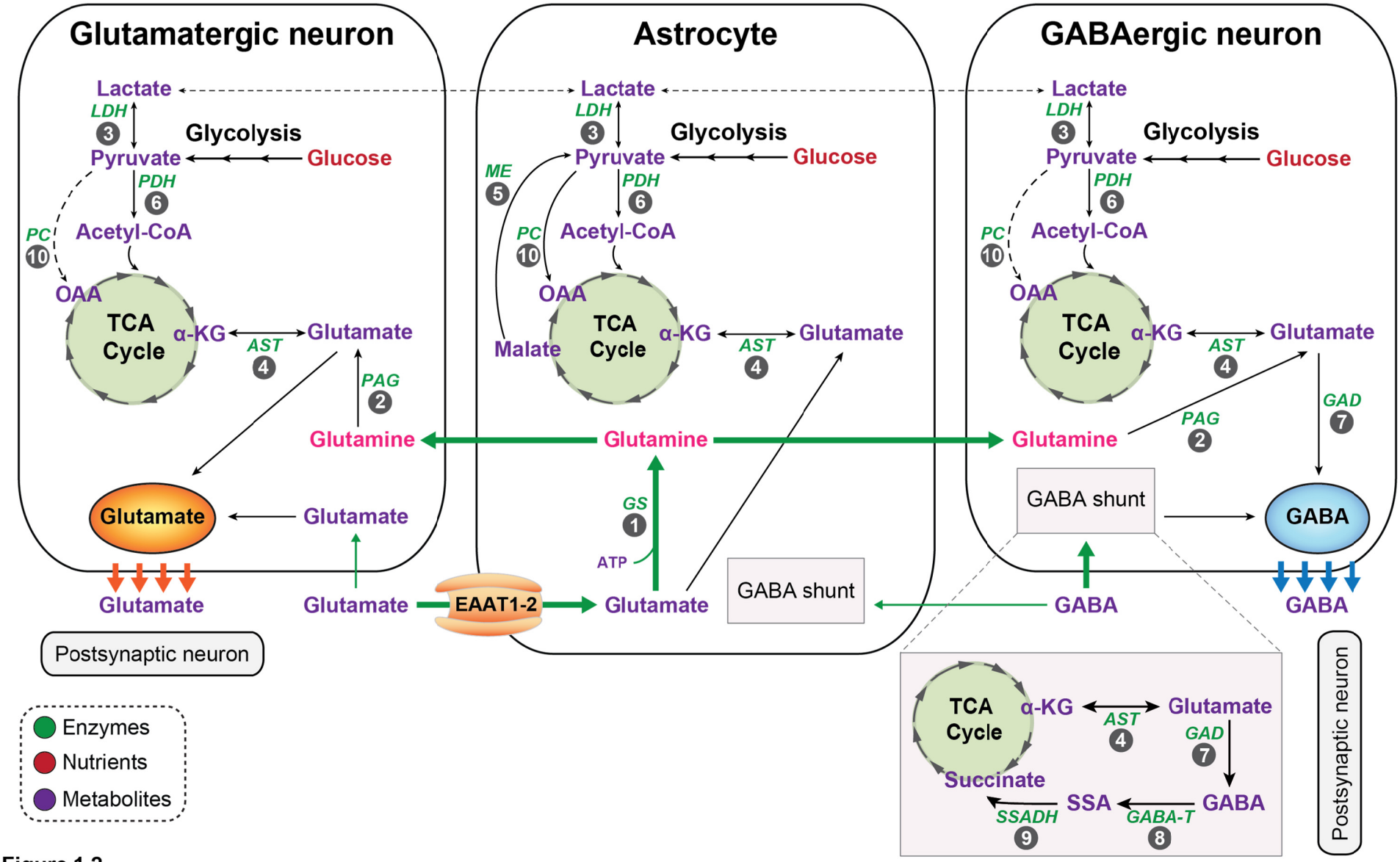
Glutamatergic neuron
Astrocyte
GABAergic neuron
Lactate
LDH
3
Glycolysis
Pyruvate
Glucose
PDH
6
PC
10
Acetyl-CoA
OAA
TCA Cycle
α-KG
AST
4
Glutamate
PAG
2
Glutamine
ME
5
Malate
GS
1
ATP
GAD
7
GABA shunt
GABA
Glutamate
EAAT1-2
Postsynaptic neuron
Enzymes
Nutrients
Metabolites
Succinate
SSA
SSADH
9
GABA-T
8

Figure 1.2

1.3 Ketogenic diet as a treatment for epilepsy

Ketone bodies and certain fatty acids (octanoate) can cross the BBB and provide up to 60% of the energy requirement in the brain, particularly in cases of low glucose availability (DeVivo et al., 1978; Ebert et al., 2003; Owen et al., 1967). The metabolism of fatty acids and ketone bodies is integrated through acetyl-CoA pools (Figure 1.1). In addition, ketone bodies can be synthesized locally by astrocytes (Auestad et al., 1991; Blazquez et al., 1998). The capacity of mitochondria to process carbohydrates and ketone bodies can influence neuronal excitability. For example, the ketogenic diet (KD), which reduces glucose metabolism and promotes the breakdown of fatty acids to generate ketone bodies, is an effective treatment for pharmacoresistant epilepsy (Hartman et al., 2007; Lutas and Yellen, 2013). The classic KD consists of a 4:1 ratio of fat to protein and carbohydrates, and it stimulates the production of high amounts of the 3 ketone body species acetone, β-hydroxybutyrate, and acetoacetate by the liver, which are in turn secreted to the bloodstream and used as fuel by the brain (Lutas and Yellen, 2013). Though the effectiveness of the KD for the treatment of drug-resistant epilepsy is well documented and further underscored by a randomized clinical trial (Neal et al., 2009), the molecular underpinnings of the KD-induced glucose-to-ketone-body fuel switch and the attendant changes in neuronal activity are not fully understood.

The anticonvulsant mechanisms of the ketogenic diet

Several mechanisms have been put forward to explain the anticonvulsant effect of the KD. These mechanisms, which need not be mutually exclusive, range from direct influence of ketone bodies on neuronal excitability to effects on glucose metabolism and neurotransmission, ultimately regulating neuronal excitability. For example, one study showed that acetoacetate inhibits the vesicular glutamate transporter, VGLUT2, reducing glutamate transport into synaptic vesicles and consequently decreasing seizure intensity by dampening glutamatergic neurotransmission (Juge et al., 2010). This is likely mediated by competitive binding of acetoacetate to a site in VGLUT2 that is normally engaged by its allosteric activator, the chloride ion (Juge et al., 2010). Other groups have shown that the KD-induced switch from glucose to ketone body metabolism leads to increased GABA synthesis, counteracting

excessive excitatory neurotransmission observed in seizures (Erecinska et al., 1996; Yudkoff et al., 2007). Specifically, increases in KB-derived acetyl-CoA and citrate synthesis in the TCA cycle decrease the availability of oxaloacetate for the transamination of glutamate to aspartate, making more glutamate available for GABA synthesis (Yudkoff et al., 1997; Yudkoff et al., 2005; Yudkoff et al., 1994). Astrocytes are also thought to play a role in this process as the increase in ketone body metabolism stimulates glutamine production by astrocytes and its transfer and subsequent conversion to glutamate for GABA synthesis in GABAergic neurons via the glutamate-glutamine cycle (Melo et al., 2006; Yudkoff et al., 2005).

Ketone bodies can also affect neuronal ionic balance by modulating the activity of ATP-sensitive potassium (K_{ATP}) channels, which are inhibited by ATP and help maintain a hyperpolarized state in neurons (Lutas and Yellen, 2013; Yellen, 2008). Therefore, the opening of these channels reduces neuronal excitability by preventing excessive neuronal firing and/or expediting recovery of ionic balance post excitation by triggering influx of potassium ions into the cell. As many glycolytic enzymes are localized near the plasma membrane, it is proposed that K_{ATP} channels may be especially senstive to fluctuations of glycolytically-derived ATP in this micro-environment (Lutas and Yellen, 2013). Consistent with this idea, the open probability of these channels is increased following inhibition of glycolysis (Lutas et al., 2014). However, the open probability of these channels is also increased upon exposure to ketone bodies such as β-hydroxybutyrate, which can be metabolized to generate ATP (Ma et al., 2007; Tanner et al., 2011). Whether the effect of ketone bodies on the opening of these channels is mediated by their capacity to inhibit glycolysis as previously proposed (Garriga-Canut et al., 2006), or by a more direct effect of their metabolism is not fully known.

Other mechanisms for the anticonvulsant effects of the ketogenic diet include adenosine signaling via A1 receptors (Masino et al., 2011), as well as changes in redox balance (Kim et al., 2007; Maalouf et al., 2007). Overall, this body of evidence suggests that multiple mechanisms are likely involved in the potent seizure protection conferred by the ketogenic diet. However, the complex systemic effects of dietary treatments and the different levels of protection observed in humans and rodent animal models have made it difficult to obtain a clear picture of how KD-induced changes in brain metabolism lead to altered neuronal

excitability. Therefore, the identification of cell-intrinsic molecular modulators that can induce a similar glucose-to-ketone body fuel switch in the absence of dietary manipulations will greatly aid the molecular understanding of the link between metabolism and excitability. As detailed below, recent findings from the Danial lab have implicated the BCL-2 family protein BAD as such a cell-intrinsic modulator of fuel choice in the brain and seizure sensitivity independently of any dietary treatments (Gimenez-Cassina et al., 2012).

1.4 BAD regulates the reciprocal utilization of glucose and ketone bodies

BAD [B cell lymphoma (BCL)-2-associated Agonist of Cell Death] is a member of the BCL-2 family of cell death/survival proteins (Chi et al., 2014; Czabotar et al., 2014; Danial and Korsmeyer, 2004; Moldoveanu et al., 2014). Separate from its well established role in apoptosis, BAD modulates glucose metabolism in multiple cell types (Figure 1.3) (Danial, 2008; Gimenez-Cassina and Danial, 2015). The first evidence for the involvement BAD in systemic glucose homeostasis emerged from the identification of the direct interaction between BAD and glucokinase (GK, hexokinase IV) – the maturity-onset diabetes of the young type 2 (MODY2) gene product (Danial et al., 2003; Danial et al., 2008; Gimenez-Cassina et al., 2014; Szlyk et al., 2014). GK is a key component of the mammalian glucose-sensing machinery with tissue-restricted roles in insulin secretion by pancreatic islet β-cells, glucose utilization and storage in hepatocytes, as well as central glucose sensing (Matschinsky, 2009). Compared to other hexokinase isoforms, unique kinetic properties such as lack of product inhibition by glucose-6-phosphate, a high *K*m (low affinity) for glucose, and positive substrate cooperativity, render the GK-catalyzed reaction essentially a substrate-driven process particularly well-suited for regulation of blood glucose levels. BAD directly activates GK (Szlyk et al., 2014). This requires phosphorylation of Ser155 within and α-helix known as the BAD BH3 domain (Figure 1.3) (Danial et al., 2008; Szlyk et al., 2014). The notion that the BAD–GK partnership is physiologically relevant for glucose sensing and systemic glucose homeostasis is consistent with several metabolic alterations that are phenocopied *in vivo* and *in vitro* upon ablation or depletion of each protein in β-cells and liver. These aberrations include reduced glycolysis and mitochondrial handling of glucose, fasting hyperglycemia, loss of glucose

responsiveness of insulin secretion in β-cells, impaired glucose tolerance, and hepatic insulin resistance (Figure 1.3) (Danial et al., 2003; Danial et al., 2008; Gimenez-Cassina et al., 2014).

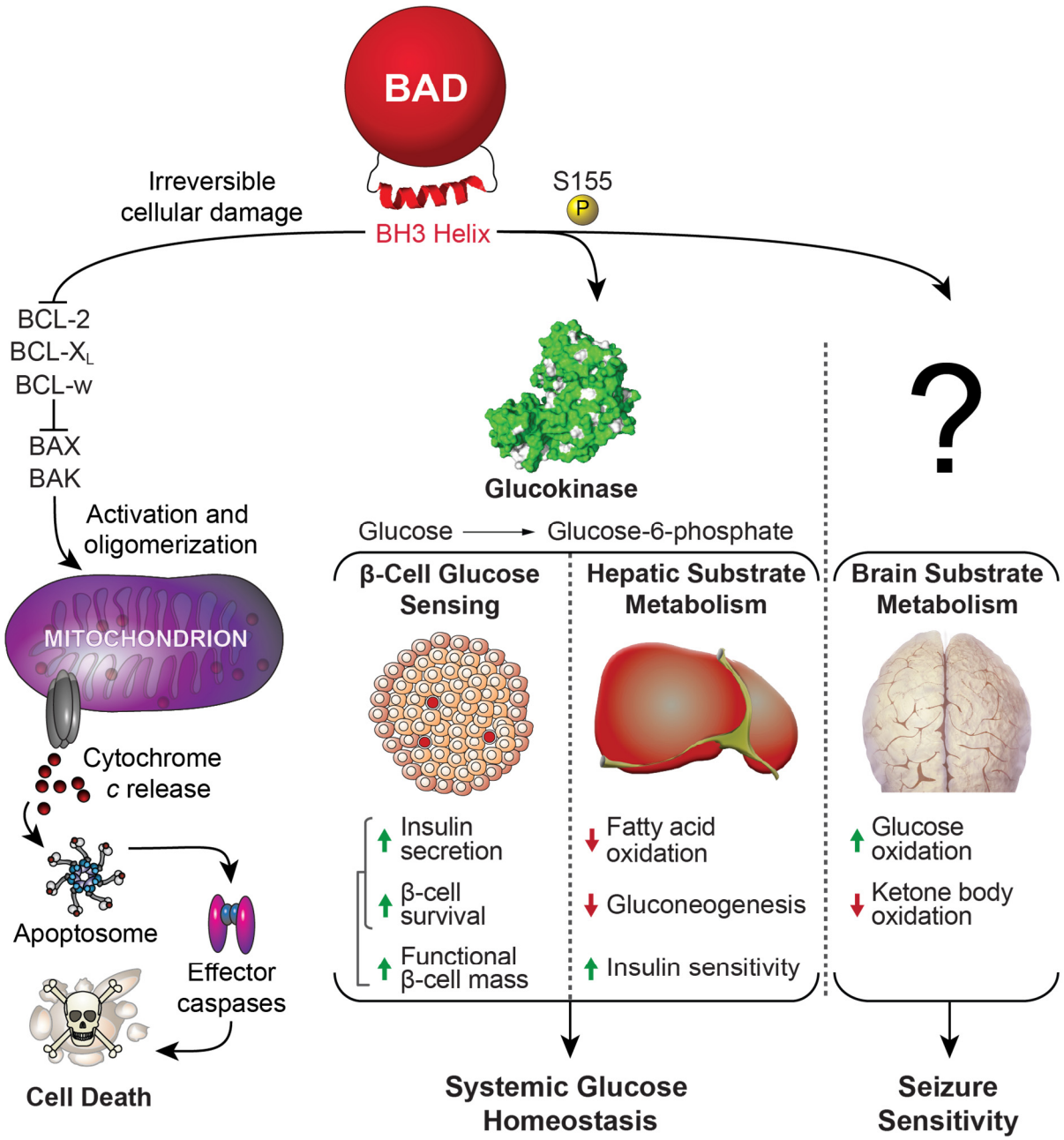

Figure 1.3 Dual roles of BAD in apoptosis and fuel metabolism

Regulation of glucose metabolism by BAD is not limited to tissues that express GK, suggesting that cell type-specific mechanisms/binding partners mediate the metabolic function of BAD in different tissues (Deng et al., 2008; Gimenez-Cassina et al., 2012). In particular, BAD modulation of fuel choice in the brain is relevant for neuronal excitability and seizure sensitivity (Gimenez-Cassina et al., 2012). Specifically, Ser155 phosphorylation within the BAD BH3 helix normally stimulates mitochondrial metabolism of glucose but inhibits ketone body utilization (Figures 1.3 and 1.4). Consequently, BAD deficiency or interference with its phosphorylation produces a glucose-to-ketone-body fuel switch in neural cells that is seizure protective. An electrophysiological consequence of this fuel switch is a marked increase in the open probability of the metabolically sensitive K_{ATP} channel in dentate granule neurons (Gimenez-Cassina et al., 2012), an area believed to function as a 'seizure gate' in the brain (Dunn-Meynell et al., 1998; Karschin et al., 1997; Zawar et al., 1999). This is further associated with reduction in electrographic and behavioral seizures *in vivo* (Gimenez-Cassina et al., 2012). Seizure resistance in this setting cannot be explained by changes in neural cell apoptosis following BAD modifications, rather genetic evidence indicates that the opening of the K_{ATP} channel is a necessary downstream mediator of the effect of BAD on neuronal excitation and seizure responses (Gimenez-Cassina et al., 2012). The precise mechanism of K_{ATP} channel activation by BAD-dependent metabolic changes is not fully known. Glucose deprivation or elevation of ketone body metabolism can each increase K_{ATP} channel activity (Ma et al., 2007; Tanner et al., 2011). Additional data indicate that seizure resistance in BAD-deficient mice is likely related to changes in neural metabolism rather than systemic metabolic alterations. Consistent with this idea, the whole-brain content of the ketone body species β-hydroxybutyrate is significantly higher in *Bad* -/- mice, while its serum levels are not altered (Gimenez-Cassina et al., 2012). This suggests potential BAD-dependent local changes in ketone body generation and handling such as ketogenesis by astrocytes. Because ketone bodies can increase the activity of the K_{ATP} channel in central neurons (Ma et al., 2007; Tanner et al., 2011), their higher content in this setting may explain, at least in part, the observed increase in K_{ATP} channel activity. In addition, the contribution of other mechanisms beyond changes in K_{ATP} channel activity downstream of BAD cannot be ruled out.

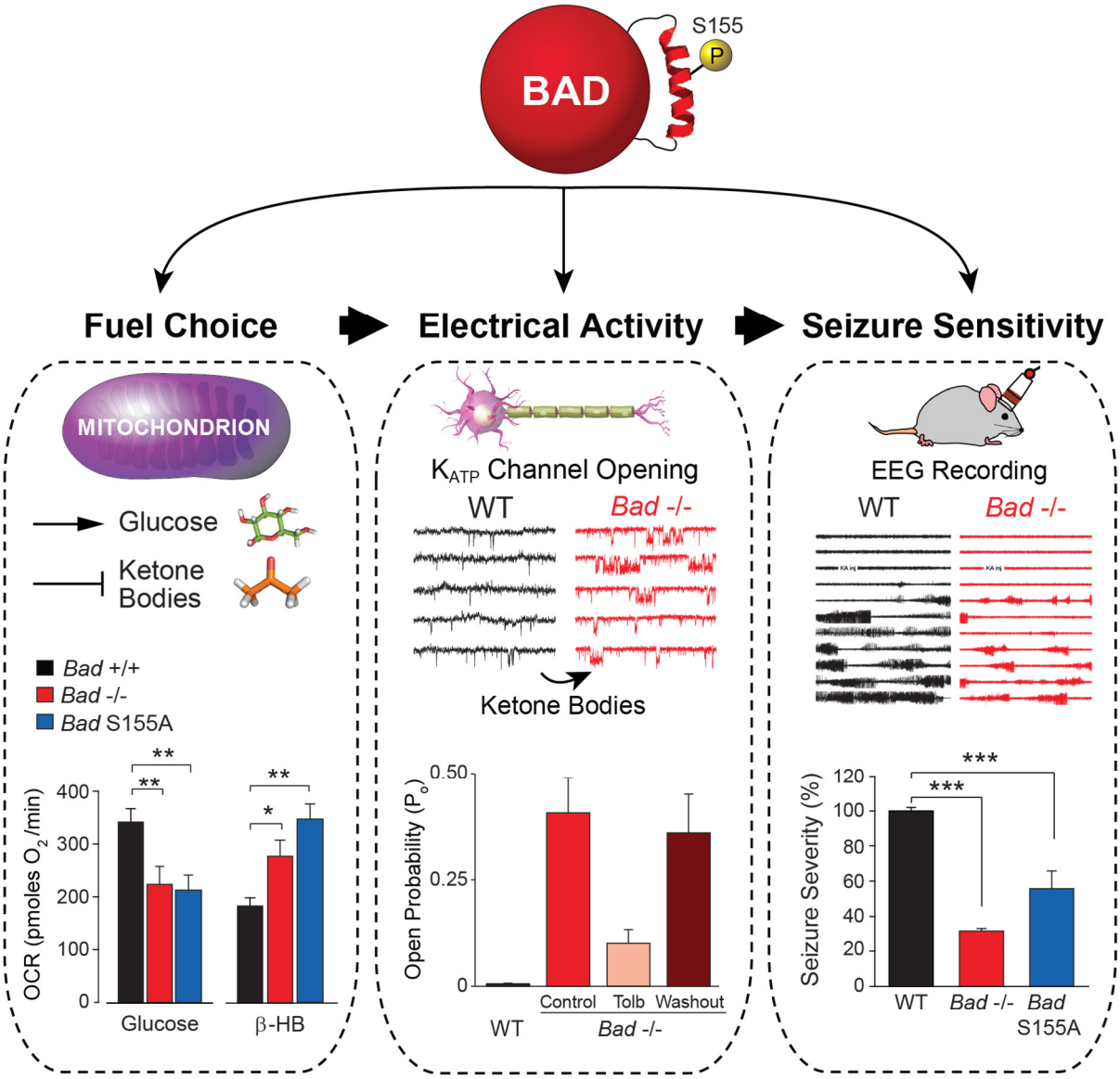

Figure 1.4 BAD-dependent glucose-to-ketone body fuel switch and metabolic control of neuronal excitability

BAD phosphorylation on Ser155 sets the preference for carbon substrate utilization in the brain, favoring mitochondrial oxidation of glucose as the main source of energy over ketone bodies. Consequently, BAD deficiency or interference with its phosphorylation triggers a glucose-to-ketone body fuel switch that is associated with opening of the K_{ATP} channels. The increase in K_{ATP} channel activity significantly buffers excessive neuronal firing under pathological conditions such as epilepsy. These effects are independent of BAD's effect on apoptosis.

1.5 Objectives and overview of this dissertation

The glucose-to-ketone-body fuel switch induced by BAD modification recapitulates the actual change in fuel consumption by the brain under fasting or on ketogenic diet. However, these BAD-dependent changes occur in the absence of any dietary manipulation, providing a new molecular and cellular handle on the metabolic control of neuronal activity by fuel substrate switching. Compared with the systemic effects of dietary alterations, seizure resistance in *Bad*-null and S155A mice is likely due to alterations in neural cell metabolism rather than systemic changes. Therefore, these findings present a unique opportunity to test and define the underlying metabolic mechanisms that control neuronal activity in a way that has not been easy with dietary manipulations given their systemic effects.

The studies described in this dissertation aimed at determining the mechanistic underpinnings of the metabolic alterations associated with BAD modifications. Specifically, our efforts focused on defining the metabolite signature of the glucose-to-ketone-body fuel switch that are directly and acutely associated with BAD modifications, as well as to identify potential BAD-interacting partners in the brain that mediate this metabolic phenotype (Figure 1.5). Our work towards these aims integrates a range of approaches, including state of the art targeted metabolomics and ^{13}C isotopomer tracing studies, quantitative proteomics, and biochemical assays, together with genetic manipulation of BAD, to answer the key question: *What are the precise steps at which the metabolism of glucose and ketone bodies is changed when BAD is modified, and how are they mediated at the molecular level?* Chapter 3 investigates the steps in glucose metabolism that are modified by BAD and uncovers a BAD-dependent metabolic lesion in the lower glycolytic pathway, which consequently leads to reduced input of glucose-derived carbons in the TCA cycle. Chapter 4 identifies specific candidate novel interaction partners for BAD that may mediate its effect on fuel utilization in the brain. Chapter 5 follows the fate of carbons derived from ketone bodies to define how the metabolism of these fuel substrates is altered upon BAD modifications.

In the fullness of time, the work described here and our ongoing experiments to complete these integrative studies will give an integrated picture of the mechanistic pathway connecting BAD-dependent control of fuel choice in the brain to changes in neuronal

excitability. This line of investigation may also have broader implications by revealing potential targetable metabolic nodes that control seizure responses in a cell-autonomous manner, which may serve as an alternative strategy to ketogenic diet for the treatment of pharmacoresistant epilepsies.

Thesis Project at a Glance

Overarching question: what are the metabolic signatures and the molecular mediators of the glucose-to-ketone-body fuel switch that regulate neuronal excitability and seizure sensitivity in a BAD-dependent manner?

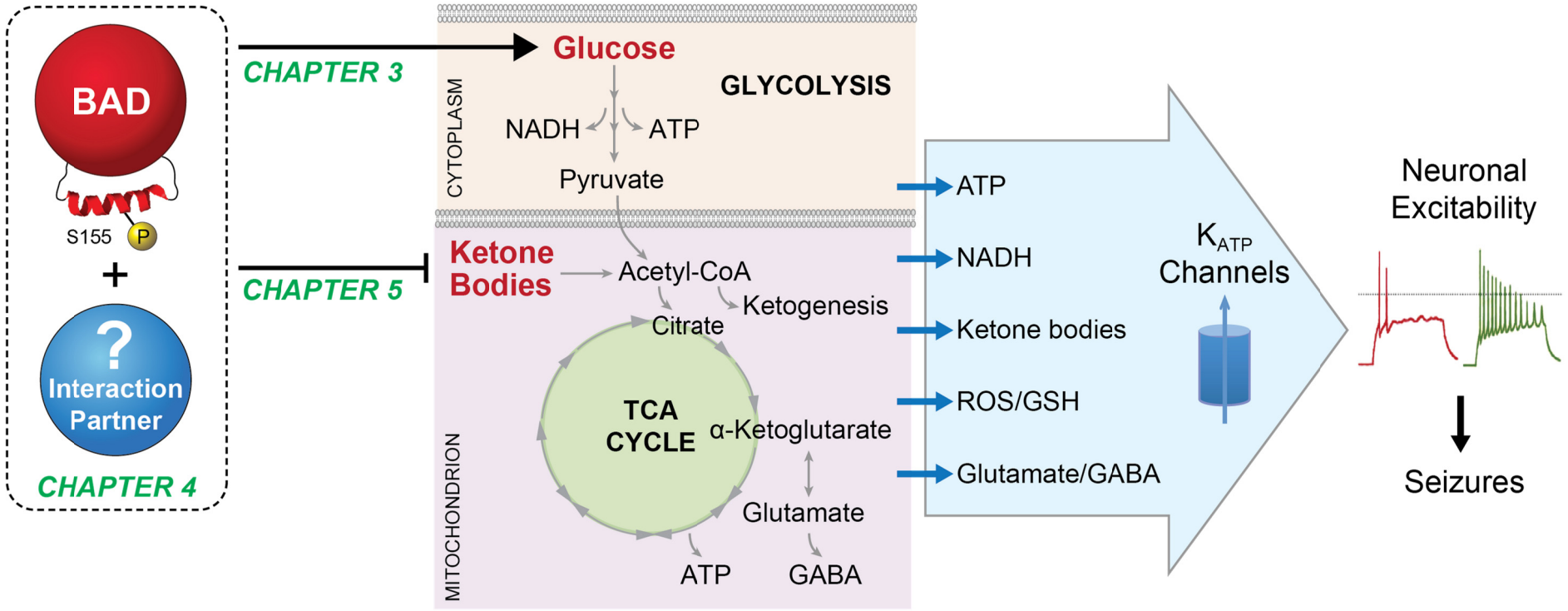

Figure 1.5

CHAPTER 2

Materials and Methods

METHODS USED IN CHAPTERS 3 AND 5

Animals

The *Bad* +/+ (WT), *Bad* -/- and *Bad* S155A knockin mice used throughout these studies have been previously described (Danial et al., 2008; Gimenez-Cassina et al., 2012). *Bad* genetic models were bred into the C57BL/6J genetic background for at least 14 generations and were validated by genome scanning to be 99.9% congenic with C57BL/6J. Mice received a standard chow diet and were housed in a barrier facility with 12 hr light and dark cycles. All animal procedures were approved by the Institutional Animal Care and Use Committee of Dana-Farber Cancer Institute and Harvard Medical School. Pregnant females bearing E16-17 embryos were used to generate neuronal cultures. Eight to 12-week-old male mice were used to harvest cortical brain tissue.

Primary cultures of neurons

Primary cortical neurons were cultured according to established protocols with some modifications (Gimenez-Cassina et al., 2012). Cortices from E16-17 mouse embryos were dissected in pre chilled Hank's buffered salt solution (HBSS) supplemented with Ca^{2+} and Mg^{2+}. After removal of the meninges, striatum, and hippocampus, the intact cortices were cut into small pieces, washed 3 times in HBSS (free of Ca^{2+}/Mg^{2+}), and incubated in a HBSS solution containing 0.25% trypsin (Sigma-Aldrich, St. Louis, MO) and 1 mg/mL DNaseI (Roche Diagnostics, Indianapolis, IN, USA) for 15 min at 37^{o}C with gentle shaking every 3-4 min. The digested tissue was washed twice in HBSS solution and mechanically dissociated in plating medium, composed of Neurobasal medium (Thermo Fisher Scientific, Waltham, MA) supplemented with 10% horse serum (Thermo Fisher Scientific, Waltham, MA) and 1% penicillin and streptomycin mix (100 U/mL and 100 mg/mL, respectively) by pipetting up and down. The cell suspension was then passed through a 70 µm-cell strainer and diluted to a final volume (mL) of 1.5 times the number of brains dissected and pooled. Cell number was determined and cells were seeded onto poly-L-lysine (PLL)-coated tissue culture dishes or

multi-well plates at the following densities: 2.5-3 x 10^6 cells in 60 mm dishes, 6.5 x 10^5 cells in 12-well multiwell plates, and 3.5 x 10^5 cells in 12-well multiwell plates containing coverslips. Three hr after seeding, the medium was changed to culture medium composed of Neurobasal medium supplemented with 2% B-27 (Thermo Fisher Scientific, Waltham, MA), 2 mM GlutaMAX (Thermo Fisher Scientific, Waltham, MA), and 1% penicillin and streptomycin mix. Cells were re-fed every 3 days by replacing one-third of the medium with fresh culture medium. At 3 days in vitro (DIV 3), cells were treated with 10 μM cytosine arabinoside (AraC) (Sigma-Aldrich, St. Louis, MO) to prevent glial cell proliferation. Cells were cultured for 5 days prior to all experiments.

Immunofluorescence

Neurons cultured in PLL-coated glass coverslips were fixed with 4% paraformaldehyde solution for 30 min at room temperature, followed by 3 washes with phosphate buffered saline (PBS) solution. Cells were then permeabilized and blocked with a blocking solution composed of 0.1% Triton X-100 and 1% BSA diluted in PBS solution, for 30 min at room temperature. Cells were incubated with a mix of primary antibodies, anti-β-tubulin III (1:500, Sigma-Aldrich, St. Louis, MO) and anti-GFAP (1:100, Sigma-Aldrich, St. Louis, MO) in blocking solution, overnight at 4°C. Following 3 washes with PBS, secondary antibodies Alexa 488-conjugated anti-rabbit (1:200) and Alexa 568-conjugated anti-mouse (1:200) (both from Thermo Fisher Scientific, Waltham, MA) were added for 1 hr at room temperature, protected from light. After 3 washes with PBS, coverslips were mounted on glass slides using mounting media (Vectashield), containing DAPI, and sealed with clear nail polish. Images were acquired on a Zeiss fluorescence microscope.

Western blots

Whole cell protein lysates were obtained by scrapping cells with lysis buffer, 20 mM HEPES pH 7.4, 100 mM NaCl, 100 mM NaF, 1 mM Na_3VO_4, 1% Triton X-100, and 5 mM EDTA supplemented with protease inhibitors (Roche Diagnostics, Indianapolis, IN, USA) and phosphatase inhibitors (Roche Diagnostics, Indianapolis, IN, USA), followed by 15 min

incubation on ice. The supernatants were cleared by centrifugation at 14 000 rpm for 10 min at 4°C. Protein concentration was determined using the Pierce BCA protein assay kit (Thermo Fisher Scientific, Waltham, MA) according to manufacturer's instructions. Protein lysates were denatured with 4x Laemmli buffer, 8% SDS, 40% glycerol, 20% β-mercaptoethanol, 250 mM Tris-HCl pH 6.8 and bromophenol blue, for 8 min at 90°C. Twenty-five µg of protein lysate were loaded per lane (unless otherwise indicated in the figure legend) of a 4-12% gradient Bis-Tris NuPAGE gel (Thermo Fisher Scientific, Waltham, MA). Protein transfer was carried out in an XCell SureLock™ Mini-Cell Electrophoresis System (Thermo Fisher Scientific, Waltham, MA) using nitrocellulose membranes. Membranes were blocked for 1 hr at room temperature in blocking solution, 5% (m/v) fat-free milk prepared in PBS solution containing 0.1% Tween-20 (PBST). Primary antibodies were diluted in blocking solution and incubated for 1h or overnight at 4°C. The following primary antibodies, concentrations and incubation times were used: rabbit anti-BAD (Cell Signaling Technology, Danvers, MA), 1:1000, overnight; rabbit anti-β-tubulin III (Sigma-Aldrich, St. Louis, MO), 1:10000, 1 hr; mouse anti-GFAP (Sigma-Aldrich, St. Louis, MO), 1:1000, 1 hr; mouse anti-β-actin (Sigma-Aldrich, St. Louis, MO), 1:10000; rabbit anti-BCL-X_L (Cell Signaling Technology, Danvers, MA), 1:2000, overnight. The following secondary antibodies, concentrations and incubation times were used: goat anti-rabbit HRP (Jackson ImmunoResearch Laboratories, West Grove, PA), 1:10000, 1 hr; goat anti-mouse HRP (Jackson ImmunoResearch Laboratories, West Grove, PA), 1:1000, 1 hr. Membranes were washed 3 times for 10 min with PBST solution and incubated with HRP-conjugated secondary antibodies diluted in blocking solution for 1 hr at room temperature. Membranes were washed again 3 times for 10 min with PBST and developed with Western Lightning Plus ECL (PerkinElmer) according to manufacturer's instructions.

PDH activity assay

PDH activity was assessed in 25 µg of isolated mitochondria from adult mouse cortices using a microplate assay kit (MitoSciences, Eugene, OR). Briefly, cortices from 8- to 12-week old adult male mice were dissected and homogenized in ice-cold mitochondria isolation buffer

(MIB) containing 200 mM mannitol, 70 mM sucrose, 1 mM EGTA, 10 mM HEPES and protease inhibitors, using a glass dounce homogenizer. Homogenates were cleared by centrifugation, repeated twice, at 1000 × g for 5 min at 4°C, and supernatant were recovered. Mitochondria were pelleted by centrifugation of the supernatant at 9000 × g for 20 min at 4°C, and were washed in MIB followed by centrifugation at 9000 × g for 20 min at 4°C. Isolated mitochondria were resuspended in MIB and protein concentration was determined using the BCA protein assay kit. The concentration of the mitochondrial preparation was adjusted to 5.3 mg/mL with PBS and the remainder of the PDH activity assay was performed according to manufacturer's instructions.

Glucose uptake

Glucose uptake was measured as previously described with some modifications (Furukawa et al., 2005; Heidenrich et al., 1989). Primary cortical neurons were grown in 12-well multiwell plates and 3-6 h before the experiment. The medium was changed to fresh neuronal culture medium, and cells were rinsed 3 times with KRH buffer containing 50 mM HEPES pH 7.4, 136 mM NaCl, 1.25 mM $MgSO_4$, 1.25 mM $CaCl_2$ and 4.7 mM KCl, and incubated in KRH buffer for 20 min in the 37°C cell culture incubator. KRH buffer containing 0.5 mM 2-DG (non-radiolabeled) and 0.25μCi of [^{3}H]-2-deoxyglucose (DG) (American Radiolabeled Chemicals, St Louis., MO) was added to each well followed by a 10 min incubation at 37°C. Cells were rinsed 3 times with KRH buffer containing 200mM glucose, lysed in 200 μL of 0.1% SDS, and 100 μL of cell lysate were used to measure ^{3}H disintegrations per minute (dpm) in a TriCarb liquid scintillation counter (PerkinElmer, Boston, MA). The remaining cell lysate was used for protein quantification with the BCA protein assay kit to normalize glucose uptake rates across genotypes.

Isotopic labeling

For isotopic labeling experiments, primary neurons were cultured in PLL-coated 60mm dishes for 5 days prior to the experiments. Labeling experiments were carried out in labeling media composed of glucose- and pyruvate-free Neurobasal-A medium supplemented with 2% B-27,

2mM GlutaMAX, 1% penicillin and streptomycin mix and the tracer of interest. The tracers used were 10 mM $U^{13}C$-glucose, 5 mM $U^{13}C$-pyruvate, and 5 mM $U^{13}C$- β-hydroxybutyrate (all from Cambridge Isotope Laboratories, Tewksbury, MA). Cells were incubated in labeling medium for 0, 2, 4, 8 and 24 hr for glucose tracer and 2 hr for pyruvate and β-hydroxybutyrate tracers.

Metabolite extraction and derivatization

Metabolite were extracted as previously described (Faubert et al., 2014; Mamer et al., 2013). Polar metabolites were extracted using -80°C cold methanol:water (80:20 v/v). Briefly, 10 µL of extracellular medium were collected into a tube containing 500 µL of -80°C cold methanol:water. The remaining supernatant was removed and cells were gently rinsed twice with 2 mL of ice-cold isotonic saline solution (9 g/L NaCl) and maintained on ice throughout the procedure. After the saline washes, plates were transferred onto dry ice and 800 µL of -80°C cold methanol:water were added to each plate. Cells were scraped and collected into a pre-chilled tube. Cell suspensions were quickly vortexed and then sonicated on an ice bath for 2 cycles of 10 min (30 s ON, 30 s OFF) in the ‘‘high’’ setting, using the BioRuptor (UCD-200 TM, Diagenode). Metabolite suspensions were centrifuged for 10 min at 21,000 × g at 4°C. The supernatant was transferred into a fresh pre-chilled tube containing 1 µL of 750 ng/ µL D27-myristic acid dissolved in pyridine, as an internal standard. Samples were dried overnight in a vacuum centrifuge (Labconco, Kansas City, MO, USA) at – 4°C. Extracellular media samples were processed similarly to cell extracts but skipping the sonication step. Dried cell extracts and media samples were then derivatized. Briefly, 30 µL of MOX solution (10 mg Methoxyamine:HCl in 1 mL anhydrous pyridine) were added to each dried sample, which were then sonicated for 15 sec and vortexed for 15 sec twice at room temperature. The samples were centrifuged for 10 min at >10,000 rpm, incubated at room temperature for 30 min and then centrifuged again for 2 min. The supernatants were transferred to GC-MS vials containing 70 µL of *N-tert*-butyldimethylsilyl-*N*-methyltrifluoroacetamide (MTBSTFA). The GC-MS vials containing metabolite extracts, MOX and MTBSTFA were incubated for 1 hr at 70°C in order to carry out the derivatization reactions (Mamer et al., 2013).

Metabolite analysis by GC-MS

GC/MS analyses were performed as previously described (Faubert et al., 2014; Mamer et al., 2013; McGuirk et al., 2013; Vincent et al., 2015). Samples were analyzed on an Agilent 5975C mass selective detector coupled to a 7890A gas chromatograph (Agilent J&W, Santa Clara, CA) fitted with a 7693 autosampler and a DB-5MS+DG capillary column (30 m plus 10 m Duraguard®), diameter 0.25 mm, film thickness 0.25 µm (Agilent J&W, Santa Clara, CA, USA). All data were collected by electron ionization set at 70 eV. 1 µL of the derivatized sample was injected in the GC in splitless mode with inlet temperature set to 280°C, using helium as a carrier gas with a flow rate of 1.5512 mL/min (rate at which myristic acid elutes at 17.94 min). The quadrupole was set at 150°C and the GC/MS interface at 285˚C. The oven program for all metabolite analyses started at 60°C held for 1 min, then increasing at a rate of 10°C/min until 320˚C. Bake-out was at 320°C for 10 min. Sample data were acquired both in scan (1-600 m/z) and selected ion monitoring (SIM) modes. All metabolites used in this study were previously validated using authentic standards to confirm mass spectra and retention times (Mamer et al., 2013).

GC-MS data analysis

Integration of ion intensities was done using the Agilent MSD ChemStation software (Agilent J&W, Santa Clara, CA). U^{13}C-glucose, U^{13}C-pyruvate, and U^{13}C-β-hydroxybutyrate flux analysis was performed by mass isotopomer distribution analysis using an in-house algorithm developed at McGill University as previously described (Faubert et al., 2014; McGuirk et al., 2013; Nanchen et al., 2007; Vincent et al., 2015). The atomic composition of the TBDMS-derivatized metabolite fragments (M-57 ions) was determined and, using the algorithm, matrices correcting for natural contribution of isotopomer enrichment were generated for each metabolite (C_{total}^{-1}). The mass distribution of each metabolite was normalized (such that the sum of the distribution equals 1) and rearranged in vector form. The resulting mass distribution vector (MDV), also known as mass isotopomer distribution (MID) vector, was multiplied into

the appropriate correction matrix ($MDV^* = C_{total}^{-1} \cdot MDV$). The corrected mass distribution vector (MDV*) was again normalized to 1. These values correspond to the proportional metabolite flux in the cell, and ion level values are expressed as fractions of the total pool of the particular metabolite examined. These values are referred in the text as mass isotope distributions (MIDs) (McGuirk et al., 2013; Nanchen et al., 2007). To take into account potential differences in the total metabolite pool size, a different methodology was used to evaluate "flux". First, the steady state level of each metabolite and its corresponding isotopologue levels were determined by multiplying the MDV* by the total ion count (TIC) of each metabolite and then summing all integrated ion intensities for a given metabolite (total pool). Then each corrected total ion count or isotopologue count was normalized to the signal of the internal standard, D27-myristic acid (McGuirk et al., 2013). Internal standard corrected values were subsequently normalized by the mean total protein level of 3 neuronal culture plates of the same genotype grown in parallel to the experimental "flux" plates to correct for any differences in cell number across genotypes.

METHODS USED IN CHAPTER 4

Preparation of cortical lysates for size exclusion chromatography (SEC)

Cortical lysates were prepared from brains of 8- to 12-week old adult WT and *Bad* -/- male mice. Cortices were dissected, washed in ice-cold PBS and flash frozen until use. Six to eight cortices were used to obtain enough protein (7-10 mg) for each round of size exclusion chromatography (SEC). Frozen cortices were lysed in ice-cold lysis buffer containing 50 mM Tris-HCl pH 7.5, 150 mM NaCl, 1 mM EDTA, 0.3% CHAPS, 10% glycerol, protease inhibitors and phosphatase inhibitors. Each cortex was homogenized in 250 µL of lysis buffer using a mini portable pestle mixer. Tissue homogenates were incubated on ice for 15 min and centrifuged at 14 000 rpm for 20 min at 4^{o}C. The supernatants were transferred using a 23G1 needle attached to a 1 mL syringe and combined into a single 1.5 mL tube. Centrifugation of the cleared supernatant was repeated 2 more times at 14 000 rpm for 15 min at 4^{o}C. The supernatant was then filtered through an Ultra Free-MC 0.2 µm filter unit (Thermo Fisher Scientific, Waltham, MA) by centrifugation at 12 0000 × g for 10 min at 4^{o}C. Protein concentration of the filtered lysate was determined using the BCA protein assay kit.

Superdex 200 10/300 GL calibration

The Superdex 200 column was calibrated using a high molecular weight calibration mix containing the following standard proteins: Ferritin (440 KDa), Catalase (250 KDa), Aldolase (161 KDa), Albumin (67 KDa), Ovalbumin (43 KDa) and Chymotrypsinogen (25 KDa). The protein calibration mix was prepared at a concentration of 4 mg/mL for each protein, except for Ferritin (0.4 mg/mL) and Aldolase (1.6 mg/mL). Five hundred µL the protein calibration mix were injected and subjected to chromatography in a running buffer composed of 50 mM Tris-HCl pH 7.5, 150 mM NaCl, 1 mM EDTA, 0.3% CHAPS and, 10% glycerol at a flow rate of 0.2 mL/min on an Akta Explorer system (Ge Healthcare). To determine the void volume (V_o) of the column, 100 µL of Blue Dextran 2000 (~2000 KDa, 1 mg/mL) was injected and chromatography was performed at a flow rate of 0.4 mL/min in a 50 mM sodium phosphate

buffer, pH 7.0, containing 150 mM NaCl. Peak elution volumes (V_e) for each standard protein and for Blue Dextran 2000 (V_o) were determined from the chromatogram using the Unicorn V5 software (Ge Healthcare). These elution volumes were used to calculate the partition coefficient (K_{av}) for each standard protein using the equation: $K_{av} = (V_e - V_o) / (V_t - V_o)$, where V_o is the void volume, V_e is elution volume, and V_t denotes total bed volume (24 mL). The correlation between the partition coefficient and the molecular weight (Log MW) of each standard protein was determined through a linear regression, which was then used to determine the size of the chromatographic fractions and of the BAD-containing complexes.

Size exclusion chromatography

Cortical lysates were injected into a Superdex 200 10/300GL column (GE Healthcare) for separation of BAD-containing complexes using an Akta Explorer system (Ge Healthcare). A volume of 500 µL was injected per chromatography run, containing an average of 7-10 mg of protein. Before injection, the column was equilibrated with 50 mL of running buffer composed of 50 mM Tris-HCl pH 7.5, 150 mM NaCl, 1 mM EDTA, 0.3% CHAPS, 10% glycerol and protease inhibitors, and the chromatography run was carried out at 4^{o}C and a flow rate of 0.25 mL/min. After injection, eluted proteins were collected using an automated sample collector (Frac-950, GE Healthcare) in 1 mL fractions. Elution was carried out for 32.5 mL (1.3 column volumes). Fractions were pooled according to the chromatogram (fractions A-F) and concentrated to ~ 200 µL in Amicon-Ultra 4 mL concentrators (Thermo Fisher Scientific, Waltham, MA). The protein content of the concentrated fractions was determined using the BCA protein assay kit.

Native PAGE western blots

Concentrated fractions from SEC (50-100 µg) were applied and run on 4-16% Bis-Tris native gels (Thermo Fisher Scientific, Waltham, MA) according to manufacturer's instructions. Native gels were fixed for 15 min in 40% methanol, 10% acetic acid solution. After fixation, gels were denatured by shaking in 50 mM Tris-HCl buffer, pH 6.8, containing 2% SDS and 50 mM DTT for 45 min at room temperature. This step is required as the BAD antibody used in these blots

does not recognize BAD epitopes in their native conformation. Denatured native gels were transferred onto PVDF membranes and probed with BAD or BCL-X_L antibody as described above for regular western blots.

BAD immunoaffinity capture

BAD-containing complexes were immunocaptured using an immunoaffinity column generated by cross-linking a BAD antibody (Yang et al., 1995) with Protein A-Sepharose CL-4B beads (GE Healthcare). Briefly, beads and antibody were incubated overnight at 4°C at a final concentration of 2 mg anti-BAD antibody per mL of beads. The mix was washed with 20 mM Tris-HCl buffer, pH 7.5, containing 137 mM NaCl, 10% glycerol, 2 mM EDTA, 0.5% CHAPS, protease inhibitors and phosphatase inhibitors. After another wash with 0.2 M sodium borate pH 9.0, the beads-antibody mix was cross-linked with dimethyl pimelimidate dihydrochloride (DMP) dissolved in 20 mM sodium borate for 30 min at room temperature. Cross-linked antibody-beads were washed once with 0.2 M sodium borate and the reaction was quenched with 0.2 M ethanolamine, pH 8, for 2 hr at room temperature followed by 2 washes with 150 mM NaCl, 10 mM sodium phosphate, pH 7.4, containing 50% glycerol. Size exclusion fractions were pre-cleared with non-crosslinked Sheparose A beads for 30 min at 4°C followed by overnight incubation with the antibody-beads resin at 4°C. The immunocaptured complexes and resin were washed 3 times with the Tris buffer above and eluted with 0.2 M glycine buffer, pH 2.6, and eluates were neutralized with 125 mM Tris buffer, pH 8.0. Samples were either denatured with 4x Laemmli buffer for western blot analysis or precipitated with tricloroacetic acid (TCA) and air dried for LC-MS/MS analysis.

Chemical cross-linking and BAD immunoprecipitation

Size exclusion fractions were subjected to chemical cross-linking using bis(2-[succinimidoxy-carbonyloxy]ethyl)sulfone (BSOCOES) (Thermo Fisher Scientific, Waltham, MA). For these experiments, cortical lysates were fractionated with an amine-free lysis buffer containing 25 mM HEPES pH 7.4, 120 mM NaCl, 1.5 mM $MgCl_2$ and 0.2% CHAPS. BSOCOES was solubilized with DMSO immediately before use, and then added to concentrated SEC fractions

to a final concentration of 3.75 mM. The cross-linking reaction was carried out at 4°C for 2 hr and subsequently quenched with 50 mM Tris-HCl solution, pH 8.0, for 15 min at 4°C. Cross-linked samples were diluted in amine-free lysis buffer containing protease inhibitors and phosphate inhibitors. The volume of reaction for BAD-immunoprecipitation (IP) was adjusted to 500 µL with 20 mM Tris, 137 mM NaCl, 1.5 mM MgCl2, 1mM EDTA and 0.2% CHAPS. Cross-linked fractions were then incubated overnight with an anti-BAD antibody (Yang et al., 1995) at 4°C, Protein G magnetic beads were subsequently added followed by 1 hr incubation at 4°C. Immunoprecipitated samples were washed twice with the Tris buffer as above, also containing 1% NP-40 and 0.1% SDS, before denaturing with NuPAGE® 4X LDS Sample Buffer (Thermo Fisher Scientific, Waltham, MA) for 3 min at 90°C. Samples were analyzed by western blot and SDS-PAGE gel bands containing the complexes of interest were cut and subjected to LC-MS/MS analysis.

Protein digestion and isobaric TMT labeling

Gel bands were dehydrated with acetonitrile and dried. BAD-immunoaffinity eluates were precipitated with TCA and air dried. Dried samples were ressuspended in 50 mM ammonium bicarbonate (pH 8.5) containing 500 ng of sequencing-grade trypsin (Promega, Madison, WI), and incubated for 8 hr at 37°C. Digested samples were then loaded onto StageTips (Thermo Fisher Scientific, Waltham, MA) and desalted (Rappsilber et al., 2007). Peptides were eluted with 50% acetonitrile, 5% formic acid, dried using a Speed-Vac apparatus, and resuspended in 25 µl of HEPES, pH 8.5. Peptides were labeled with 6-plex tandem mass tag (TMT) reagents, TMT-126, TMT-127, TMT-128, TMT-129, and TMT-130 (Thermo Fisher Scientific, Waltham, MA). After 1 hr of incubation at room temperature, the reaction was quenched with hydroxylamine and acidified with formic acid to pH ~2. TMT labeled peptides were combined, desalted by StageTips, dried and resuspended in 10 µl of 1% formic acid.

LC-MS/MS parameters

All spectra were acquired using an Oribtrap Fusion mass spectrometer (Thermo Fisher Scientific, Waltham, MA) in line with an Easy-nLC 120 (Thermo Fisher Scientific, Waltham, MA) ultra-high pressure liquid chromatography (UHPLC) pump. TMT-labeled peptides (4 µL) were separated onto a 75 µM inner diameter column containing 1 cm of Magic C4 resin (5 µm, 100 Å, Michrom Bioresources) followed by 35 cm of Sepax Technologies GP-C18 resin (1.8 µm, 120 Å) with a gradient consisting of 4–30% (ACN, 0.125% FA) over 90 min at ~250 nl/min. For all LC-MS/MS experiments, the mass spectrometer was operated in the data-dependent mode where the MS1 spectra was set at a resolution of 120,000, with an AGC target of 150,000 and a max injection time of 100 ms. The ten most intense ions were selected for MS2. MS1 precursor ions were excluded using a dynamic window (60 seconds +/- 10 ppm) and the MS2 precursors were isolated with a quadrupole mass filter set to a width of 0.5 DA. For MS3 based TMT quantitation, MS2 spectra were collected at an AGC of 4000, max injection time of 150 ms, and CID collision energy set at 35%. MS3 spectra were acquired in the Orbitrap parameters where the HCD collision energy was increased to 55%. Synchronous-precursor-selection (SPS) was enabled to include up to six MS2 fragment ions for the MS3 spectrum.

Data dissemination and MS2 spectra assignment

A compendium of in-house software was used to convert.raw files to mzXML format that adjusted monoisotopic *m/z* measurements and corrected erroneous peptide charge state assignments. Assignment of MS2 spectra was performed using the SEQUEST algorithm (Eng et al., 1994). All searches utilized the mouse UniProt database (downloaded 6/10/2016), where reversed protein sequences and known contaminants (keratins, etc.) were included. SEQUEST searches were performed using a 10 ppm precursor ion tolerance and requiring each peptide's N/C terminus to have tryptic specificity and allowing up to three missed cleavages. An MS spectra assignment false discovery rate (FDR) of less than 1% was achieved by applying the target-decoy database search strategy (Elias and Gygi, 2007).

Determination of TMT reporter ion intensities

For quantification, a 0.03 *m/z* window centered on the theoretical DA value of each reporter ion was utilized for the nearest maximal signal intensity. Reporter ion intensities were adjusted to correct for the isotopic impurities from the different TMT reagents as per manufacturer's specifications. The signal to noise values for all peptides were summed within each TMT channel. For each peptide, a total minimum sum signal to noise value of 200 and an isolation purity greater than 70% was required (McAlister et al., 2014).

Statistical Analysis

Statistical analysis was performed in Graph Pad Prism 6 software. All values are presented as mean ± SEM. Statistical significance was determined using two tailed Student's *t*-test, one-way or two-way analysis of variance (ANOVA) with multiple comparisons. The specific tests used are indicated in each figure legend. Significance indicated by p-values is as follows: n.s, non-significant; *$p < 0.05$; **$p < 0.01$; ***$p < 0.001$.

CHAPTER 3

Dissecting BAD-dependent changes in glucose metabolism using ^{13}C isotopomer analysis

INTRODUCTION

We have previously shown that modulation of mitochondrial fuel handling by BAD in the brain involves the reciprocal utilization of glucose *versus* ketone bodies. BAD phosphorylation on S155 not only stimulates mitochondrial metabolism of glucose but also inhibits ketone body utilization (Gimenez-Cassina et al., 2012). Consequently, BAD deficiency or interference with its phosphorylation as in the *Bad* S155A knockin allele is associated with diminished glucose utilization and a concomitant shift to ketone body metabolism (Gimenez-Cassina et al., 2012). Blunted glucose oxidation in neural cell types derived from *Bad* genetic models may be due to defects in glucose uptake, cytosolic processing, mitochondrial import of glucose-derived pyruvate and its subsequent metabolism in the TCA cycle. The studies described in this chapter were designed to map the specific lesion in glucose metabolism when BAD is modified, as to gain insights into how BAD might alter the branch points at which glucose carbons are metabolized, including the pentose phosphate pathway (PPP), lactate production or entry into the TCA cycle. To this end, we carried out targeted gas chromatography-mass spectrometry (GC-MS)-based metabolomics analyses in primary *Bad* -/- and S155A neurons to quantify the incorporation of glucose-derived carbons into downstream metabolites. Throughout these studies, we used primary cortical neurons derived from control and BAD mutant mice given the well-recognized importance of the cortex as a key region of the brain in the control of seizure initiation and propagation (Bertram, 2009; Kramer and Cash, 2012).

RESULTS

3.1 Assessment of glucose uptake in BAD-deficient primary cortical neurons

BAD-dependent changes in glucose metabolism could stem from altered glucose uptake. To examine this possibility, we performed glucose uptake assays in *Bad* +/+ (WT) and -/- cortical neurons using [^{3}H]-2-deoxy-glucose (DG) (Furukawa et al., 2005; Heidenrich et al., 1989). Upon uptake, [^{3}H]-2-DG is converted to [^{3}H]-2-deoxy-glucose-6-phosphate, [^{3}H]-2-DG-6-P, which cannot be further metabolized. Thus, intracellular [^{3}H]-2-DG-6-P levels measured by liquid scintillation counting in these assays report on glucose uptake. WT and *Bad* -/- neurons had comparable [^{3}H]-2-DG-6-P content (Figure 3.1), indicating that diminished glucose metabolism in the absence of BAD cannot be explained by defects in glucose uptake.

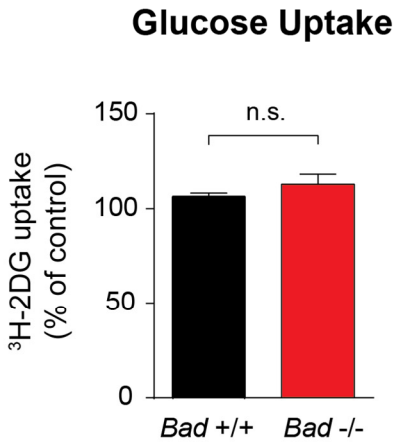

Figure 3.1 Assessment of glucose uptake in BAD-deficient primary cortical neurons

Glucose uptake in WT and *Bad* -/- primary neurons. Cells were treated with [^{3}H]-2-deoxyglucose (^{3}H-2DG, 0.25 µCi/well) for 10 min, and ^{3}H disintegrations per minute (dpm) was measured by liquid scintillation counting. Data are mean ± SEM of 4 independent neuronal cultures derived from 4 embryos (E16-17) per genotype, for which 4 wells per culture were analyzed. n.s., non-significant; two-tailed Student's *t*-test.

3.2 Metabolomics workflow for ^{13}C-glucose tracer analysis in primary cortical neurons derived from *Bad* genetic models

We next optimized conditions for ^{13}C-glucose tracer labeling in primary cortical neurons (see Chapter 2 for experimental details). To ensure highly pure neuronal preparations, neuronal cultures were treated with cytosine arabinoside (AraC) 3 days following isolation [days in vitro (DIV) 3] as previously described (Seibenhener and Wooten, 2012; White et al., 1998). We confirmed the purity of these cultures by immunofluorescence and western blot detection of the neuronal marker β-tubulin III (Tuj1), and ascertained the absence of signal for the glial marker glial fibrillary acid protein (GFAP) (Figure 3.2A). Pilot studies were then performed to determine the optimal labeling conditions for detection of glycolytic and TCA cycle metabolites, including optimal cell number and labeling medium (see Chapter 2 for experimental details).

To determine isotopic steady state, a point when ^{13}C enrichment into a particular metabolite is constant over time, we incubated DIV 5 neurons with a uniformly labeled glucose tracer (U^{13}C-glucose) over a 0-24 hr period and analyzed metabolites using GC-MS (Figure 3.2B). Isotopic steady state varies depending on several parameters, including the metabolite of interest, the particular ^{13}C tracer used, and the size of the metabolite pool (Buescher et al., 2015). We predicted that the above time course would be sufficient for all ^{13}C-labeled species of the metabolites of interest also known as isotopologues to reach isotopic steady state. This reasoning is based on the fact that DIV 5 cortical neurons are likely at metabolic steady state as they are non-dividing and differentiated cells, but have not fully matured into neurons that fire action potentials, a process associated with significant increases in glucose metabolism (Agostini et al., 2016; Buescher et al., 2015; Mergenthaler et al., 2013; Okada and Lipton, 2007).

Overall, these time course studies indicated that neurons rapidly metabolize glucose through glycolysis and the TCA cycle. ^{13}C-enriched glycolytic metabolites such as dihydroxyacetone phosphate (DHAP) and lactate reached isotopic steady state within the first 2 hr of labeling, while labeling of the TCA cycle intermediates such as citrate and malate reached steady state between 4 and 8 hr (Figure 3.2C and Supplementary Figure 3-S1).

Based on these data, all subsequent analyses with U^{13}-glucose tracer were carried out following 8 hr of tracer incubation, a time point at which all isotopologues for metabolites of interest are at isotopic steady state.

Figure 3.2 Metabolomics workflow for U^{13}C-glucose tracer analysis in primary cortical neurons derived from *Bad* genetic models

(**A**) Purity of DIV 5 primary cortical neuronal cultures used throughout these studies as assessed by immunofluorescence (top) of the neuronal marker β-tubulin III (green) and the absence of a signal for the glial marker GFAP (red). DAPI (blue) is used as a nuclear stain. Western blot analysis (bottom) of protein lysates derived from the above neuronal cultures probed with β-tubulin III and GFAP antibodies, while the β-actin signal was used as loading control.

(**B**) Schematic of workflow for U^{13}C-glucose tracer analysis. DIV 5 primary cortical neurons derived from WT and *Bad* genetic models were labeled with 10 mM U^{13}C-glucose tracer for 0-24 hr. At the end of each labeling period, polar metabolites were extracted with 80% methanol and derivatized with MOX and MTBSTFA for GC-MS analysis. Data analysis was carried out initially using the MSD ChemStation software (Agilent Technologies) for peak integration. Mass isotopomer distribution (MID) vectors, also known as mass distribution vectors (MDVs), were determined for each metabolite and corrected for natural abundance using correction matrices as previously described (Nanchen et al., 2007). MDVs express the fractional abundance of each isotopologue normalized to the sum of all possible isotopologues, which equals to 1 or 100% (Buescher et al., 2015). Total pools (peak areas) were also determined for each metabolite.

(**C**) Time-course of ^{13}C enrichment in glycolytic and TCA cycle metabolites in WT and *Bad* -/- neurons labeled with 10 mM U^{13}C-glucose. Data are shown as percentage of ^{13}C incorporation (^{13}C Enrichment) with labeled portion (^{13}C, SUM of M+1…M+n, where n is the number of carbons) in blue and unlabeled portion (^{12}C, M+0) in black. Data are mean ± SEM of cortical neurons derived from 8 embryos (E16) seeded and analyzed in 2 plates per genotype. These experiments were independently repeated in an additional set of cultures derived from 6 embryos. See also Figure 3-S1.

Abbreviations: DHAP: dihydroxyacetone phosphate; MOX: methoxyamine hydrochloride; MTBSTFA: *N*-*tert*-butyldimethylsilyl-*N*-methyltrifluoroacetamide.

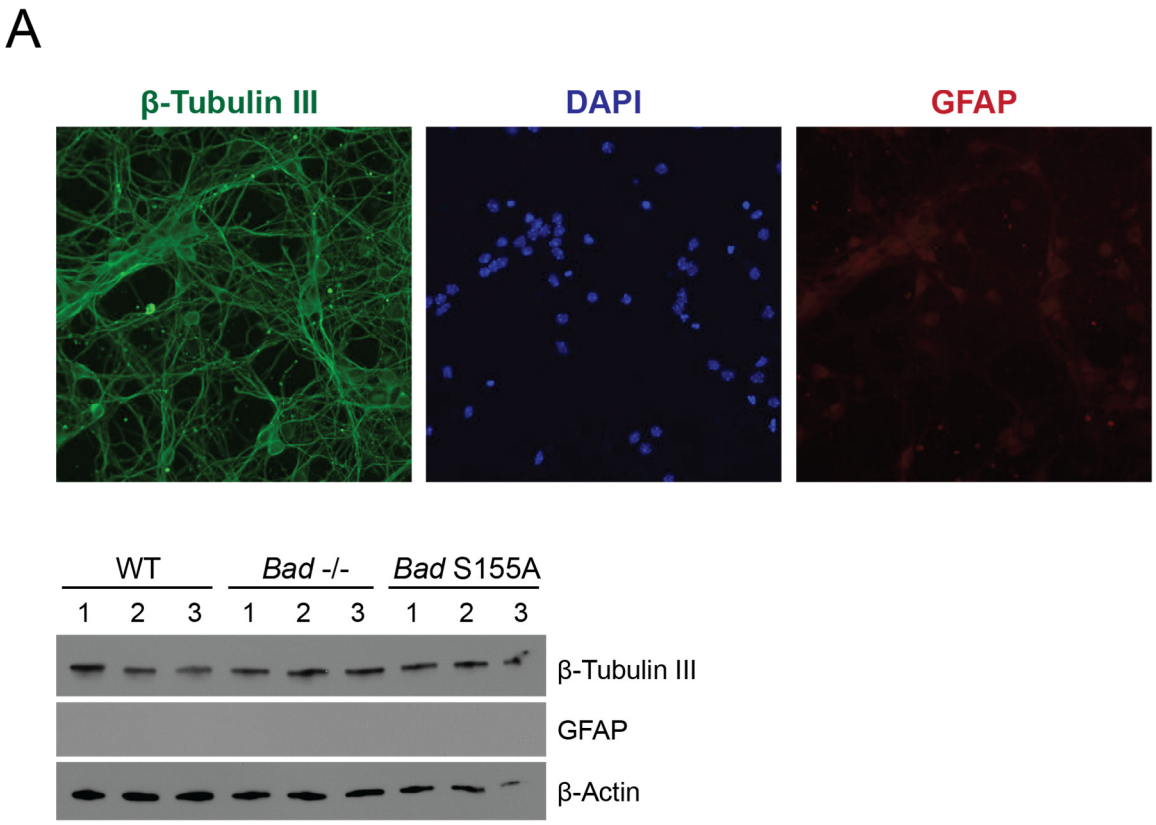
A
β-Tubulin III
DAPI
GFAP
WT
Bad -/-
Bad S155A
1 2 3 1 2 3 1 2 3
β-Tubulin III
GFAP
β-Actin
B
Dissect E16-17 cortices and digest with trypsin
Seed 2.5x10^6 cells in PLL-coated 60 mm dishes
DIV3 neurons Refresh medium and add AraC
DIV 5 neurons Label with 10 mM U13C-glucose for 0-24 hrs
Metabolite extraction with 80% MeOH
CH3ONH2 . HCl
+
Derivatization with MOX and MTBSTFA
Metabolite detection by GC-MS
Data Analysis

Figure 3.2

C

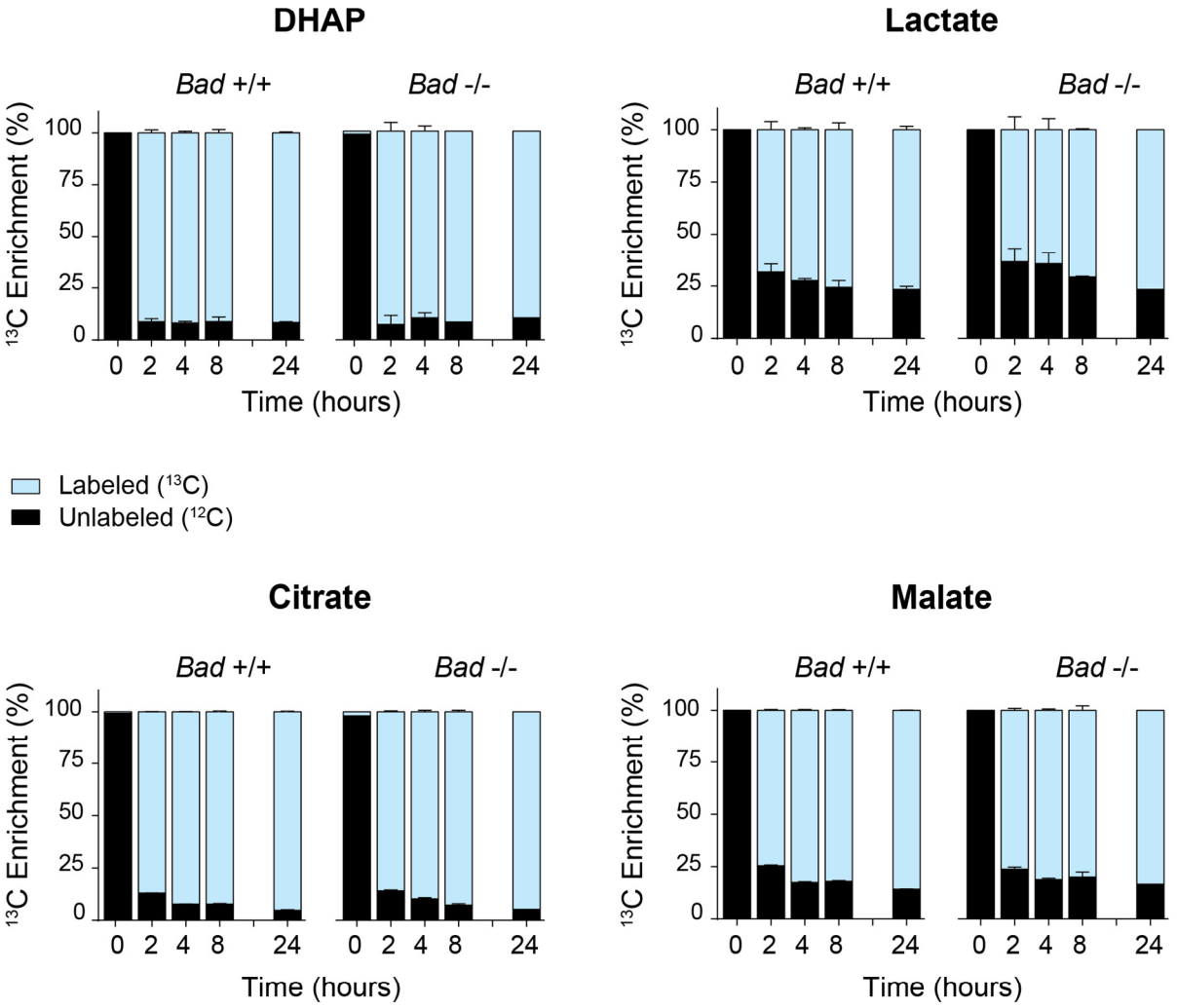

Figure 3.2 (continued)

3.3 Reduced glucose oxidation in *Bad* -/- and S155A neurons maps upstream of the mitochondrial entry of glucose-derived pyruvate

Six-carbon labeled glucose gives rise to 3-carbon labeled glycolytic intermediates downstream of the aldolase (ALD) step, referred to as M+3 isotopologues (Figure 3.3A). The abundances of labeled M+3 isotopologues for DHAP were comparable among the 3 genotypes, while those of 3PG, PEP, pyruvate, and alanine, which is in isotopic equilibrium with pyruvate via alanine aminotransferase (AST), were significantly reduced in *Bad* -/- and S155A neurons compared to WT counterparts (Figure 3.3B). These observations suggest reduced flux through the lower part of the glycolytic pathway. Notably, the total pools of the above metabolites, which reflect the sum of all isotopologues, also followed a similar pattern with significant reduction in 3PG, PEP, pyruvate and alanine and no alterations in DHAP (Table 1). Taken together, these data suggest a BAD-dependent diminution in pyruvate production from glucose, which likely occurs after DHAP synthesis (Figure 3.3A).

Consistent with reduced pyruvate labeling from glucose, incorporation of glucose carbons into TCA cycle intermediates was also lower in *Bad* -/- and S155A neurons. M+3 pyruvate formed from U^{13}C-glucose yields 2-carbon labeled (M+2) acetyl-CoA, which upon condensation with oxaloacetate, produces M+2 citrate in the first round of the TCA cycle (Figure 3.3A). After several turns of the TCA cycle, ^{13}C labeling will appear in more carbons, eventually leading to the appearance of fully labeled TCA cycle species. Our data show a reduction in the levels of the M+2 isotopologues for citrate, succinate, malate and aspartate in *Bad* -/- and S155A neurons (Figure 3.3C). Aspartate is in isotopic equilibrium with oxaloacetate through the transamination reaction catalyzed by aspartate amino transferase (AST), and although oxaloacetate was not detected in our metabolomics platform, its labeling pattern can be inferred from that of aspartate (Figure 3.3A). Interestingly, M+2 α-ketoglutarate and fumarate levels were unaltered (Figure 3.3C), which can be potentially explained by their use in multiple metabolic reactions other than the TCA cycle, which may dilute the ^{13}C label. Another possible explanation is the presence of GlutaMAX in the labeling media, which could serve as a source of unlabeled glutamine that can exchange with glutamate pools and consequently affect α-ketoglutarate labeling (Buescher et al., 2015).

Beyond reduced M+2 isotopologues, which are produced in the first turn of the TCA cycle, M+3 to M+6 citrate and M+3 to M+4 succinate, malate and aspartate, which are produced upon subsequent turn of the TCA cycle, were also significantly reduced in *Bad* -/- and S155A neurons (Figure 3.3C). These data indicate an overall reduction in the flux of glucose-derived pyruvate in the TCA cycle. Furthermore, the total metabolite pool levels for citrate, succinate, fumarate, malate and aspartate were also significantly decreased (Table 1).

Taken together, the above changes in ^{13}C incorporation of glucose-derived carbons into TCA cycle intermediates corroborate our previous observation that *Bad* -/- and S155A neurons have reduced mitochondrial oxygen consumption in response to glucose (Gimenez-Cassina et al., 2012). Citrate, succinate and malate all feed coupled reactions, where NADH or $FADH_2$ are produced and supply the electron transport chain (ETC) with reducing equivalents. Imbalances in the levels of glucose-derived TCA cycle intermediates can, therefore, affect the availability of reducing equivalent required for electron transport and oxygen consumption. A summary of the changes in glucose metabolism observed in *Bad* -/- and S155A neurons upon U^{13}C-glucose labeling is shown in Figure 3.3A as orange and blue arrows denoting no change and reduction, respectively.

Figure 3.3 Reduced glucose oxidation in *Bad* -/- and S155A neurons maps upstream of mitochondrial entry of glucose-derived pyruvate

(**A**) Schematic representation of glycolysis and TCA cycle pathways. $U^{13}C$-glucose is represented by 6 green beads and the downstream labeling patterns for glycolytic and TCA intermediates are also shown. ^{13}C-labeled carbons are in green and unlabeled carbons are in white. Only the first turn of the TCA cycle is represented. Arrows indicating no alteration (↔) or decrease (↓) summarize data shown in (B) and (C) below in terms of metabolite changes in *Bad* -/- and S155A neurons labeled with $U^{13}C$-glucose.

(**B-C**) Intracellular metabolite levels of glycolytic (B) and TCA cycle (C) metabolites in WT, *Bad* -/- and S155A neurons labeled with 10 mM $U^{13}C$-glucose for 8 hr. Data are mean ± SEM of cortical neurons derived from 6 embryos (E16) seeded and analyzed in 3 plates per genotype. These experiments were independently repeated in an additional set of cultures derived from 6 embryos. Asterisks compare the M+3 and M+2 metabolite abundances in (B) and (C), respectively. *p < 0.05; **p < 0.01; ***p < 0.001; n.s, non-significant; two-way ANOVA with multiple comparisons.

Abbreviations: 3PG: 3-phosphoglycerate; ALD: fructose 1,6-bisphosphate aldolase; ALT: alanine aminotransferase; AST: aspartate aminotransferase; DHAP: dihydroxyacetone phosphate; ENO: enolase; GAPDH: glyceraldehyde 3-phosphate dehydrogenase; GPI: glucose-6-phosphate isomerase; IDH: isocitrate dehydrogenase; LDH: lactate dehydrogenase; MDH: malate dehydrogenase; PC: pyruvate carboxylase; PDH: pyruvate dehydrogenase; PEP: phospho-enolpyruvate. HK: hexokinase; PFK: phosphofructokinase; PGAM: phosphoglycerate mutase; PGK: phosphoglycerate kinase; PKM: pyruvate kinase; SDH: succinate dehydrogenase; TPI: triose-phosphate isomerase.

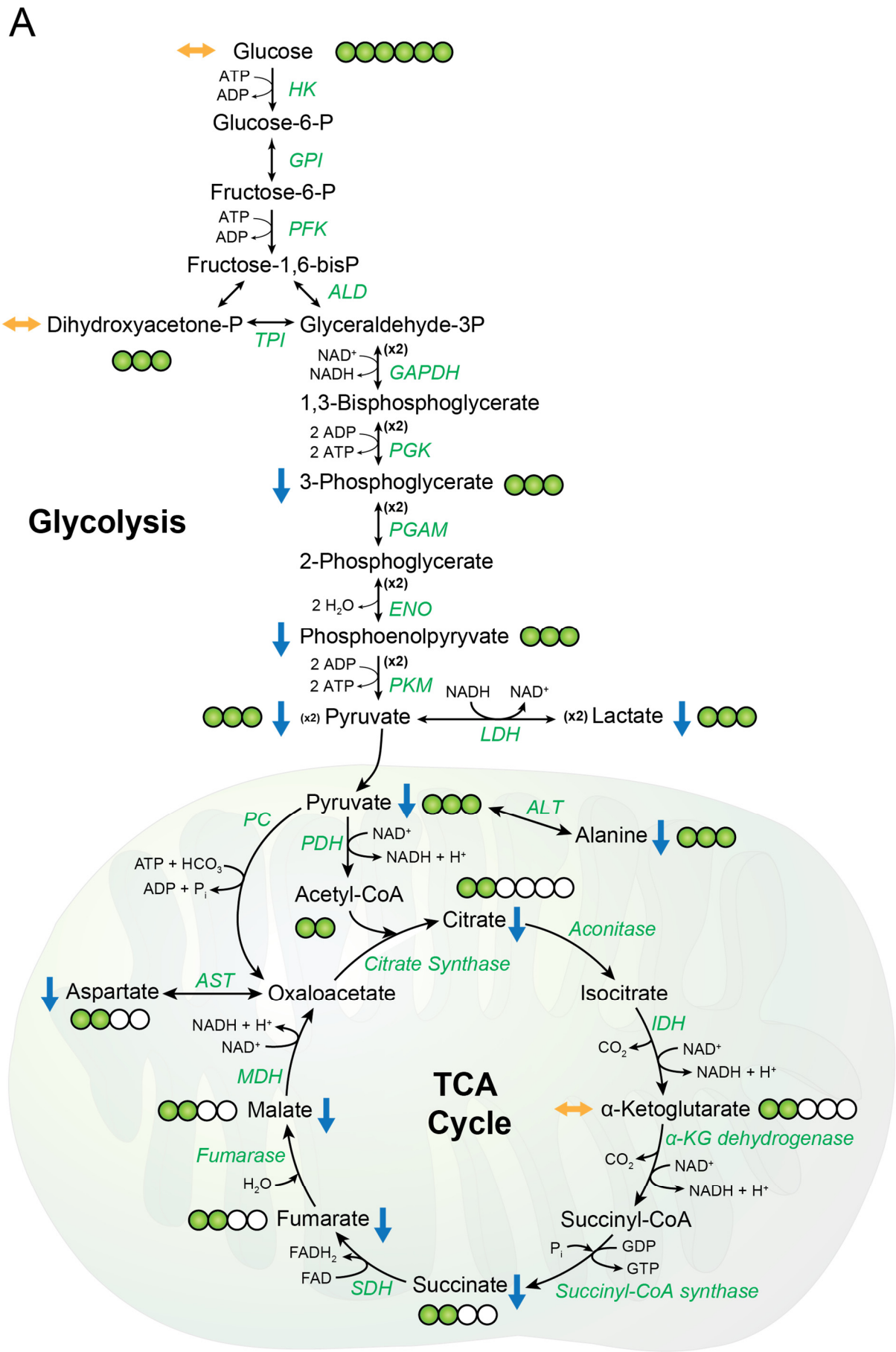
A
Glucose
ATP
ADP
HK
Glucose-6-P
GPI
Fructose-6-P
ATP
ADP
PFK
Fructose-1,6-bisP
ALD
Dihydroxyacetone-P
TPI
Glyceraldehyde-3P
NAD+
NADH
(x2)
GAPDH
1,3-Bisphosphoglycerate
2 ADP
2 ATP
(x2)
PGK
3-Phosphoglycerate
Glycolysis
(x2)
PGAM
2-Phosphoglycerate
2 H2O
(x2)
ENO
Phosphoenolpyryvate
2 ADP
2 ATP
(x2)
PKM
NADH
NAD+
(x2) Pyruvate
LDH
(x2) Lactate
Pyruvate
PC
PDH
NAD+
NADH + H+
ALT
Alanine
ATP + HCO3
ADP + Pi
Acetyl-CoA
Citrate
Aconitase
Citrate Synthase
AST
Aspartate
Oxaloacetate
Isocitrate
NADH + H+
NAD+
MDH
IDH
CO2
NAD+
NADH + H+
TCA
Cycle
Malate
α-Ketoglutarate
α-KG dehydrogenase
Fumarase
CO2
NAD+
NADH + H+
H2O
Fumarate
Succinyl-CoA
FADH2
FAD
SDH
Pi
GDP
GTP
Succinate
Succinyl-CoA synthase

Figure 3.3

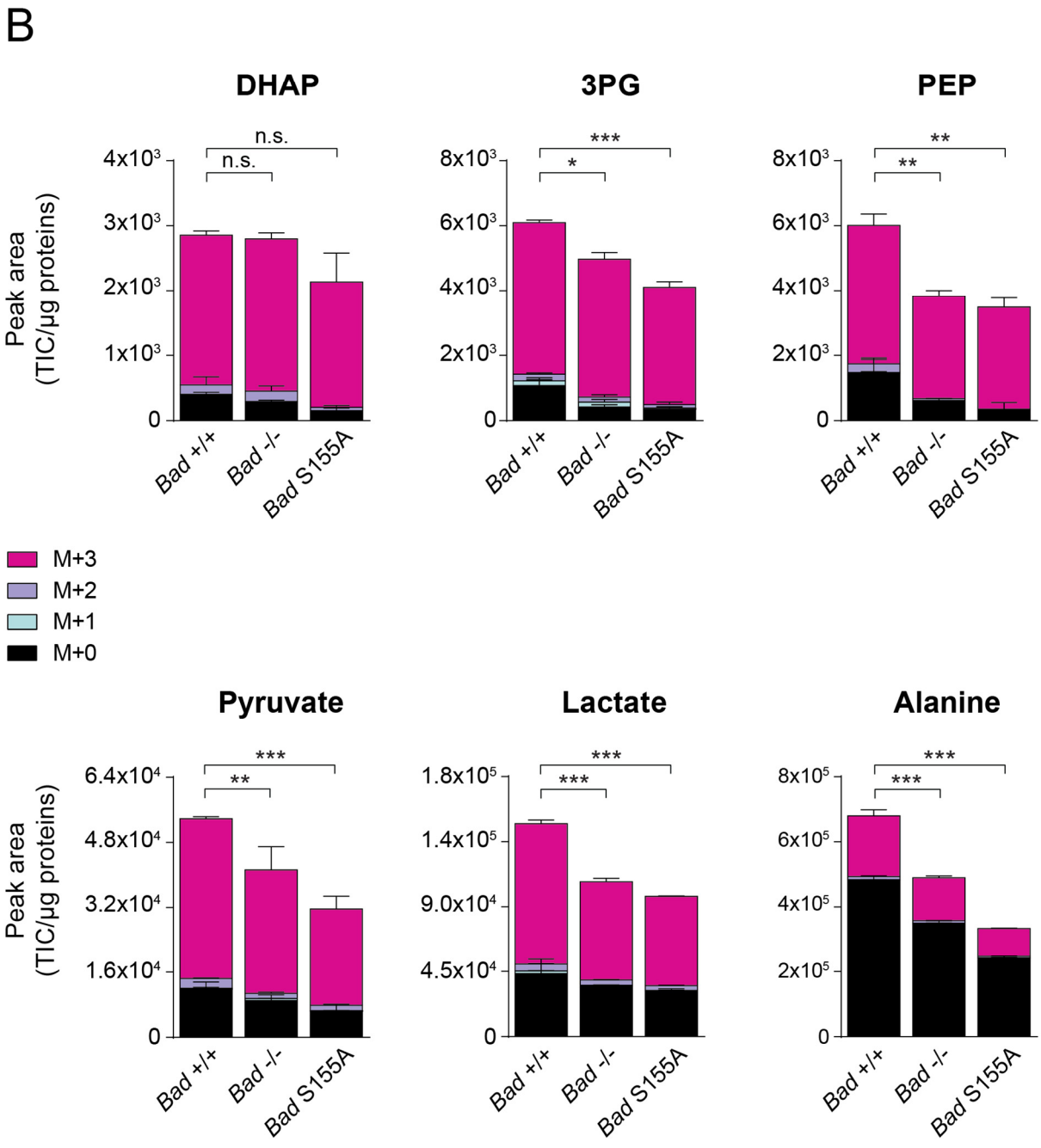

Figure 3.3 (continued)

C

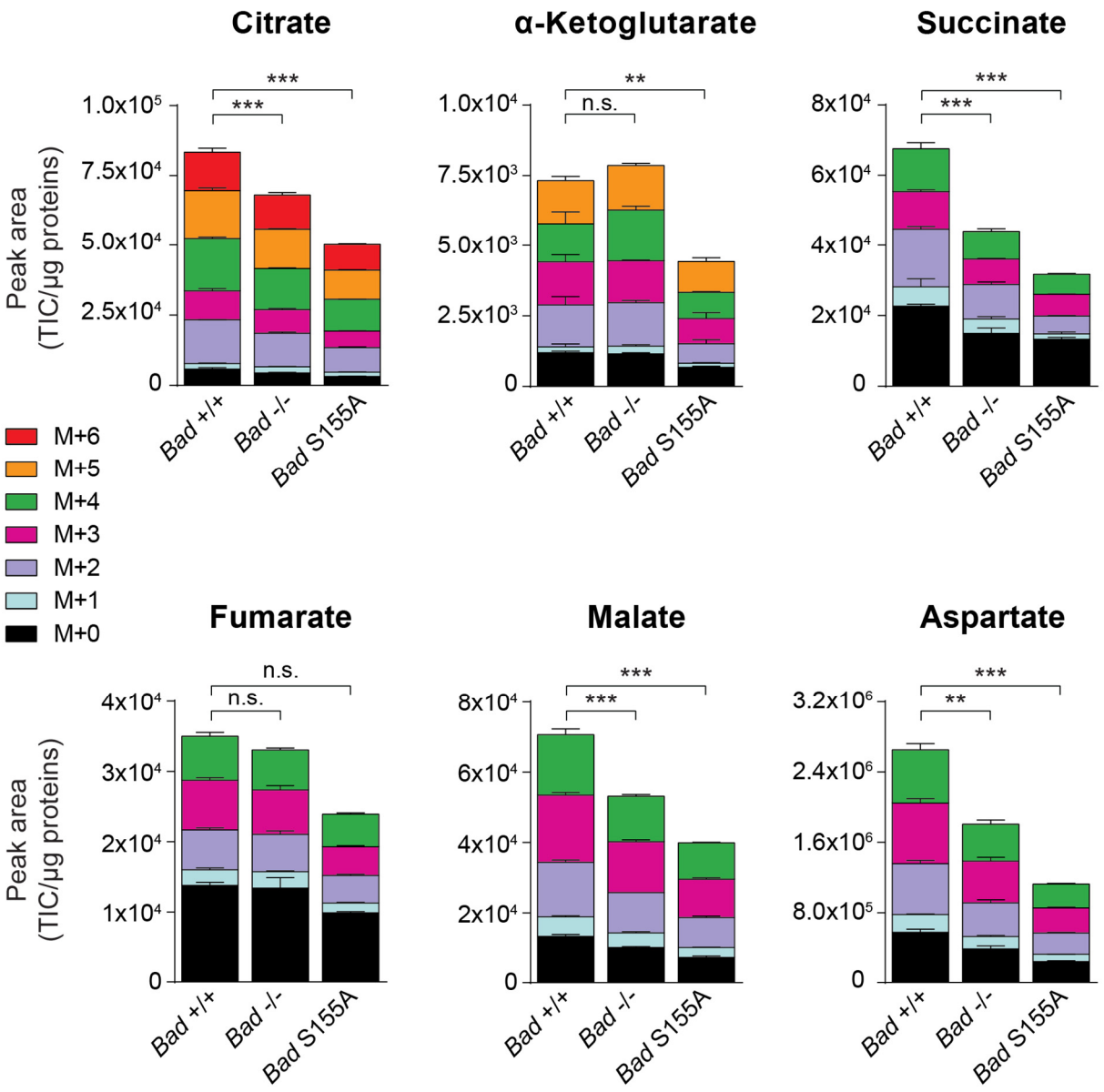

Figure 3.3 (continued)

Table 1 Summary of fold change (FC) relative to WT of total metabolite pools in *Bad* -/- and S155A neurons labeled with U^{13}C-glucose

Total metabolite pools were determined by the sum of peak areas of all possible isotopologues for each indicated metabolite. Results are presented as fold change (FC) of total metabolite pools in *Bad* -/- and S155A neurons relative to WT control. Data are mean FC ± SEM of pooled metabolite measurements from two independent neuronal cultures, each derived from 6 embryos (E16) seeded and analyzed in 3 plates per genotype. *p < 0.05; **p < 0.01; ***p < 0.001; n.s., non-significant; one-way ANOVA with multiple comparisons.

Abbreviations: 3PG: 3-phosphoglycerate; DHAP: dihydroxyacetone phosphate; PEP: phosphoenolpyruvate.

Metabolite	Mean ± SEM *Bad* -/- (FC of WT)	p value	Mean ± SEM *Bad* S155A (FC of WT)	p value
Intracellular				
DHAP	0.979 ± 0.070	n.s.	0.967 ± 0.180	n.s.
3PG	0.624 ± 0.081	**	0.570 ± 0.053	**
PEP	0.663 ± 0.078	*	0.625 ± 0.120	*
Pyruvate	0.703 ± 0.066	**	0.555 ± 0.030	***
Lactate	0.819 ± 0.077	n.s.	0.718 ± 0.081	n.s.
Alanine	0.729 ± 0.040	***	0.575 ± 0.021	***
Citrate	0.753 ± 0.055	***	0.650 ± 0.010	***
α-Ketoglutarate	0.943 ± 0.221	n.s.	0.721 ± 0.062	n.s.
Succinate	0.628 ± 0.038	***	0.530 ± 0.009	***
Fumarate	0.830 ± 0.048	**	0.740 ± 0.027	***
Malate	0.757 ± 0.031	***	0.641 ± 0.025	***
Aspartate	0.585 ± 0.049	**	0.477 ± 0.015	***
Secreted				
Pyruvate	0.966 ± 0.019	n.s.	0.916 ± 0.034	n.s.
Lactate	0.802 ± 0.063	n.s.	0.871 ± 0.092	n.s.
Alanine	0.754 ± 0.067	n.s.	0.815 ± 0.080	n.s.

3.4 Effect of BAD modifications on the levels of secreted metabolites

To determine any potential changes in glucose-derived secreted metabolites in BAD mutant neurons, we similarly analyzed the media collected from the above glucose labeling experiments. Extracellular M+3 pyruvate and M+3 alanine levels were comparable among the 3 genotypes, while secreted M+3 lactate levels were reduced in *Bad* -/- and S155A neurons, analogous to the intracellular M+3 lactate levels. However, the total metabolite pools for all of these secreted metabolites were unchanged when compared to WT (Table 1). Taken together, these data indicate that the diminution in intracellular glucose-derived metabolites cannot be explained by changes in their secretion to the extracellular media.

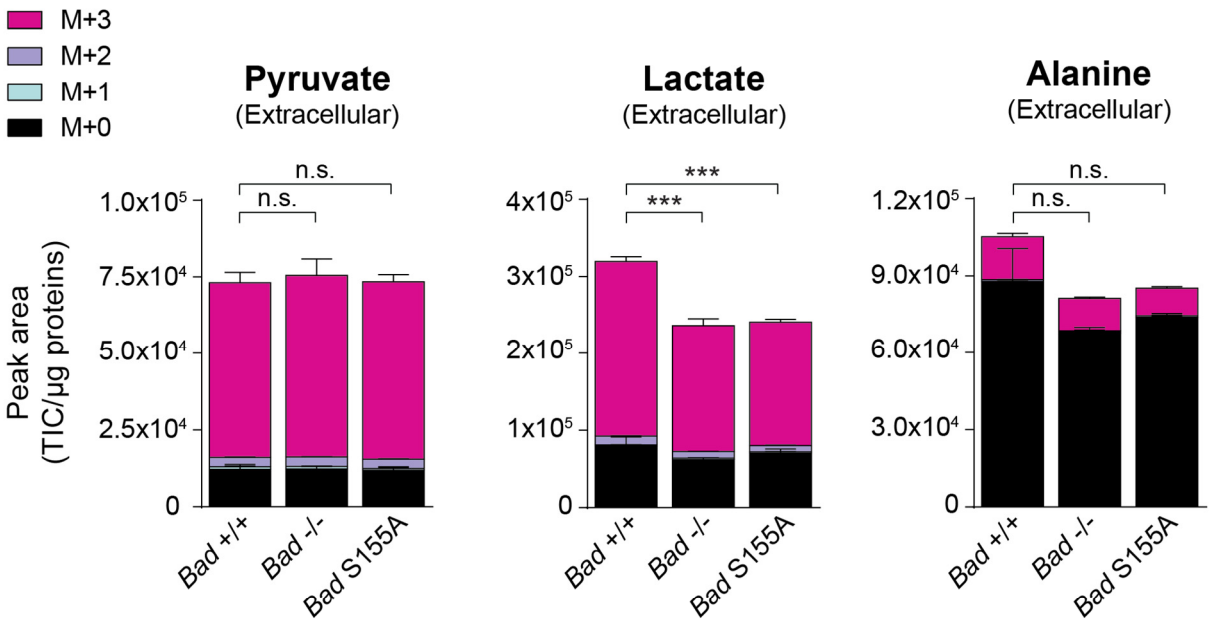

Figure 3.4 Effect of BAD mutations on the levels of secreted glucose-derived metabolites

Extracellular levels of secreted pyruvate, lactate and alanine following labeling of WT, *Bad* -/- and S155A neurons with 10 mM $U^{13}C$-glucose for 8 hr. Data are mean ± SEM of cortical neurons derived from 6 embryos (E16) seeded and analyzed in 3 plates per genotype. These experiments were independently repeated in an additional set of cultures derived from 6 embryos. Asterisks compare the M+3 levels of the indicated metabolite pools. ***p < 0.001; n.s, non-significant; two-way ANOVA with multiple comparisons.

3.5 Mitochondrial pyruvate entry is not affected by BAD mutations

The above tracer studies map BAD-dependent changes in glucose oxidation to cytosolic processing of glucose in the lower half of the glycolytic pathway, culminating in diminished glucose-derived pyruvate available for mitochondrial oxidation. To definitively determine whether changes in mitochondrial pyruvate entry and processing contribute to lower glucose oxidation in BAD mutant neurons, we labeled *Bad* -/- neurons with $U^{13}C$-pyruvate. As these experiments were carried out in the absence of glucose, which can affect the health/survival of neuronal cultures, we purposely chose a shorter labeling period of 2 hr instead of 8 hr. We then measured the incorporation of pyruvate-derived carbons into the TCA cycle intermediates. We found that the levels of labeled M+2 citrate, succinate and aspartate isotopologues, which were reduced in *Bad* -/- neurons upon glucose labeling (Figure 3.3C), were comparable among genotypes after pyruvate labeling (Figure 3.5A). Moreover, the total pools of these metabolites were also unaltered in *Bad* -/- neurons.

The above pyruvate tracing studies indicate that reduced mitochondrial glucose handling and mitochondrial respiration on glucose in BAD mutant neurons cannot be explained by changes in pyruvate processing in the TCA cycle. This conclusion is further consistent with independent measurements of pyruvate dehydrogenase (PDH) activity in the absence of BAD. PDH, which converts pyruvate to acetyl-CoA, initiates the oxidative arm of mitochondrial pyruvate processing. PDH activity was comparable in mitochondria isolated from WT and *Bad* -/- cortices (Figure 3.5B). Overall, these data rule out aberrations in the mitochondrial handling of pyruvate per se as an explanation for reduced entry of glucose carbons in the TCA cycle in BAD mutant neurons.

Figure 3.5 Mitochondrial pyruvate entry is not affected by BAD mutations

(**A**) Intracellular levels of TCA cycle metabolites and their corresponding isotopologues (M+0, …, M+6) following labeling of WT and *Bad* -/- neurons with 5 mM $U^{13}C$-pyruvate for 2 hr. Data are mean ± SEM of cortical neurons derived from 4 embryos (E16) seeded and analyzed in 2 plates per genotype. Comparisons for M+2 isotopologue levels are shown. n.s, non-significant; two-tailed Student's *t*-test.

(**B**) PDH activity in mitochondria isolated from WT and *Bad -/-* cortices using an immune-capture-based enzyme activity assay (MitoSciences, Eugene, OR). Data are presented as mean ± SEM of cortices from n=7 mice per genotype analyzed in 2 technical replicates. n.s., non-significant; two-tailed Student's *t*-test.

A

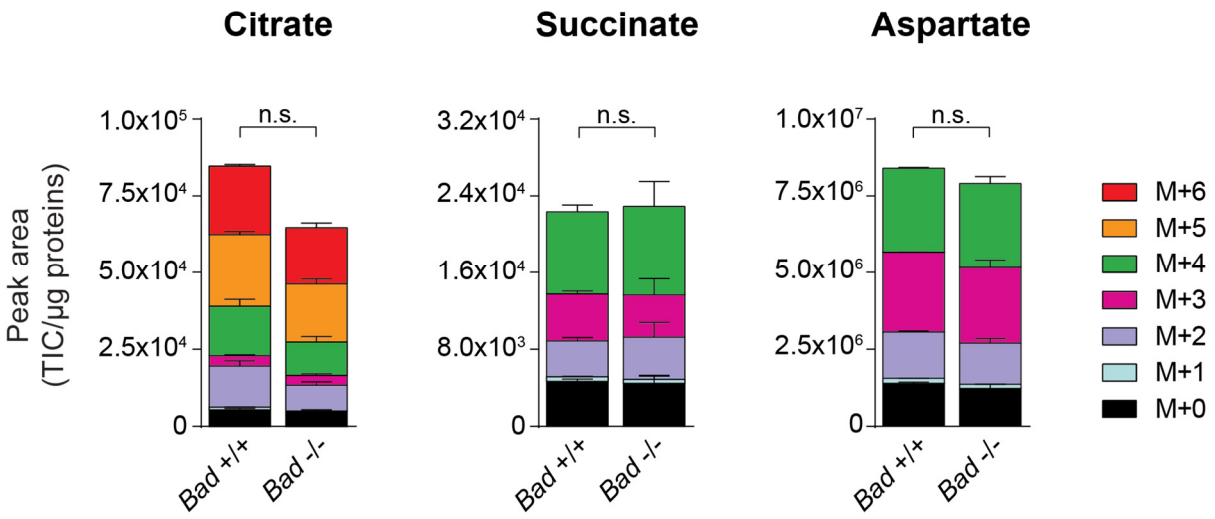
Citrate
Succinate
Aspartate
Peak area
(TIC/µg proteins)
1.0x10⁵
7.5x10⁴
5.0x10⁴
2.5x10⁴
0
3.2x10⁴
2.4x10⁴
1.6x10⁴
8.0x10³
1.0x10⁷
7.5x10⁶
5.0x10⁶
2.5x10⁶
n.s.
Bad +/+
Bad -/-
M+6
M+5
M+4
M+3
M+2
M+1
M+0

B

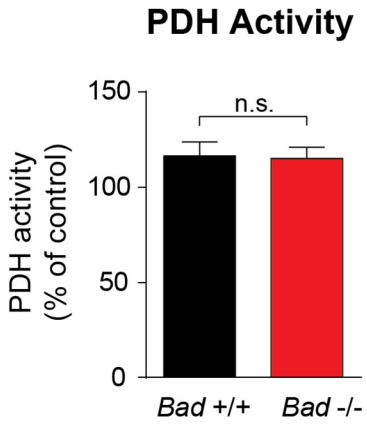
PDH Activity
PDH activity
(% of control)
150
100
50
0
n.s.
Bad +/+
Bad -/-

Figure 3.5

DISCUSSION

Using primary neuronal cultures derived from *Bad* genetic models and $U^{13}C$-glucose tracing, we have found that glycolytic metabolism, specifically the lower portion of the pathway post DHAP production, is diminished in BAD mutant cells. This leads to significantly lower entry and incorporation of glucose-derived carbons in the TCA cycle. BAD-dependent alterations in glycolysis do not originate from changes in glucose uptake or secretion of metabolites such as lactate, pyruvate and alanine. Bypassing glycolysis by directly supplying the TCA cycle with pyruvate further confirmed that the glycolytic lesion in *Bad* -/- and S155A neurons is upstream of pyruvate entry and processing in the TCA cycle. These observations also rule out any pleiotropic effects of BAD modifications on mitochondrial processing of fuel-derived carbons per se.

While our studies narrowed down the BAD-dependent lesion in glucose handling to the lower part of glycolysis, the exact enzymatic step or particular regulatory mechanism that might bring about these changes requires further investigation. Enzyme-specific alterations in metabolic pathways often manifest in altered mass isotopomer distributions of corresponding metabolites (Cardaci et al., 2015; DeNicola et al., 2015; Metallo et al., 2012; Montal et al., 2015; Vincent et al., 2015; Yang et al., 2014). Our data indicate significant diminution of glucose-derived pool sizes for 3PG, PEP, pyruvate, citrate, succinate, malate and aspartate without changes in mass isotopomer distributions (Figures 3.3 B-C and Table 1). These findings are most consistent with overall reduction of glycolytic flux without pinpointing a singular enzymatic step.

How can an overall reduction in glycolytic flux be explained in the absence of changes at a single enzymatic step? Several scenarios may be at play in this context including: (i) diversion of glycolytic intermediates to side reactions, (ii) changes in cytosolic redox balance that limit NAD^+ regeneration and/or availability for glycolysis to proceed, and (iii) simultaneous reduction in the activity of several glycolytic enzymes as in altered transcriptional and/or post-transcriptional regulatory pathways or signaling mechanisms that may lead to programmatic

reduction in glycolysis (Faubert et al., 2014). Side reactions downstream of the DHAP step [scenario (i) above] could include diversion of 3PG to *de novo* serine biosynthesis or glyceraldehyde-3P to the pentose phosphate pathway (Supplementary Figure 3-S2). These possibilities can be directly and rigorously tested by interrogating the enrichment of glucose-derived carbons in serine and pentose phosphate pathway metabolites using $U^{13}C$-glucose and [1,2-$^{13}C_2$]-glucose tracers, respectively (Ahn and Antoniewicz, 2013; Pacold et al., 2016; Possemato et al., 2011). Mechanisms that might reduce availability of cytosolic NAD^+ [scenario (ii) above] include, but are not limited to, changes in the activity of glycerol-phosphate shuttle (GPS), malate-aspartate shuttle (MAS) or lactate dehydrogenase (LDH) (Lewis et al., 2014; McKenna et al., 2006) (Supplementary Figure 3-S2). By increasing the cytosolic NAD^+ to NADH ratio, GPS, MAS and LDH can help sustain glycolysis. Both GPS and MAS have cytosolic and mitochondrial components that collectively function to transfer an electron from NADH to mitochondria, leading to regeneration of cytosolic NAD^+ (Supplementary Figure 3-S2). While the expression and relative predominance of MAS *versus* GPS in neurons has been debated, pharmacologic evidence as well as gene expression data indicate that both shuttles are present and relevant in neurons (McKenna et al., 2006). Our preliminary data indicate reduced NAD^+ to NADH ratio in BAD mutant neurons, which is further consistent with overall reduction of glycolytic flux in these cells (data not shown). The precise molecular underpinning of this potential BAD-dependent alteration in redox balance, including the activity of GPS and MAS, requires further investigation. An intriguing question for future studies is whether any biochemical explanation for diminished glucose flux in *Bad* -/- and S155A neurons might sufficiently explain the concomitant increase in ketone body utilization in these cells.

While the aforementioned scenarios may help narrow down the BAD-specific effect on glycolysis, distinguishing between them will be greatly aided by the identification of specific and direct BAD-interacting proteins in the cortex. This latter point is the subject of the work described in Chapter 4.

Figure 3-S1 Time course of glucose-derived ^{13}C enrichment in glycolytic and TCA cycle metabolites

(**A-B**) Time-course of ^{13}C enrichment in glycolytic (A) and TCA cycle (B) metabolites in WT and *Bad* -/- neurons labeled with 10 mM U^{13}C-glucose for 0, 2, 4, 8, and 24 hr. Data are shown as percentage of ^{13}C incorporation (^{13}C Enrichment) over time in M+0 and M+3 isotopologues for glycolytic intermediates (A) and for M+0, M+2, M+3 and M+4 isotopologues for TCA cycle intermediates (B). Data are mean ± SEM of cortical neurons derived from 8 embryos (E16) seeded and analyzed in 2 plates per genotype. These experiments were independently repeated in an additional set of cultures derived from 6 embryos.

Abbreviations: 3PG: 3-phosphoglycerate; DHAP: dihydroxyacetone phosphate; PEP: phosphoenolpyruvate.

A

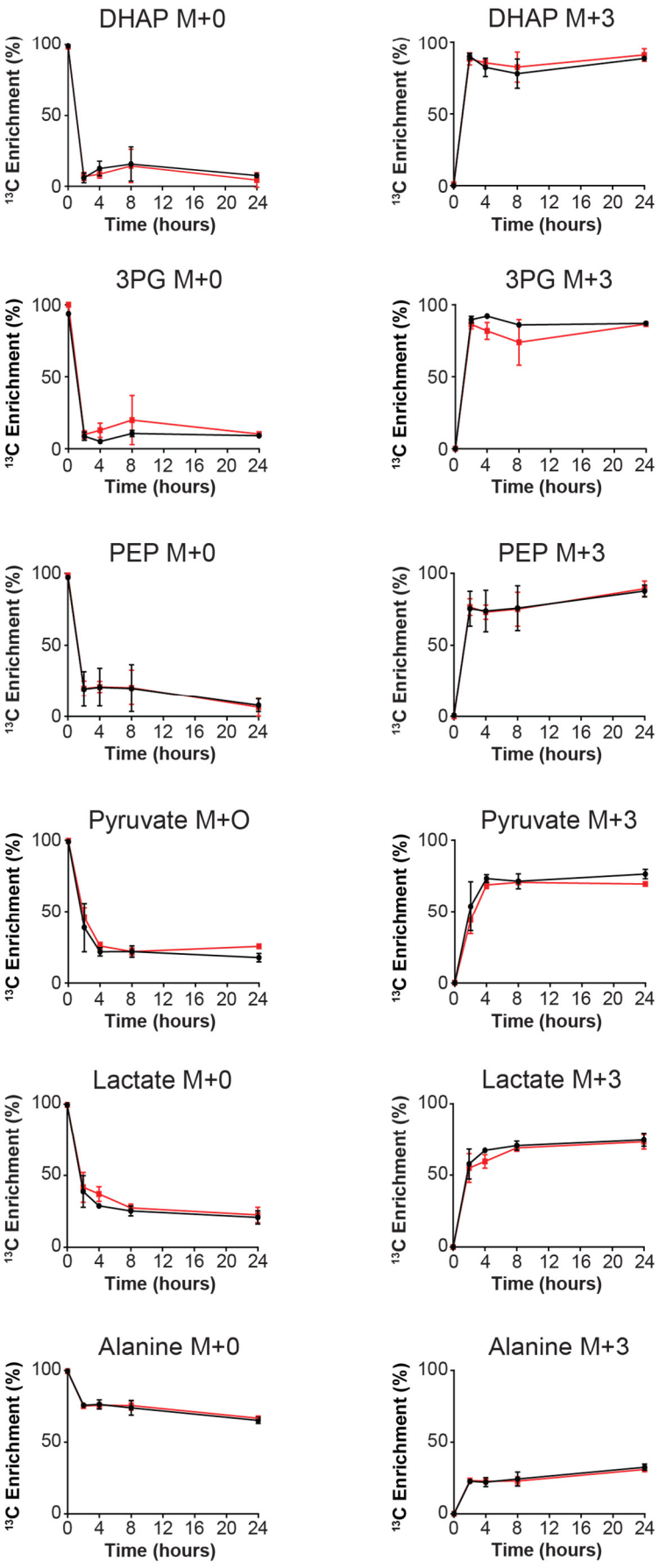

Supplementary Figure 3-S1

B

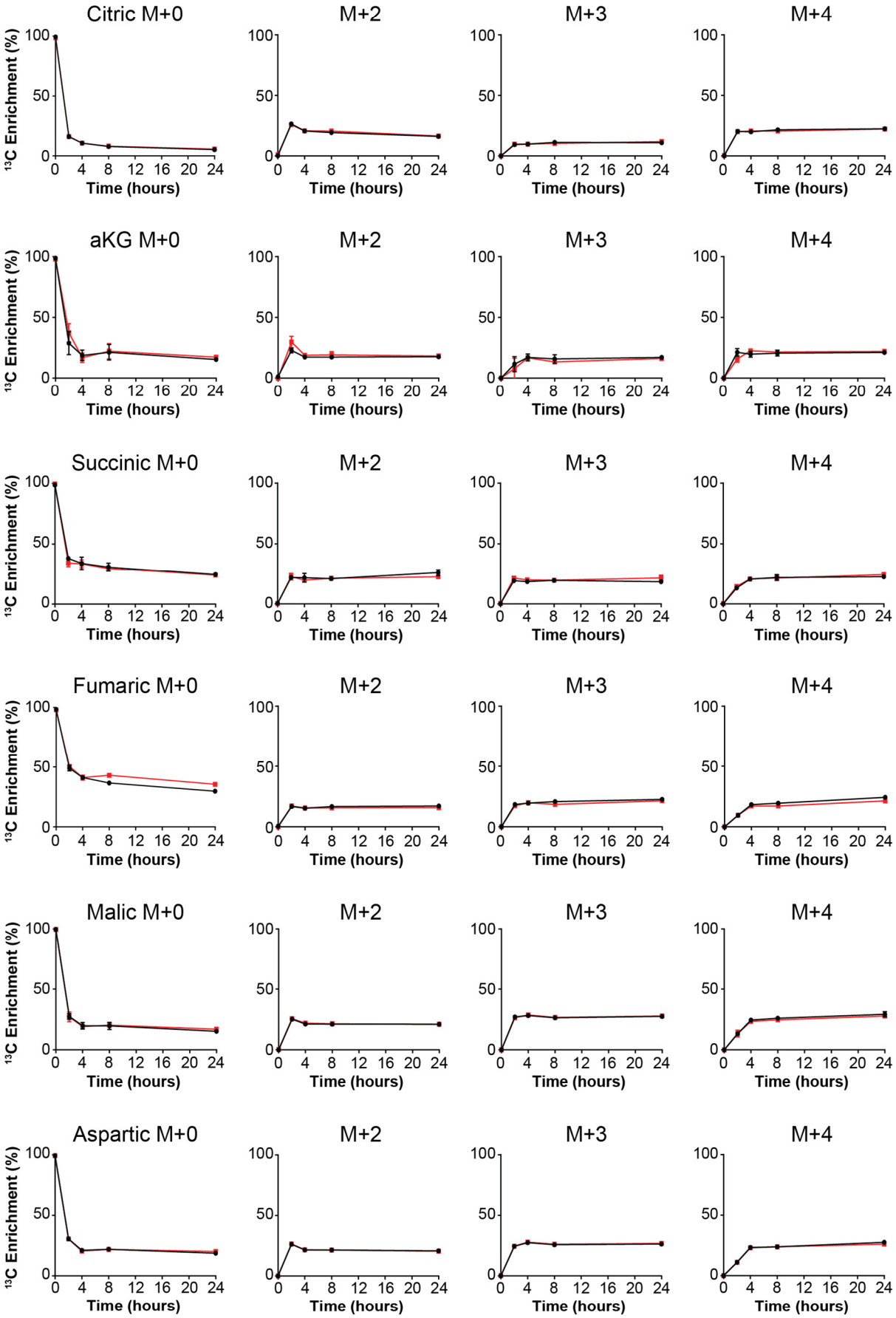

Supplementary Figure 3-S1 (continued)

Figure 3-S2 Diversion of glycolytic intermediates to side reactions and pathways for NAD^+ regeneration

Abbreviations: Asp: aspartate; DHAP: dihydroxyacetone phosphate; G6PDH: glucose-6-phosphate dehydrogenase; GAPDH: glyceraldehyde 3-phosphate dehydrogenase; GPDH-C: cytosolic glycerol-3-phosphate dehydrogenase; GPDH-M: mitochondrial glycerol-3-phosphate dehydrogenase; LDH: lactate dehydrogenase; MDH1: cytosolic malate dehydrogenase; MDH2: mitochondrial malate dehydrogenase; PHGDH: phosphoglycerate dehydrogenase.

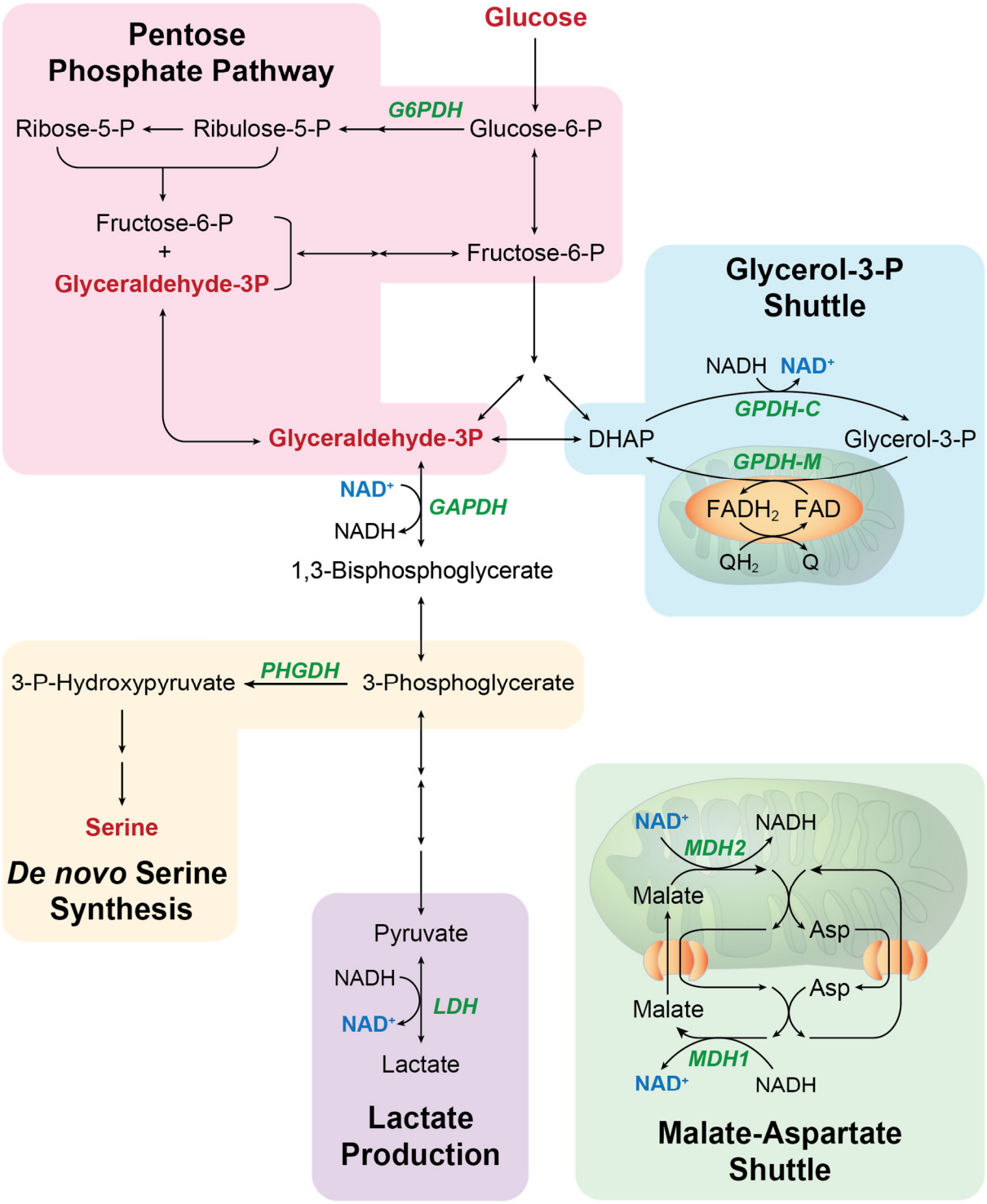

Supplementary Figure 3-S2

CHAPTER 4

Identifying novel interaction partners for BAD in the brain

INTRODUCTION

The findings described in the previous chapter indicate that *Bad* -/- and S155A neurons have a defect in glucose handling that appears to map to the lower arm of the glycolytic pathway. The work described in this chapter was motivated by the question that stems from these findings: *What is the precise molecular mechanism whereby BAD modulates glucose utilization in neurons?* Our prediction is that BAD's effect on glycolysis is mediated through specific interacting proteins that, in turn, regulate one or several steps of the glycolytic pathway. These molecular interactions may include, but are not limited to, glycolytic enzymes. This prediction suggests that in scenarios where BAD is not present or not phosphorylated, such as in *Bad* -/- and S155A neurons, these interactions and/or their functional outcomes, such as specific metabolic reactions, may be diminished. This possibility is in line with the glucose isotopomer tracing studies described in Chapter 3. In order to define the molecular underpinnings of BAD-dependent changes in glucose handling, we adopted a multidisciplinary and integrative biochemical approach. These collective efforts, which are outlined in Figure 4.1, consisted of purification and isolation of higher molecular weight complexes containing endogenous BAD in cortical tissue, and identification of direct BAD-interacting proteins using chemical cross-linking and immunocapture coupled with state-of-the-art quantitative proteomics using Tandem Mass Tags (TMTs).

Figure 4.1 Schematic of the integrative biochemical approach used for uncovering BAD interaction partners in the cortex

WT and *Bad* -/- cortices were fractionated by size exclusion chromatography (SEC). (1) Fractions enriched in BAD-containing complexes were initially analyzed by native gels and western blot (WB). (2) BAD-containing fractions were subjected to immunoaffinity capture followed by TMT-coupled proteomics. (3) In a parallel approach, BAD-containing fractions were cross-linked with a chemical cross-linker to capture the most proximal BAD-interacting protein. Cross-linked complexes were then immunoprecipitated with an anti-BAD antibody and subjected to quantitative proteomics.

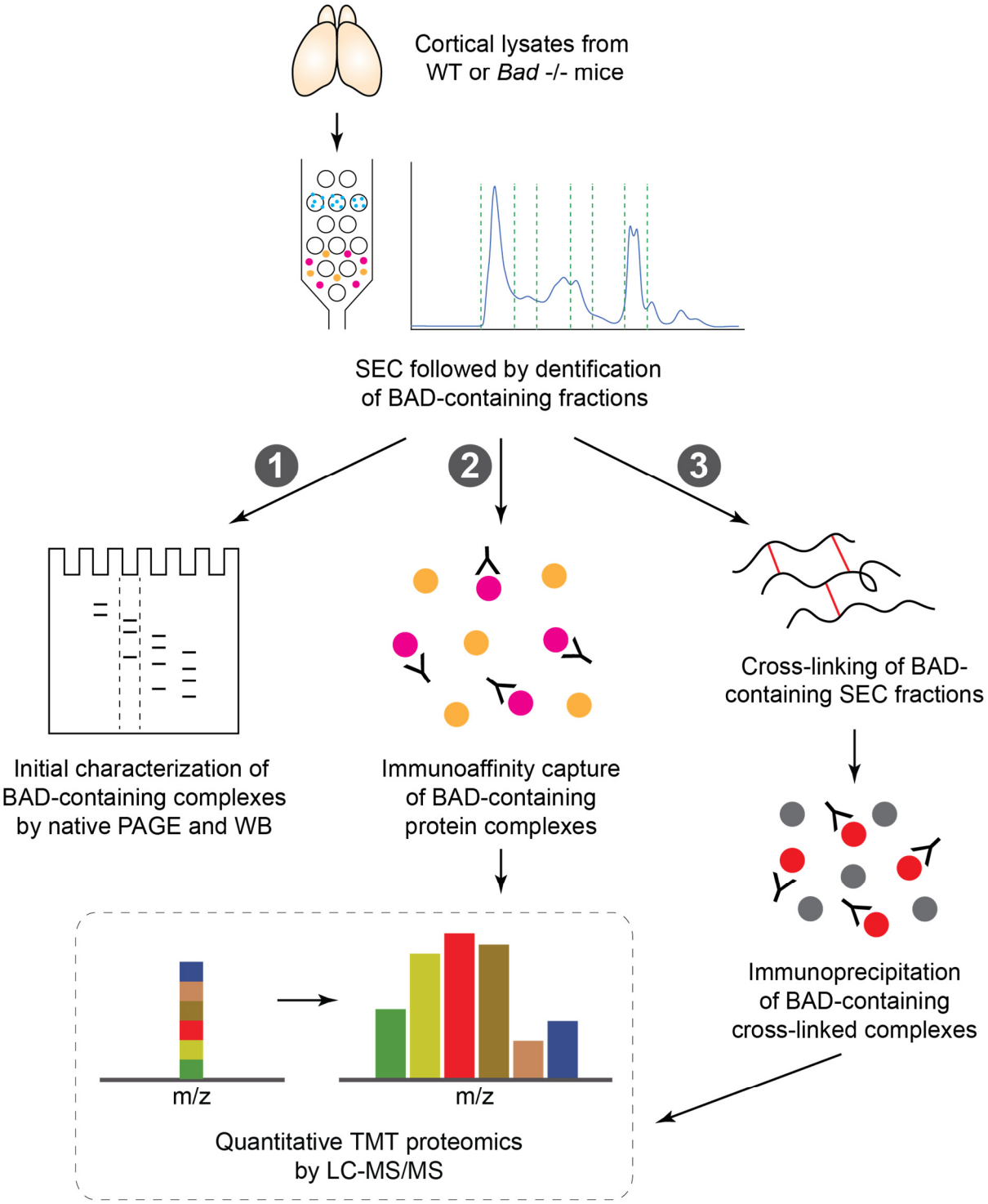
Cortical lysates from
WT or Bad -/- mice
SEC followed by dentification
of BAD-containing fractions
1
2
3
Initial characterization of
BAD-containing complexes
by native PAGE and WB
Immunoaffinity capture
of BAD-containing
protein complexes
Cross-linking of BAD-
containing SEC fractions
Immunoprecipitation
of BAD-containing
cross-linked complexes
m/z
m/z
Quantitative TMT proteomics
by LC-MS/MS

Figure 4.1

RESULTS

4.1 Isolation of higher molecular weight BAD-containing protein complexes in the cortex

As an initial purification step for BAD-containing cortical complexes, we subjected cortical tissue derived from WT mice to size exclusion chromatography (SEC) (Figure 4.2A and Supplementary Figure 4-S1). BAD primarily eluted in a fraction corresponding to 130-350 kDa complexes (fraction C, Figure 4.2B). Occasionally, BAD was also detected in SEC fractions >350 kDa (fraction B), however, this represented a minor portion of BAD-containing complexes. Notably, BAD was not detected in fractions E and F, which would correspond to its monomeric form, the 23 kDa short isoform (BAD_S) and the 28 kDa long isoform (BAD_L) of murine BAD (Danial et al., 2003; Ranger et al., 2003). This is consistent with the interpretation that the majority of BAD in the cortex resides in higher molecular weight protein complexes.

To narrow down the size and number of predominant, distinct BAD-containing complexes, we next performed non-denaturing, native PAGE analyses of fractions A-D from WT cortices. Additionally, fraction C derived from *Bad* -/- cortices was used as a control for specificity. Immunoblotting of native gels indicated that BAD was present in higher molecular weight protein complexes with estimated sizes ranging from 40 to 146 KDa (Figure 4.2C and D). These BAD-containing complexes were specifically present in fraction C from WT cortices. The different bands that react with the anti-BAD antibody in these native gels may correspond to different BAD-containing complexes or to degradation products of the same complex species (Figure 4.2C and D). It is important to note that these results do not rule out the presence of BAD-containing complexes of other sizes that might not be compatible with the lysis conditions we used or stable enough to be captured as distinct complexes on native gels. BAD's presence in these distinct higher molecular weight complexes prompted efforts to identify complexes constituents. To this end, we undertook two parallel and complementary biochemical approaches (Figure 4.1); (i) immunoaffinity capture (section 4.2 below),

and (ii) chemical cross-linking followed by immunoprecipitation (section 4.3 below) both coupled to TMT proteomics.

Figure 4.2 Isolation of higher molecular weight BAD-containing complexes in the cortex

(**A**) Representative chromatogram of size excluded WT cortical lysates showing fractions A-F and their corresponding size ranges.

(**B**) Representative western blot of SEC fractions (25 µg per lane) from WT or *Bad* -/- cortices probed with an anti-BAD antibody. The 23 and 28 kDa bands correspond to the short (BAD_S) and long (BAD_L) isoforms of BAD, respectively.

(**C**) Short (left) and long (right) exposures of native (non-denaturing) PAGE analysis of SEC fractions A, B C and D (50 µg per lane) from WT cortices probed with an anti-BAD antibody.

(**D**) Short (left) and long (right) exposures of native (non-denaturing) PAGE analysis of fraction C (50 µg per lane) from two independent SEC runs of WT and *Bad* -/- cortices probed with an anti-BAD antibody.

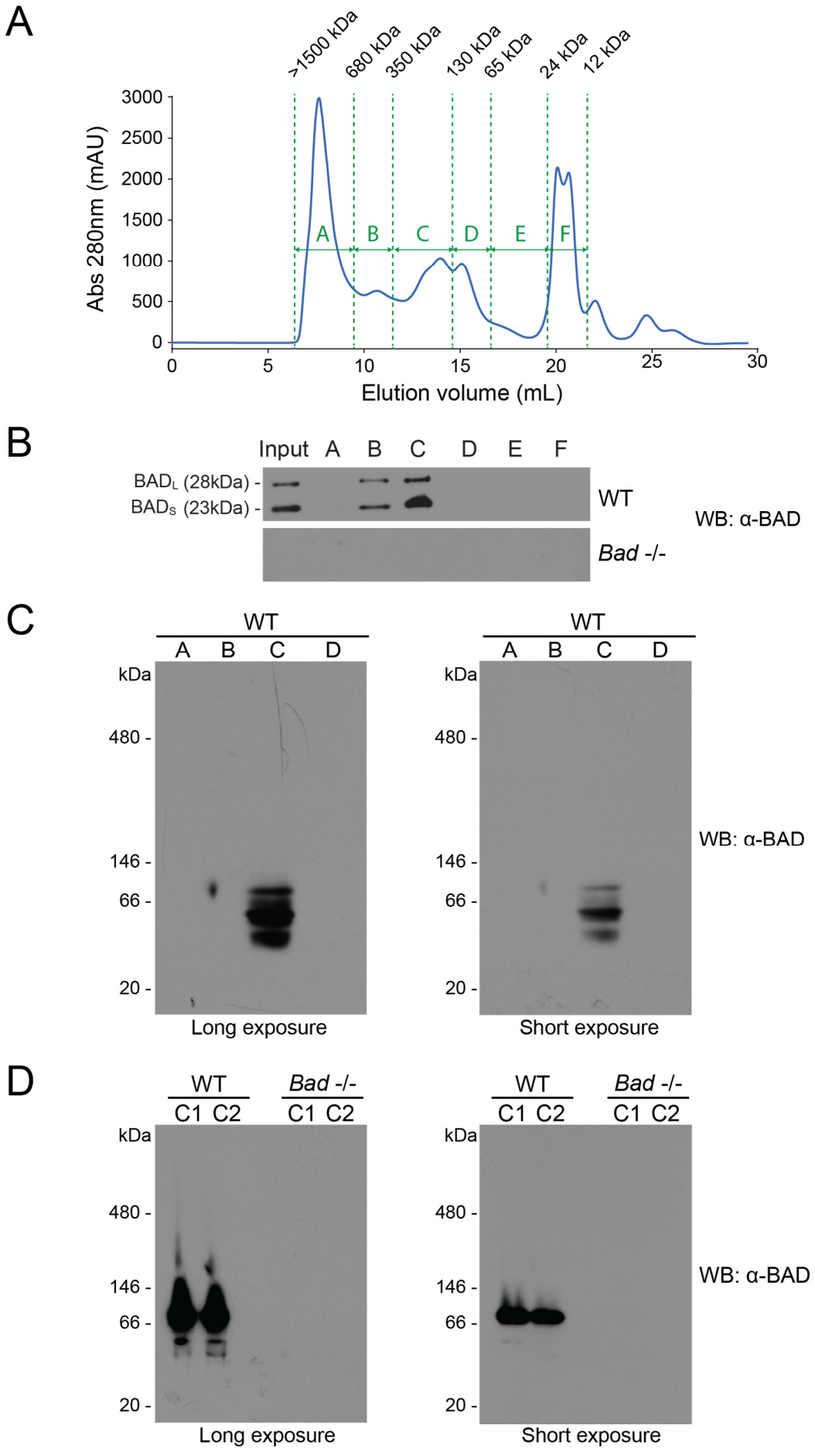
A
>1500 kDa
680 kDa
350 kDa
130 kDa
65 kDa
24 kDa
12 kDa
Abs 280nm (mAU)
Elution volume (mL)
A B C D E F
B
Input A B C D E F
BADL (28kDa) -
BADS (23kDa) -
WT
Bad -/-
WB: α-BAD
C
WT
A B C D
kDa
480 -
146 -
66 -
20 -
Long exposure
Short exposure
WB: α-BAD
D
WT
Bad -/-
C1 C2
Long exposure
Short exposure
WB: α-BAD

Figure 4.2

4.2 Identification of novel BAD-interacting proteins using immunoaffinity capture

BAD-containing complexes in fraction C were first purified using an immunoaffinity column, which sufficiently captures BAD (see Chapter 2 for experimental details) (Gimenez-Cassina et al., 2014; Yang et al., 1995). Throughout these studies, two independent negative controls were used to ensure specificity; (i) fraction C derived from *Bad* -/- cortices, and (ii) fraction D from WT and *Bad* -/- cortices, which is devoid of BAD (Figure 4.2B). Immunocaptured complexes were subjected to TMT proteomics using liquid chromatography-tandem mass spectrometry (LC-MS/MS) to quantify tryptic peptides and their corresponding proteins that are specifically enriched in WT fraction C relative to negative controls (see also Supplementary Figure 4-S2). As a proof of concept positive control, the presence of BCL-X_L, a well-known BAD-interacting protein, was confirmed among immunocaptured complexes using this method (data not shown).

Among the candidate BAD-interacting proteins identified using this unbiased approach, we initially focused on glycolytic enzymes; PFK, ALDO, TPI, GAPDH, ENO, PKM, and LDH (Figure 4.3 and Table 2). Remarkably, the majority of these enzymes map to the lower arm of glycolysis, which is in accordance with the findings described in Chapter 3. We are currently in the process of independently validating these candidates, including assessment of potential BAD-dependent effects on their enzyme activity (see also discussion below).

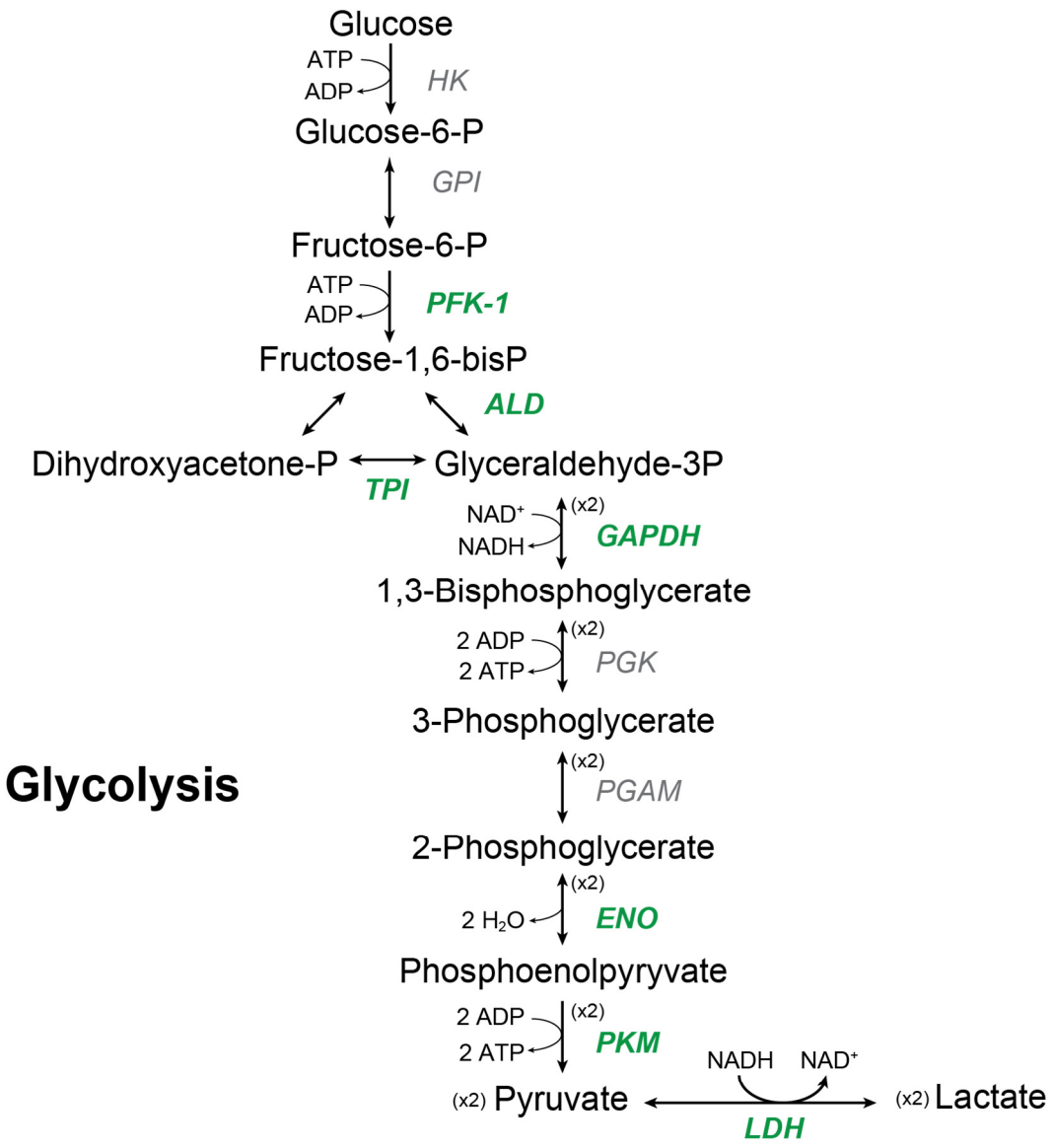

Figure 4.3 Candidate glycolytic enzymes as potential BAD-interacting proteins in the brain

Schematic of the glycolytic pathway, where the candidate glycolytic enzymes identified as BAD-interacting proteins are highlighted in green.

Abbreviations: ALD: fructose 1,6-bisphosphate aldolase; ENO: enolase; GAPDH: glyceraldehyde 3-phosphate dehydrogenase; GPI: glucose-6-phosphate isomerase; HK: hexokinase; LDH: lactate dehydrogenase; PFK: phospho-fructokinase; PGAM: phosphoglycerate mutase; PGK: phosphoglycerate kinase; PKM: pyruvate kinase; TPI: triose-phosphate isomerase.

Table 2 List of candidate glycolytic enzymes identified as BAD-interacting proteins using immunoaffinity capture

The number of quantified tryptic peptides for each candidate enzyme is shown. Signal abundance was derived by summing TMT signal-to-noise (S/N) reporter ion intensities for all peptides per protein. The ratio of TMT reporter ion signal for WT/*Bad* -/- samples is also indicated.

Gene Symbol	Protein Name	Total Quantified Peptides	S/N Reporter Ion Intensity (WT)	S/N Reporter Ion Intensity (*Bad* -/-)	Ratio WT/*Bad* -/-
PFKP	6-Phosphofructokinase type C	7	1841	198	9.29
ALDOA	Fructose-bisphosphate aldolase A	2	332	52	6.37
TPI1	Triose phosphate isomerase	4	1158	201	5.77
GAPDH	Glyceraldehyde-3-phosphate dehydrogenase	25	13105	1443	9.08
ENO1	Alpha-Enolase	13	8244	1001	8.24
PKM	Isoform M1 of Pyruvate kinase	6	1181	500	2.36
LDHB	L-Lactate dehydrogenase B chain	5	1466	166	8.81

Table 2

4.3 Identification of novel BAD-interacting proteins using chemical cross-linking

Most protein interactions are of transient nature *in vivo*, rendering their characterization a considerable challenge. Chemical cross-linkers can overcome this challenge by converting non-covalent interactions between two or more molecules into covalent bonds, facilitating the capture of “nearest neighbor” protein-protein interactions (Holding, 2015; Perkins et al., 2010; Rappsilber, 2011). An added advantage of chemical cross-linking for protein interaction studies is the high likelihood for identifying direct protein interactions given the spacer arm length of chemical cross-linkers. We also reasoned that this approach would effectively complement the immunoaffinity capture of BAD-containing complexes described in section 4.2 above, and enable us to more effectively narrow down the identified BAD-interacting candidates to the most proximal interactor(s).

Cross-linking reagents contain at least two reactive ends that can target the majority of functional groups in proteins or peptides depending on the cross-linker’s chemical reactivity, spacer arm length, hydrophobicity, and cleavability. We selected bis(2-[succinimidoxy-carbonyloxy]ethyl)sulfone (BSOCOES), a homobifunctional NHS-ester cross-linker with a base-cleavable spacer arm for reversible cross-linking between primary amines (Fenton et al., 2007; Grinberg et al., 2005; Zarling et al., 1980). BSOCOES is a membrane permeable cross-linker with a spacer arm length of 13.0 Å, which makes it ideal for intermolecular cross-linking (Figure 4.4A). Fraction C derived from WT and *Bad* -/- cortices were incubated with BSOCOES and quenched cross-linking reactions were either fractionated directly using SDS-PAGE or immunoprecipitated (IP) with an anti-BAD antibody prior to fractionation on SDS-PAGE and immunoblotting for BAD (Figure 4.4B-D). We found that treatment with BSOCOES for 2 hr effectively produced specific BAD-containing cross-linked complexes, which were not present in WT samples treated with DMSO control or in similarly cross-linked lysates of fraction C derived from *Bad* -/- cortices (Figure 4.4C and D). These experiments provided evidence for two reproducible BAD-containing complexes; a slower migrating ~80 kDa complex (complex 1), and a faster migrating ~50 kDa complex (complex 2) (Figure 4.4C-D).

We next set out to identify the components of the two BAD-containing complexes. We reasoned that BCL-X_L, which is a known BAD-interacting protein that was also detected in the

eluates from the BAD antibody column (section 4.2), should be present in at least one of these cross-linked complexes. Indeed, an anti-BCL-X_L antibody reacted with complex 2, indicating the presence of both BAD and BCL-X_L in this complex (Figure 4.4E). The approximate 50 kDa size of complex 2 is consistent with a monomer of each protein forming this complex; BAD_S (23 kDa) and BCL-X_L (30 kDa). Interestingly, cross-linked BAD complex 1 did not react with anti- BCL-X_L antibody, indicating a novel complex. The estimated size of BAD complex 1 detected by chemical cross-linking is an approximate match to the predominant complex species detected using native PAGE (comparing Figures 4.2D with 4.4C-D). We have subjected the cross-linked complex 1 to mass spectrometry analysis to identify its precise constituents. At the time of this writing, we are awaiting the results of this analysis.

Figure 4.4 Identification of novel BAD-interacting proteins in the brain using chemical cross-linking

(**A**) Structure of bis(2-[succinimidoxycarbonyloxy]ethyl)sulfone (BSOCOES) used for chemical cross-linking experiments. BSOCOES contains two *N*-hydroxysuccinimide ester (NSH) groups, one on each end, which react with amino groups in proteins. The sulfone bond in the middle can be cleaved with alkaline conditions to reverse cross-linking. The spacer arm length of BSOCOES is 13.0 Å.

(**B**) Schematic workflow for cross-linking experiments.

(**C**) Western blot of cross-linked SEC fraction C from WT and *Bad* -/- cortices developed using an anti-BAD antibody following SDS-PAGE. These cross-linked lysates were used as the "input" for subsequent immunoprecipitation assays. Red arrows mark specific BAD-containing complexes 1 (C1) and 2 (C2).

(**D**) Isolation of cross-linked complexes 1 and 2 following immunoprecipitation and subsequent immunoblotting with an anti-BAD antibody. Yellow asterisks denote non-specific bands also present in *Bad* -/- controls.

(**E**) Immunoblot analysis of BAD-containing cross-linked complexes with an anti-BCL-X_L antibody identifying complex 2 as a BAD: BCL-X_L complex.

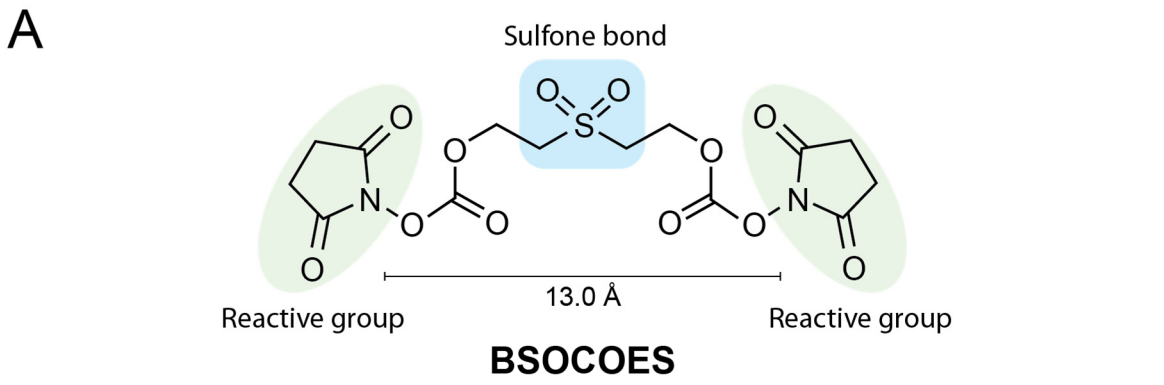
A
Sulfone bond
13.0 Å
Reactive group
Reactive group
BSOCOES

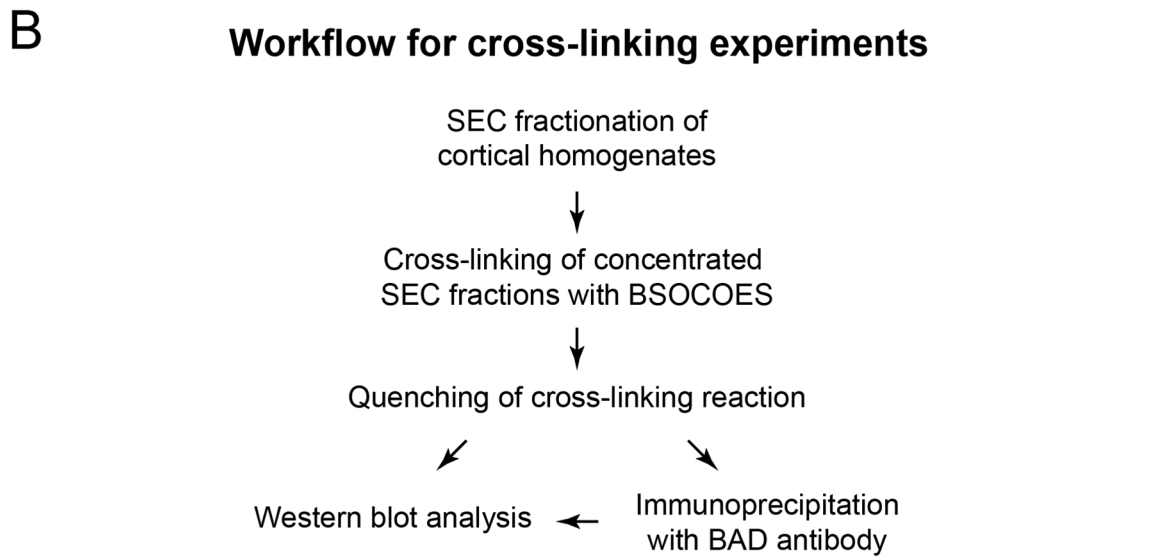
B
Workflow for cross-linking experiments
SEC fractionation of cortical homogenates
Cross-linking of concentrated SEC fractions with BSOCOES
Quenching of cross-linking reaction
Western blot analysis
Immunoprecipitation with BAD antibody

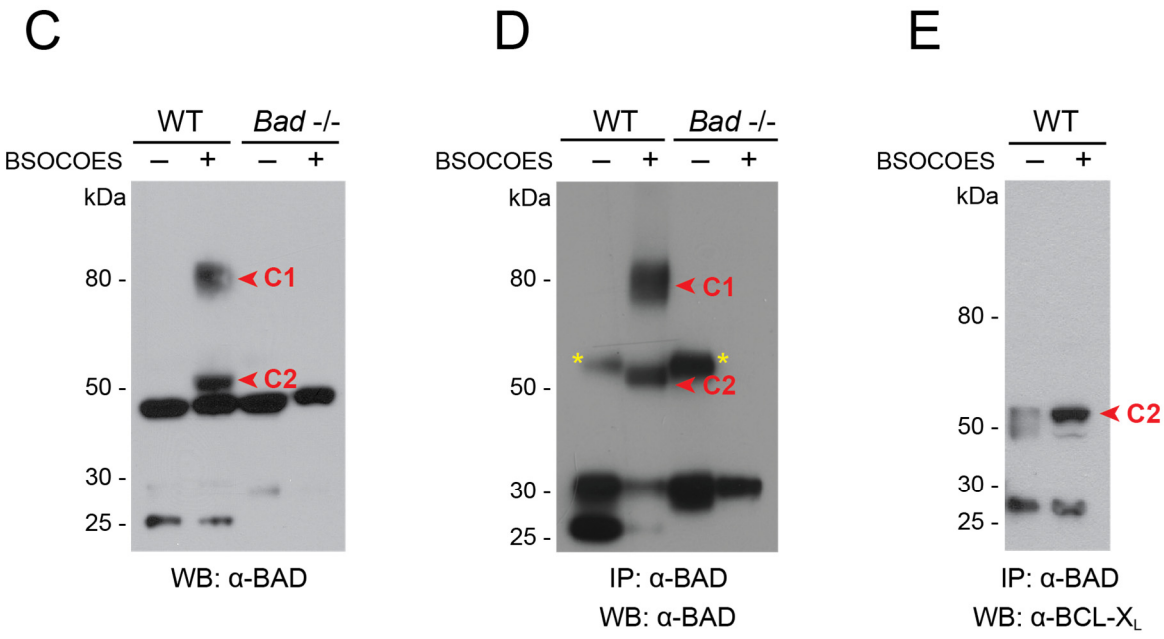
C
WT
Bad -/-
BSOCOES – + – +
kDa
80 -
50 -
30 -
25 -
C1
C2
WB: α-BAD
D
WT
Bad -/-
BSOCOES – + – +
kDa
80 -
50 -
30 -
25 -
C1
C2
IP: α-BAD
WB: α-BAD
E
WT
BSOCOES – +
kDa
80 -
50 -
30 -
25 -
C2
IP: α-BAD
WB: α-BCL-XL

Figure 4.4

DISCUSSION

The integrative biochemical approaches described in this chapter uncovered candidate glycolytic enzymes as BAD-interacting proteins in the cortex. While definitive data pointing to the precise enzyme among these candidates await completion of current ongoing experiments, we predict that BAD's direct interactor in the cortex may modulate the lower arm of glycolysis. This is consistent with the glucose tracer studies in Chapter 3.

Multiple lines of evidence indicate that BAD's ability to regulate glucose metabolism is independent of its interaction with other BCL-2 family members, namely BCL-X_L, BCL-2 and BCL-w (Gimenez-Cassina and Danial, 2015). First, the metabolic phenotype of BAD-deficient mice, including alterations in neuronal glucose handling and seizure protection, are not phenocopied in mice deficient in BCL-X_L, BCL-2 or BCL-w. Second, BAD's effect on glucose metabolism requires phosphorylation of its BH3 domain on S155, which inhibits its capacity to engage BCL-X_L, BCL-2 and BCL-w (Gimenez-Cassina and Danial, 2015). Within this context, it is relevant that BCL-X_L is only present in one of the BAD-containing cross-linked complexes (complex 2), further justifying the pursuit of complex 1 for the discovery of the binding partner(s) relevant to BAD's metabolic effect in the cortex and altered glucose handling in BAD mutant neurons.

The observation that several glycolytic enzymes simultaneously co-elute with BAD from the immunoaffinity column (Table 2) is intriguing. Previous studies have proposed that glycolytic enzymes can be present in large multi-protein complexes that might be beneficial for metabolic channeling (Genda et al., 2011; Marcondes et al., 2011; Menard et al., 2014). While additional work is required to corroborate this idea, it is possible that BAD may reside in such a complex. However, we expect that mass spectrometry identification of cross-linked BAD complex 1 (Figure 4.4C-D) will likely reveal the proximal direct binding partner of BAD in this context.

Precedence for BAD interaction with glycolytic enzymes in other cell types exists. Glucokinase (GK, hexokinase IV), a tissue restricted isoform of hexokinase, interacts with BAD in the liver and pancreatic ß-cells (Danial et al., 2003; Danial et al., 2008; Szlyk et al., 2014).

In addition, evidence for BAD interaction with PFK1 in mouse embryonic fibroblasts (MEFs) and hematopoietic cell lines (FL5.12) has been put forward (Deng et al., 2008). Both interactions lead to increased glycolysis in a cell type-specific manner but the domains of BAD required for engaging GK and PFK1 are distinct. Because GK is not expressed in the cortex, we initially considered the possibility that BAD might affect other hexokinase (HK) isoforms in the cortex despite the fact that HKI/II and GK have fundamentally distinct structural and enzyme kinetic properties. We found comparable HK activity in WT and BAD-deficient brain samples (data not shown). Likewise, we measured PFK1 activity and did not find any differences between the two genotypes or any evidence for a BAD:PFK1 complex in the cortex (data not shown). Thus, it is highly likely that our biochemical studies will ultimately identify a novel BAD-interacting protein in the cortex that mediates its effect on glycolysis.

How can BAD's effect on glycolysis be mediated by different glycolytic enzymes in different tissues? One possibility is that BAD engages certain tissue-specific isoforms of glycolytic enzymes, such as GK/HKIV in endocrine cells. We may find that BAD similarly engages brain- or neuronal-specific isoforms of certain glycolytic enzyme. Once we definitively determine the BAD-interacting partner in the cortex, we plan to carry out careful structure-function studies to define the precise domain of BAD and the partner protein required for this interaction. Furthermore, given that BAD S155 phosphorylation positively regulates glucose metabolism in neurons [(Gimenez-Cassina et al., 2012) and Chapter 3], we predict that BAD may modify the activity of such partner enzyme. Our lab has previously shown that the BAD BH3 helix directly engages GK and that S155 phosphorylation within this domain is required for BAD's capacity to increase GK activity (Gimenez-Cassina et al., 2014; Ljubicic et al., 2015; Szlyk et al., 2014). If we find that the BAD BH3 domain is similarly required for interaction with its partner protein in the cortex, then this would give rise to a testable hypothesis that the BAD BH3 helix may use a common binding pocket or structural fold/motif found in its partner proteins that are, otherwise, distinct enzymes.

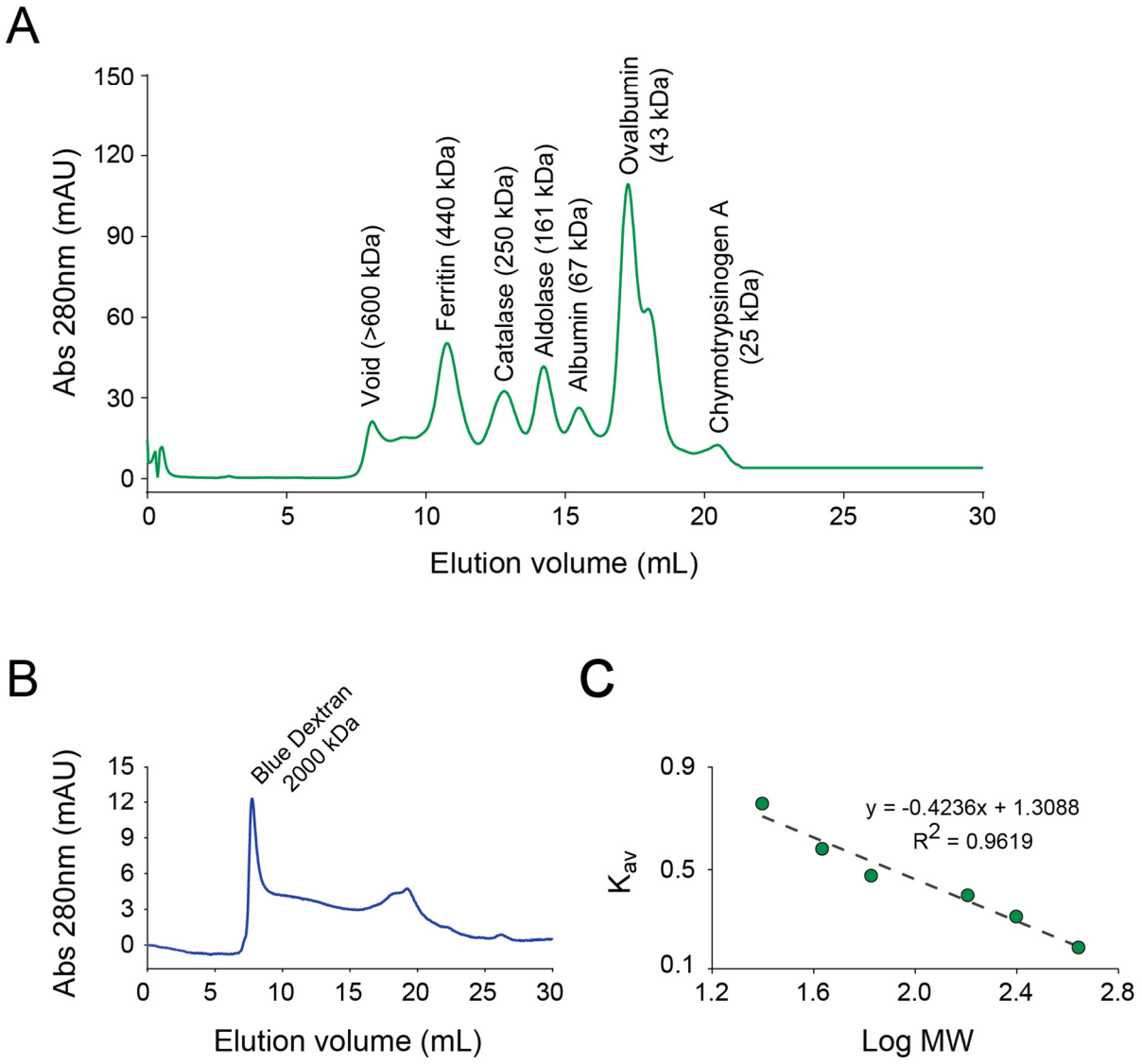

Supplementary Figure 4-S1 Calibration of the Superdex 200 column used for SEC

(**A**) Chromatogram of the high molecular weight mix used to calibrate the Superdex 200 column, which has an optimum separation range of 10-600 kDa. The chromatogram showed well resolved peaks for each of the protein standards.

(**B**) Chromatogram of Blue Dextran 2000 run used to estimate the void volume (V_o) of the Superdex 200 column.

(**C**) Calibration curve for the Superdex 200 column determined with experimental parameters from (A) and (B).

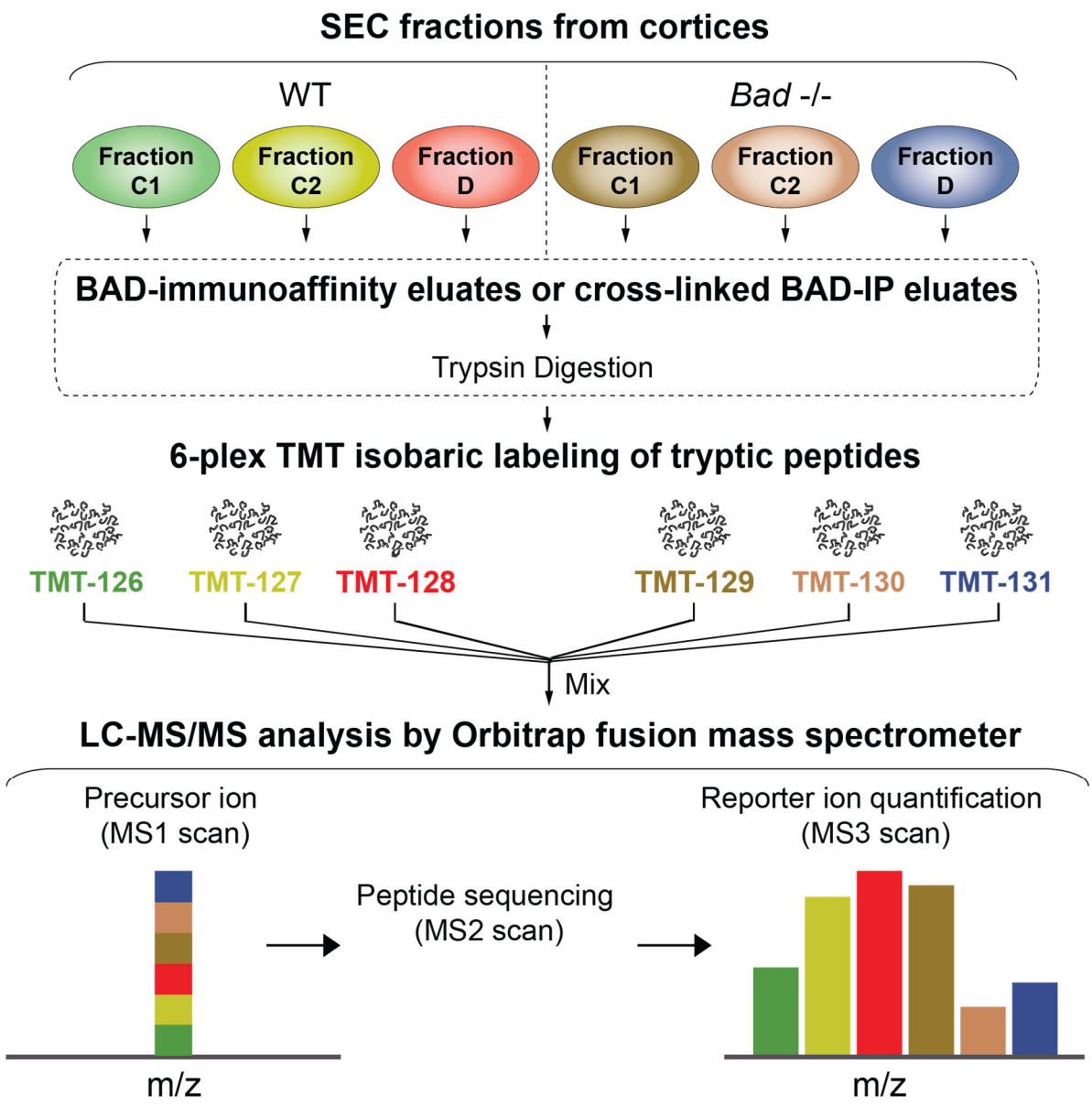

Supplementary Figure 4-S2 Schematic of TMT labeling and LC-MS/MS proteomics

Eluates from BAD immunoaffinity capture or lysates that were subjected to chemical cross-linking prior to IPs were subjected to trypsin digestion and subsequent labeling with 6-plex isobaric tandem mass tag (TMT) reagents. TMT-labeled peptides from each sample/condition were then mixed and subjected to tandem mass spectrometry (MS1 through 3) using the Orbitrap fusion instrument (Thermo Fisher Scientific). A typical mass spectrum on the bottom right shows TMT reporter peaks, which represent relative ratios of individual tryptic peptides. When fragmented during MS/MS, the reporter ions show the relative amount of the peptides in the samples. See Chapter 2 for additional experimental details.

CHAPTER 5

Dissecting BAD-dependent changes in ketone body metabolism using ^{13}C isotopomer analysis

INTRODUCTION

We have previously shown that BAD's effect on neuronal fuel metabolism extends beyond regulation of glycolysis to reciprocal modulation of glucose *versus* ketone body utilization. How does BAD affect ketone body utilization in neurons? The metabolism of ketone bodies (β-hydroxybutyrate, acetoacetate and acetone) produces acetyl-CoA and augments mitochondrial energy metabolism. The effect of ketone bodies on neuronal energetics also includes mechanisms of energy storage and release through changes in phosphocreatine to creatine ratios, which are increased in the ketotic brain (DeVivo et al., 1978; Pan et al., 1999). Furthermore, ketone bodies make important contributions to several biosynthetic outputs that are relevant to neuronal function and excitability; including GABA and glutathione (GSH) (Jarrett et al., 2008; Yudkoff et al., 2008; Yudkoff et al., 2007). In this chapter, we describe our initial efforts to determine the effect of BAD modifications on ketone body utilization using the ^{13}C-β-hydroxybutyrate tracer and targeted GC-MS metabolomics, specifically focusing on the TCA cycle flux and GABA synthesis.

RESULTS

5.1 Metabolomics workflow for U^{13}C-β-hydroxybutyrate tracer analysis in primary cortical neurons derived from *Bad* genetic models

To study the fate of ketone body-derived carbons in primary cortical neurons, we started by determining the kinetics of U^{13}C-β-hydroxybutyrate tracer uptake and ^{13}C incorporation in downstream metabolites using GC-MS analysis. To this end, WT neurons were labeled with 5 mM U^{13}C-β-hydroxybutyrate tracer for 0-8 hr. Although the majority of the TCA cycle intermediates reached isotopic steady state at 4 hr post labeling (data not shown), we decided on a 2 hr labeling period because longer incubations with the ketone body tracer led to neuronal cell death starting approximately at the 8 hr time point. This may be due to our elimination of glucose from the labeling medium given that our goal was to initially characterize β-hydroxybutyrate utilization without the confounding effects of other fuels. Using the above parameters, we next compared the uptake of U^{13}C-β-hydroxybutyrate tracer in WT and *Bad* -/- neurons, and found comparable levels of β-hydroxybutyrate in WT and *Bad* -/- neurons (Figure 5.1A). These results indicate that the increase in ketone body oxidation we previously reported in *Bad* -/- neurons cannot be explained by altered ketone body uptake.

Figure 5.1 β-hydroxybutyrate tracer uptake and metabolism in WT and *Bad* -/- neurons

(**A**) U^{13}C-β-hydroxybutyrate content in WT and *Bad* -/- neurons after labeling for 2 hr.

(**B**) Contribution of ketone body-derived carbons to TCA cycle metabolites. U^{13}C-β-hydroxybutyrate is represented by 4 orange beads and the downstream labeling patterns for TCA intermediates are also shown. Unlabeled and ^{13}C-labeled carbons are shown in white and orange, respectively. Only the first turn of the TCA cycle is shown. (**C**) Intracellular TCA cycle metabolites in WT and *Bad* -/- neurons labeled with 5 mM U^{13}C-β-hydroxybutyrate for 2 hr. Unlabeled (^{12}C, M+0, in black) and labeled (^{13}C, SUM of M+1, …, M+6, in blue) isotopologues for each metabolite are shown. Data are mean ± SEM of cortical neurons derived from 6 embryos (E16) seeded and analyzed in 3 plates. Asterisks compare the ^{13}C-labeled isotopologue abundances (SUM of M+1, …., M+n, where n is the number of carbons for the given metabolite) between genotypes. *$p < 0.05$; n.s, non-significant; two-tailed Student's *t*-test.

Abbreviations: α-KG: α-ketoglutarate; AST: aspartate aminotransferase; IDH: isocitrate dehydrogenase; MDH: malate dehydrogenase; SDH: succinate dehydrogenase.

A

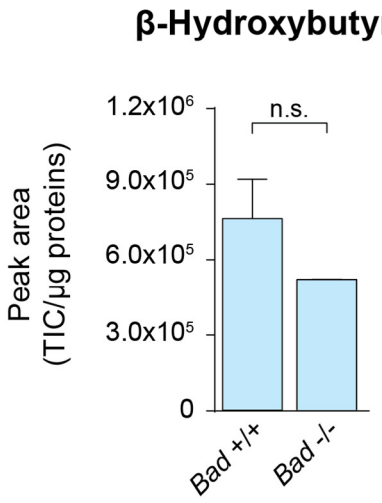
β-Hydroxybutyrate
Peak area (TIC/µg proteins)
1.2x10⁶
9.0x10⁵
6.0x10⁵
3.0x10⁵
0
n.s.
Bad +/+
Bad -/-

B

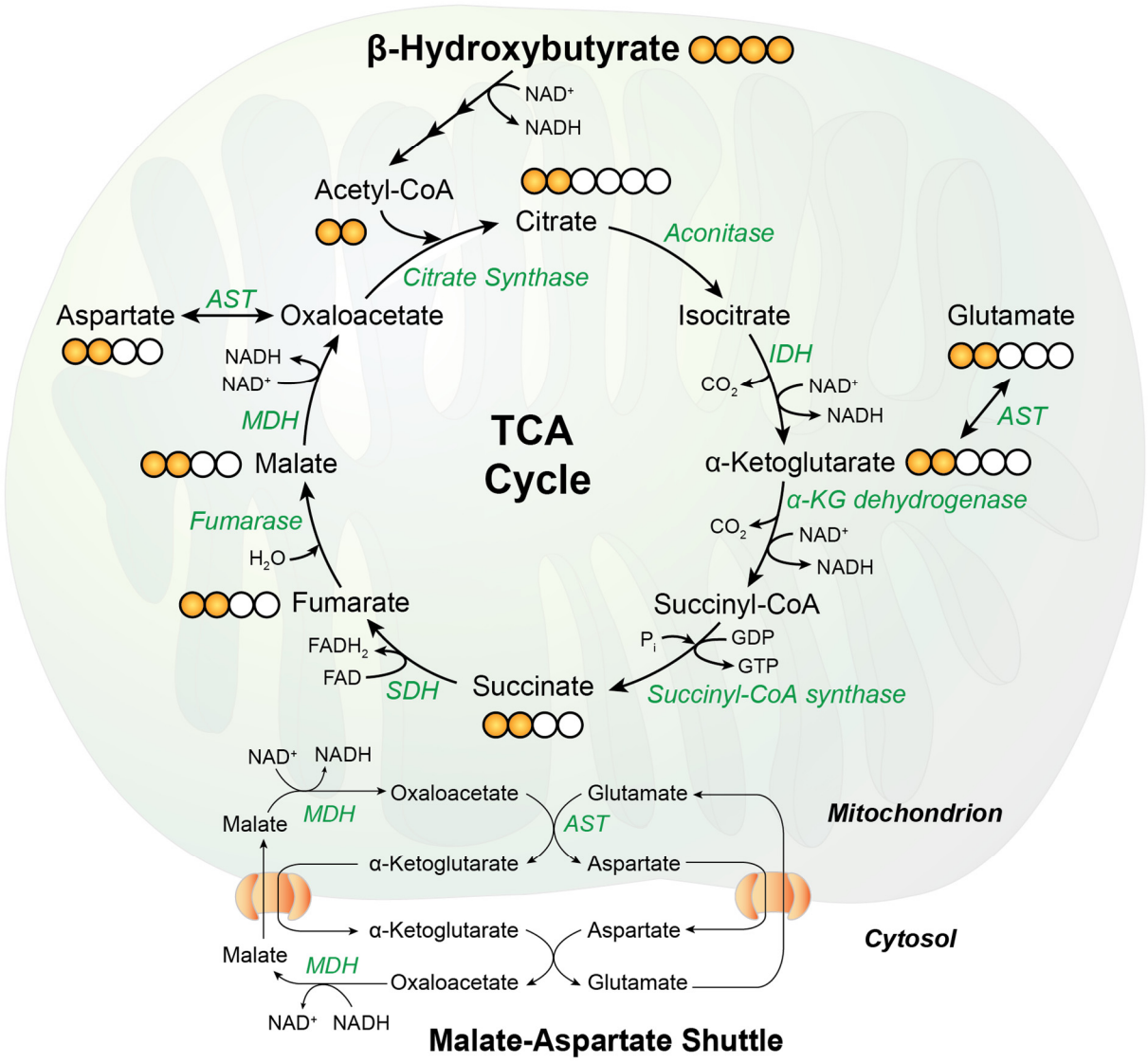
β-Hydroxybutyrate
NAD⁺
NADH
Acetyl-CoA
Citrate
Aconitase
Citrate Synthase
AST
Aspartate
Oxaloacetate
Isocitrate
IDH
CO₂
NAD⁺
NADH
Glutamate
AST
NADH
NAD⁺
MDH
Malate
TCA Cycle
α-Ketoglutarate
α-KG dehydrogenase
CO₂
NAD⁺
NADH
Fumarase
H₂O
Fumarate
Succinyl-CoA
Pi
GDP
GTP
FADH₂
FAD
SDH
Succinate
Succinyl-CoA synthase
NAD⁺ NADH
Malate
MDH
Oxaloacetate
Glutamate
AST
α-Ketoglutarate
Aspartate
Mitochondrion
α-Ketoglutarate
Aspartate
Malate
MDH
Oxaloacetate
Glutamate
Cytosol
NAD⁺ NADH
Malate-Aspartate Shuttle

Figure 5.1

C

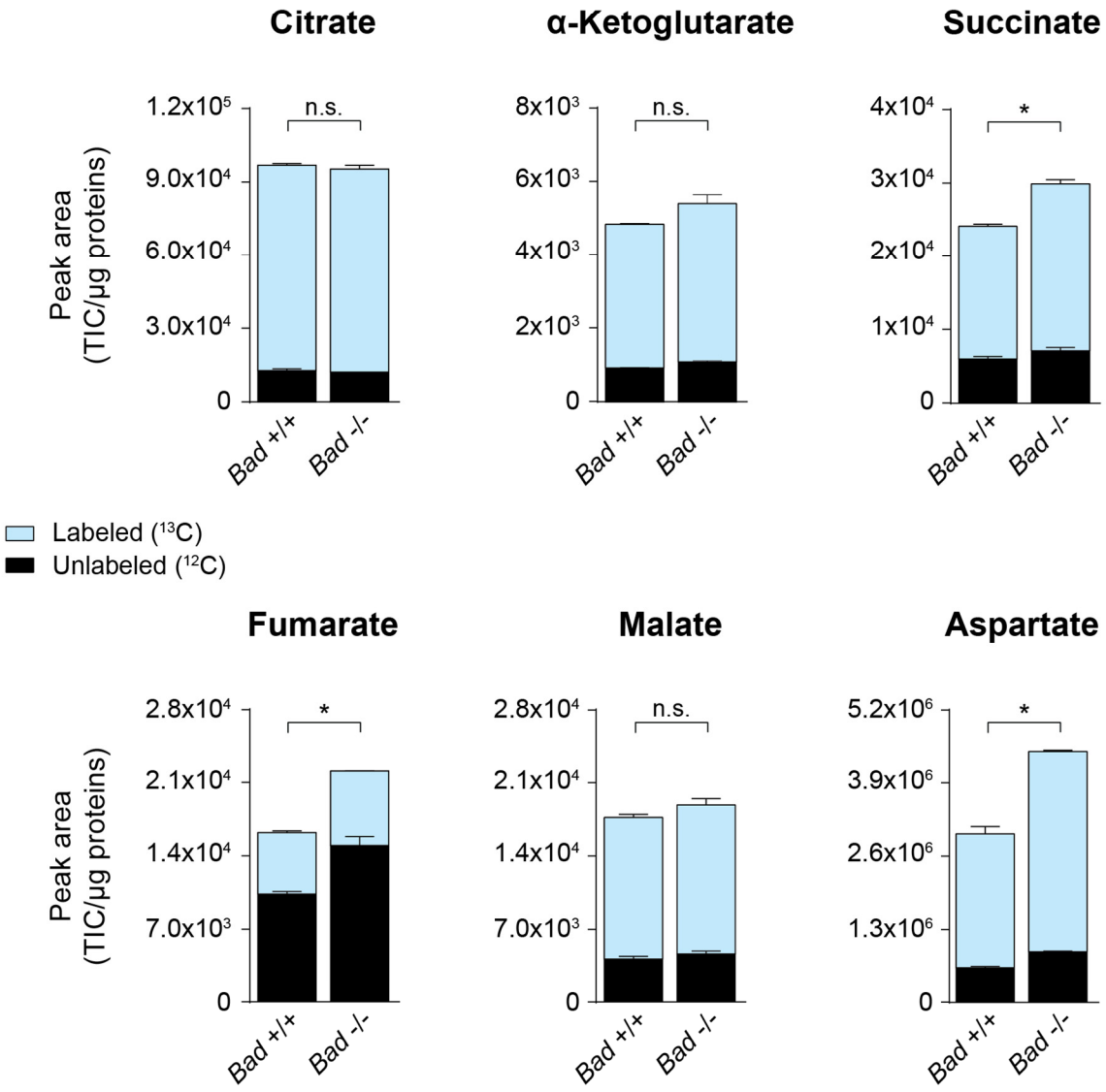

Figure 5.1 (continued)

5.2 Increased ketone body oxidation in *Bad* -/- neurons is associated with augmented TCA cycle activity

Four-carbon labeled β-hydroxybutyrate yields 2 molecules of 2-carbon labeled (M+2) acetyl-CoA, which react with oxaloacetate to form M+2 citrate in the first round of the TCA cycle (Figure 5.1B). After multiple turns of the TCA cycle, ^{13}C labeling will appear in more carbons, eventually leading to the presence of fully labeled TCA cycle metabolites. Labeling of WT and *Bad* -/- neurons with U^{13}C-β-hydroxybutyrate resulted in similar levels of labeled citrate (Figure 5.1C). However, labeled succinate, fumarate and aspartate were significantly higher in *Bad* -/- neurons compared to WT controls (Figures 5.1C). Labeled aspartate in this setting can be used as a surrogate for oxaloacetate because the two metabolites are thought to be in isotopic equilibrium through the AST reaction (Figure 5.1B). In comparison, the levels of labeled α-ketoglutarate and malate remained mostly unaffected in *Bad* -/- neurons (Figure 5.1C), which can be partly explained by their involvement in multiple reactions that can ultimately result in dilution of the ^{13}C label. Taken together, these data are consistent with the conclusion that *Bad* -/- neurons have higher TCA cycle activity in response to β-hydroxybutyrate. This further explains our previous observations that *Bad* -/- neurons have increased mitochondrial oxygen consumption rates in response to β-hydroxybutyrate in that NADH- or $FADH_2$-producing reactions, which donate electrons to the electron transport chain, will parallel the increase in TCA cycle flux in these cells.

5.3 Biosynthetic utilization of ketone body-derived carbons for amino acid and neurotransmitter synthesis

The ketogenic diet and the attendant increase in mitochondrial processing of ketone bodies increase the synthesis of the inhibitory neurotransmitter GABA (Yudkoff et al., 2008; Yudkoff et al., 2007). At the mechanistic level, increased GABA synthesis in this setting is likely due to increased availability of glutamate for the GAD reaction for at least two reasons; (i) decreased activity of AST in GABAergic neurons, which can otherwise use glutamate to generate aspartate (Figure 5.2A), and (ii) increased astrocytic glutamine synthesis and its

provision to GABAergic neurons, which can covert glutamine to glutamate for more GABA synthesis (Figure 5.2A) (Erecinska et al., 1996; Lund et al., 2009; Matsumoto and Ito, 1985; Melo et al., 2006; Yudkoff et al., 2001). We found that *Bad* -/- neurons have markedly higher levels of ^{13}C-labeled glutamate and GABA following U^{13}C-β-hydroxybutyrate labeling (Figure 5.2B and C).

Interestingly, this effect seems to be fuel-specific because unlike the scenario with U^{13}C-β-hydroxybutyrate labeling, the levels of glutamate and GABA in *Bad* -/- neurons labeled with U^{13}C-glucose were reduced (data not shown). This is further consistent with reciprocal changes in TCA cycle activity in *Bad* -/- neurons in response to glucose *versus* ketone bodies (Figure 3.3C *versus* 5.1C). In independent studies, we also found that total steady state levels of GABA are significantly higher in *Bad* -/- neurons than WT controls (data not shown). In light of the aforementioned tracer studies, we can conclude that this increase in total GABA stems from increased ketone body contribution to its synthesis in *Bad* -/- neurons.

Figure 5.2 Increased GABA synthesis in *Bad* -/- neurons incubated with U^{13}C-β-hydroxybutyrate

(**A**) Schematic representation of the GABA shunt and its relationship to the TCA cycle. (**B-C**) Intracellular metabolite levels of glutamate (B) and GABA (C) in WT and *Bad* -/- neurons labeled with 5 mM U^{13}C-β-hydroxybutyrate for 2 hr. The indicated metabolites and their corresponding isotopologues were measured as in Figure 5.1C. Data are mean ± SEM of cortical neurons derived from 6 embryos (E16) seeded and analyzed in 3 plates. Asterisks compare the ^{13}C-labeled isotopologue abundances (SUM of M+1, …., M+n, where n is the number of carbons for the given metabolite). *$p < 0.05$; two-tailed Student's *t*-test.

Abbreviations: AST: aspartate aminotransferase; GABA-T: GABA transaminase; GAD: glutamate decarboxylase; GS: glutamine synthetase; OAA: oxaloacetate; PAG: phosphate-activated glutaminase; SSA: succinate semi aldehyde; SSADH: succinate semi aldehyde dehydrogenase.

A

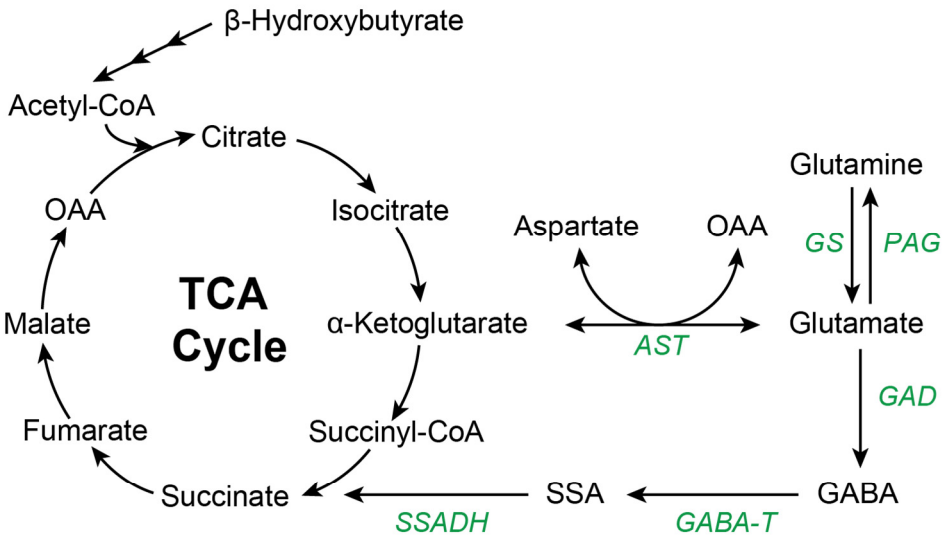

B

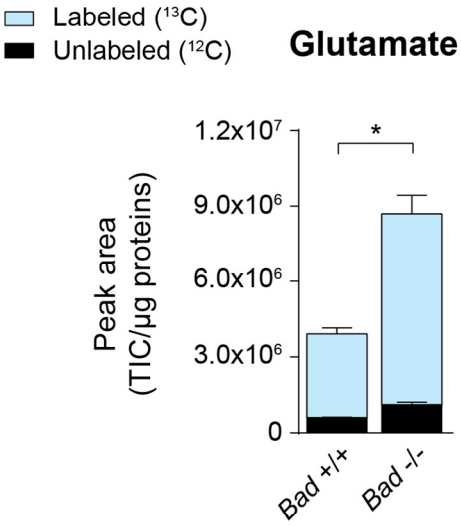

C

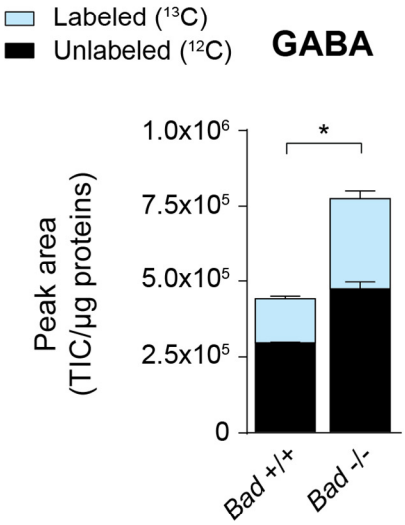

Figure 5.2

DISCUSSION

Our initial efforts to trace the fate of ketone body-derived carbons in BAD mutant neurons indicated an overall enhancement of the TCA cycle activity and higher ^{13}C enrichment in GABA pools. The contribution of β-hydroxybutyrate to the TCA cycle and mitochondrial electron transport chain is consistent with increased acetyl-CoA, succinate and NADH following its metabolism in mitochondria (Figure 1.1). Our data do not readily point to a specific step in ketone body oxidation that might be increased in BAD-deficient neurons. However, this might be due to the limited number of metabolites we measured in this targeted metabolomics study.

Our previous studies suggested that increased utilization of ketone bodies in *Bad* -/- and S155A neurons is likely derived from local metabolic alterations in the brain rather than altered metabolism in the liver, which is the body's main source of ketone body production (Gimenez-Cassina et al., 2012). Consistent with this idea, serum levels of ketone bodies are not altered in BAD mutant mice, yet the β-hydroxybutyrate content in BAD-deficient brain is significantly higher than WT. What accounts for increased tissue content of ketone bodies in the absence of BAD? One possibility is altered ketogenesis. Evidence exists that ketogenesis can occur in the brain, although to a lesser extent than liver. In particular, astrocytes can synthesize ketone bodies from octanoate *in vitro* (Auestad et al., 1991). Whether neurons are similarly capable of ketone body production is an open question. In addition to fatty acid-generated acetyl CoA, which can be used for ketogenesis, certain amino acids can also produce acetyl-CoA upon degradation. Such ketogenic amino acids include phenylalanine, tyrosine, isoleucine, leucine, tryptophan, threonine, and lysine. The metabolic precursors for ketone body synthesis in BAD mutant brain and the possibility of increased ketogenesis in BAD-deficient neurons and/or astrocytes warrant additional investigation.

While the design of our tracer studies enabled us to initially learn about increased contribution of ketone body carbons to the TCA cycle activity and GABA pools in BAD mutant neurons, they do not precisely simulate the physiologic fuel milieu of neurons in ketotic brain following starvation or ketogenic diet treatment. Although glucose concentrations are

significantly lower under these conditions, they are not nil (Roberts, 2007). Because our labeling medium did not contain glucose, it will be important to perform parallel studies with U^{13}C-β-hydroxybutyrate in the presence of minimal concentration of glucose that parallels brain glucose levels during starvation.

Increased contribution of ketone bodies to GABA pools in BAD mutant neurons is particularly interesting and previously unappreciated. This finding suggests that, in addition to increased open probability of K_{ATP} channels, which we have previously reported (Gimenez-Cassina et al., 2012), greater inhibitory neurotransmission through GABA may contribute to seizure resistance in BAD-deficient mice. The fact that increased GABA pools in *Bad* -/- neurons are associated with significantly higher ^{13}C enrichment in glutamate suggests BAD-dependent changes in glutamate handling (Figure 5.2B). This idea is further consistent with published report that ketogenic diets alter amino acid handling in the brain, leading to increased availability of glutamate for GABA synthesis (Yudkoff et al., 2008; Yudkoff et al., 2007). It has been proposed that in ketotic brain, the astrocytic glutamate-glutamine cycle is intensified (Figure 1.2), providing GABAergic neurons with more glutamine, which can be subsequently used for GABA synthesis upon conversion to glutamate (Figure 5.2A). In addition, transamination of glutamate with oxaloacetate, which generates aspartate through the AST reaction (Figure 5.2A), is diminished in ketotic brain, ensuring more glutamate is instead available for GABA synthesis. Reduced glutamine transamination in this setting is proposed to stem from lower oxaloacetate pool due to enhanced mitochondrial citrate synthesis in response to ketone bodies (Mason et al., 1995; Yudkoff et al., 2007; Yudkoff et al., 1997; Yudkoff et al., 1994).

Our data are partly consistent with the proposed effect of ketone bodies on glutamate handling as detailed above in that we find higher incorporation of β-hydroxybutyrate-derived carbons in glutamate. However, we do not detect increased citrate pools or decreased aspartate levels (Figure 5.1C). It is possible that citrate is being used immediately after production so that no differences were apparent at the time point our measurements were taken. Regardless, detailed studies using ^{15}N- and ^{13}C-labeled glutamine, glutamate and aspartate tracers are needed to establish if and how glutamate handling might be altered

following BAD modifications. It is also important to note that, given the metabolic communication between astrocytes and GABAergic neurons, similar tracer studies in experimental settings that better emulate the physiologic milieu of neurons may provide additional valuable insights. Such settings include nerve endings, synaptosomes, brain slices or neuron-astrocyte co-cultures. Lastly, it would be important to determine if any changes in glutamate handling are a mere byproduct of reduced glucose metabolism in BAD-deficient neurons or require active supply and utilization of ketone bodies.

CHAPTER 6

General Discussion and Future Perspectives

The findings and concepts described in the preceding chapters are an example of how cells' fuel choice can fundamentally and profoundly change cellular fate, function and behavior. In the case of neurons, the majority of our work continues to focus on the outcome of fuel choice on energy metabolism and biosynthetic power that culminates in the regulation of neurotransmission and ultimately affects seizure responses. Yet, we are increasingly aware that, beyond changes in ATP and biosynthetic precursors, fuel metabolism can be interlaced with every fabric of cell physiology through programmatic changes in gene expression, epigenetic modifications, as well as cellular signaling. Understanding how fuel choices are established and defining their outcomes will provide a powerful handle on modulating cellular behavior in normal physiology and in pathologic conditions. Inspired by these concepts, we have used the following sections to discuss our work in the broader context of molecular mechanisms and physiologic consequences of fuel choice.

6.1 Glucose *versus* ketone bodies: Mechanisms of fuel choice and fuel competition

Glucose and ketone bodies are both physiologic fuels in the brain. While ketone bodies are predominant under glucose limiting conditions, glucose concentrations in neurons never reach zero. This raises important questions about mechanisms of fuel selection. How are neurons cued to preferentially metabolize one particular carbon substrate when they have access to both? What are the mechanisms underlying "fuel competition"?

Perhaps one of the best understood paradigms of fuel competition is the Randle cycle, also known as the glucose-fatty acid cycle (Hue and Taegtmeyer, 2009; Roberts, 2007). This mechanism of fuel competition involves inhibition of glucose metabolism by fatty acids and ketone bodies at several steps during the glycolytic and mitochondrial processing of glucose carbons. This is predominantly brought about by the rise in the mitochondrial acetyl-CoA to CoA and NADH to NAD^+ ratios following fatty acid and ketone body utilization. Both acetyl-CoA and NADH inhibit pyruvate dehydrogenase (PDH) and subsequent oxidation of glucose-derived pyruvate in the TCA cycle. Elevated mitochondrial citrate synthesis in

response to fatty acids and ketone bodies can also lead to increased cytosolic citrate, which inhibits phosphofructokinase (PFK)1, a key regulatory enzyme of the glycolytic pathway (Figure 1.1) (Randle, 1981; Reed, 1981; Roberts, 2007). Lastly, PFK1 inhibition may result in accumulation of glucose-6-phosphate and inhibition of low *K*m hexokinase isoforms. A second, but less understood, component of the Randle cycle is glucose inhibition of fatty acid and ketone body utilization. Several biochemical explanations have been put forward for this aspect (Hue and Taegtmeyer, 2009), however, their broad applicability to cell types beyond endocrine cells is not known. It is also less clear how glucose might inhibit ketone body oxidation.

While the Randle cycle is best known for controlling fuel choice in the muscle, a similar mechanism may also exist in the brain. A recent report showed that, in hippocampal slices incubated with glucose alone or β-hydroxybutyrate and glucose, β-hydroxybutyrate becomes the predominant fuel used for acetyl-CoA production even in the presence of glucose (Valente-Silva et al., 2015). At least two testable possibilities could explain these findings. *First*, a Randle-cycle-like mechanism may be operative, whereby PFK and PDH are inhibited. *Second*, when both fuels are present, glucose may be mainly used for glycolytic ATP production while ketone bodies may sustain a higher fraction of mitochondrial metabolism in neurons, thereby increasing the provision of biosynthetic precursors for neurotransmitter synthesis (discussed in Chapters 1 and 5). A testable prediction for this second possibility is that PDH, but not PFK, is inhibited when both fuels are present. Regardless, the study by Valente-Silva *et al*. suggests that, when present, ketone bodies may trump glucose utilization. This would assign a critical regulatory role to mechanisms in charge of the supply and uptake of ketone bodies in the brain. If applicable to fuel utilization patterns in BAD mutant neurons, this could suggest that reduced glycolytic flux in *Bad* -/- and S155 neurons may be primarily the outcome of increased ketone body metabolism. This possibility can be formally tested, in part, by incubating BAD mutant neurons with both fuels and tracing the contribution of each to the TCA cycle, as well as assessing the effect of β-hydroxybutyrate on glycolytic flux. By comparing these measurements with conditions, where only glucose or β-hydroxybutyrate is present (Chapters

3 and 5), one can draw informative conclusions as to how competition between these two fuels might shape the metabolite profiles in neurons.

It is important to note that any discussion on mechanisms underlying glucose *versus* ketone body selection in the brain and its effect on neuronal excitability and seizure sensitivity should also take into account the observation that both low glycemic *and* ketogenic diets are seizure protective (Muzykewicz et al., 2009; Neal et al., 2009; Pfeifer and Thiele, 2005). In addition, published studies indicate that the effect of ketogenic diet can be reversed by glucose infusion (Pfeifer and Thiele, 2005), supporting the idea that diminished glycolysis, rather than increase ketone body oxidation, may potentially be more important. However, this conclusion is based on whole-body systemic observations, and requires biochemical characterization at the cellular level. Lastly, it is also possible that either reduced glucose utilization or increased ketone body consumption may be sufficient to produce the metabolic changes associated with a glucose-to-ketone body fuel switch. This could suggest that utilization of these two fuels is tightly cross-regulated so that reduced metabolism of one would augment that of the other and vice versa.

The above considerations emphasize the need for more detailed dissection of mechanisms underlying fuel selection. Such efforts will be best born out using experimental systems that enable acute and reversible manipulation of neuronal preference for glucose *versus* ketone bodies. Within this context, acute reconstitution of *Bad* -/- neurons with a BAD S155 phospho-mimic variant (S155D) *versus* a phospho-deficient (S155A) mutant can be a valuable approach. Based on our findings, BAD S155D will produce a metabolic scenario where glucose utilization is preferred over ketone body metabolism (Figure 1.4), while BAD S155A will have the opposite effect, providing a controlled system to then define the minimal downstream metabolic trigger that establishes the fuel preference in neurons.

6.2 Fuel-driven metabolic signaling

Fuel substrate metabolism can have important effects on neuronal fate and function beyond energy production and biosynthetic input into neurotransmitter synthesis. Within this context, the ability of certain fuel-derived metabolites to influence cell signaling and gene

expression is particularly interesting because it expands the functional consequences of fuel metabolism to additional aspects of cellular regulation.

Increasing evidence indicates specific roles for fuel substrates and their downstream metabolites in epigenetic and transcriptional regulation (Gut and Verdin, 2013; Kaelin and McKnight, 2013; Katada et al., 2012). For example, β-hydroxybutyrate is a potent endogenous inhibitor of histone deacetylases (HDACs), and its administration to cells or mice leads to dose-dependent histone hyperacetylation and Forkheadbox (Foxo) 3 upregulation (Newman and Verdin, 2014a, b; Shimazu et al., 2010). Furthermore, changes in acetyl-CoA, α-ketoglutarate, and S-adenosylmethionine (SAM) downstream of fuel substrate metabolism can impart additional epigenetic effects through changes in histone acetylation and histone/DNA methylation (Kaelin and McKnight, 2013). Ketotic state is also associated with increased activity of the peroxisome proliferator-activated receptor α (PPARα), which regulates the expression of multiple metabolic enzymes (Cullingford, 2008; Cullingford et al., 2002a; Cullingford et al., 2002b). These ketone body-dependent changes in epigenetic and transcriptional regulatory mechanisms are also consistent with microarray analyses of brain tissue from rodents treated with the ketogenic diet, which showed significant transcriptional changes in components of multiple cellular pathways (Bough et al., 2006).

In addition to effects on gene regulation, fuel metabolism can influence multiple aspects of cellular signaling. For example, several metabolic byproducts of fuel substrates, including acetyl-CoA, succinate, fumarate, S-adenosylmethionine (SAM), and UDP-GlcNAc can influence cell signaling through protein post-translational modifications (PTMs) such as acetylation, succinylation, succination, methylation, and O-GlcNAcylation (Kaelin and McKnight, 2013; Merkley et al., 2014). These modifications can have a wide range of effect on protein stability, activity, and protein-protein interaction within cells. Because distinct fuel substrates can differentially change the pool sizes of these metabolites and the PTMs they regulate, fuel-specific effects on cellular signaling can be predicted. For example, UDP-GlcNAc is generated through the hexosamine pathway downstream of glucose, and succinate can accumulate as a byproduct of ketone body breakdown as well as the GABA shunt (Figure 1.1). Therefore, a shift in fuel preference may be associated with specific alterations in PTMs

and cellular signaling. However, PTMs that are specifically triggered by altered fuel preference between glucose and ketone bodies in neurons and their functional outcomes have not been systemically explored. Given the advancements in protein mass spectrometry platforms that allow quantitative measurements of the diverse post-translational modifications (PTMs) noted above, this line of investigation is likely to yield important insights into how fuel choices may be interwoven with additional aspects of neuronal signaling and function.

6.3 Fuel preference and neurologic disorders: A therapeutic perspective

Understanding the molecular underpinnings of glucose *versus* ketone body utilization as they relate to the control of neuronal excitability will provide important insights into metabolic control of neurotransmission. However, the ultimate goal of this undertaking is to determine the implications of such metabolic regulation in the context of disease pathology. Is BAD-dependent control of fuel choice in the brain relevant to human epilepsy? The seizure protective effect of *Bad* alleles conferring a glucose-to-ketone-body fuel switch (*Bad*-null and *Bad* S155A) is evident from several chemical convulsant models of epilepsy in rodents (Gimenez-Cassina et al., 2012). These include kainic acid (KA) and pentylenetetrazole (PTZ), which stimulate excitatory glutamate receptors or antagonize GABAergic inhibitory receptors, respectively. Such acute convulsant models are an efficient way of assessing seizure susceptibility, and have been used in many small molecule screens for anticonvulsants. Although a good starting point, these pharmacologic models are, however, not sufficient for modelling human epilepsy, especially considering the multiple forms and complex etiology of epilepsy in humans. For this reason, the broad therapeutic implications of the BAD-dependent fuel preference in the control of seizure responses can be best established using a chronic epilepsy model, with the occurrence of spontaneous seizures over an extended period similar to human epilepsy. A valuable genetic tool in this case is the *Kcna*1-null mouse (Smart et al., 1998), which exhibits frequent convulsive seizures throughout adult life due to the loss of the voltage-gated potassium channel. It will be important to determine whether *Bad*-null or S155D mutations in the *Kcna*1-null genetic background will similarly confer seizure protection as in chemical convulsant models.

Altered fuel preference may also have therapeutic implications in neurologic conditions beyond seizure disorders, including neurodegeneration, traumatic brain injuries, and CNS tumors. In a recent randomized study of patients with mild to moderate Alzheimer disease, a ketogenic compound improved cognitive functions (Hertz et al., 2015). Similarly, a small cohort of Parkinson disease (PD) patients showed improvement on the ketogenic diet (Vanitallie et al., 2005). In all these cases, increased mitochondrial function and/or biogenesis has been proposed as a mechanism of neuro-protection by increased ketone body utilization. For example, ketone bodies may bypass mitochondrial respiratory complex I deficiency in PD because their breakdown can generate succinate (Figure 1.1), preferentially activating succinate dehydrogenase also known as the mitochondrial respiratory complex II. Whether the protective effects of ketone bodies in these settings also include more direct effects on neurotransmission is not clear. The efficacy of ketogenic diet may also extend to certain malignant brain tumors such as glioblastoma multiforme (GBM) (Maroon et al., 2015; Seyfried et al., 2008; Zhou et al., 2007; Zuccoli et al., 2010). As opposed to neurons and astrocytes that can consume multiple fuels, GBM cancer cells are extremely reliant on glycolysis making them especially vulnerable to the ketogenic diet. The molecular underpinning of this toxicity is not known. One possibility is that glucose dependency in these tumors is a metabolic vulnerability so that inhibition of glycolysis by ketone bodies (section 6.1 above) is particularly toxic to these cancers. Another aspect of this metabolic vulnerability could be that glucose-derived metabolites in these cancers make important contribution to biomass synthesis for tumor growth (Lunt and Vander Heiden, 2011), which is not recapitulated by ketone body-derived metabolites.

The aforementioned examples underscore the broader potential implications of altered fuel preference in disease pathophysiology. In the fullness of time, identification of the molecular mechanisms that control the reciprocal utilization of glucose and ketone bodies, and the consequences of metabolic fuel choice in the brain could profoundly impact the development of better therapies for these neurologic diseases.

CHAPTER 7

References

Agostini, M., Romeo, F., Inoue, S., Niklison-Chirou, M.V., Elia, A.J., Dinsdale, D., Morone, N., Knight, R.A., Mak, T.W., and Melino, G. (2016). Metabolic reprogramming during neuronal differentiation. Cell Death Differ.

Ahn, W.S., and Antoniewicz, M.R. (2013). Parallel labeling experiments with [1,2-(13)C]glucose and [U-(13)C]glutamine provide new insights into CHO cell metabolism. Metabolic engineering *15*, 34-47.

Auestad, N., Korsak, R.A., Morrow, J.W., and Edmond, J. (1991). Fatty acid oxidation and ketogenesis by astrocytes in primary culture. Journal of neurochemistry *56*, 1376-1386.

Bak, L.K., Schousboe, A., Sonnewald, U., and Waagepetersen, H.S. (2006). Glucose is necessary to maintain neurotransmitter homeostasis during synaptic activity in cultured glutamatergic neurons. Journal of cerebral blood flow and metabolism : official journal of the International Society of Cerebral Blood Flow and Metabolism *26*, 1285-1297.

Belanger, M., Allaman, I., and Magistretti, P.J. (2011). Brain energy metabolism: focus on astrocyte-neuron metabolic cooperation. Cell metabolism *14*, 724-738.

Bertram, E.H. (2009). Temporal lobe epilepsy: where do the seizures really begin? Epilepsy & behavior : E&B *14 Suppl 1*, 32-37.

Blazquez, C., Sanchez, C., Velasco, G., and Guzman, M. (1998). Role of carnitine palmitoyltransferase I in the control of ketogenesis in primary cultures of rat astrocytes. Journal of neurochemistry *71*, 1597-1606.

Bough, K.J., Wetherington, J., Hassel, B., Pare, J.F., Gawryluk, J.W., Greene, J.G., Shaw, R., Smith, Y., Geiger, J.D., and Dingledine, R.J. (2006). Mitochondrial biogenesis in the anticonvulsant mechanism of the ketogenic diet. Ann Neurol *60*, 223-235.

Buescher, J.M., Antoniewicz, M.R., Boros, L.G., Burgess, S.C., Brunengraber, H., Clish, C.B., DeBerardinis, R.J., Feron, O., Frezza, C., Ghesquiere, B., et al. (2015). A roadmap for interpreting (13)C metabolite labeling patterns from cells. Current opinion in biotechnology *34*, 189-201.

Cardaci, S., Zheng, L., MacKay, G., van den Broek, N.J., MacKenzie, E.D., Nixon, C., Stevenson, D., Tumanov, S., Bulusu, V., Kamphorst, J.J., et al. (2015). Pyruvate carboxylation enables growth of SDH-deficient cells by supporting aspartate biosynthesis. Nature cell biology *17*, 1317-1326.

Cavallucci, V., Fidaleo, M., and Pani, G. (2016). Neural Stem Cells and Nutrients: Poised Between Quiescence and Exhaustion. Trends in endocrinology and metabolism: TEM.

Chi, X., Kale, J., Leber, B., and Andrews, D.W. (2014). Regulating cell death at, on, and in membranes. Biochimica et biophysica acta *1843*, 2100-2113.

Chih, C.-P., Lipton, P., and Roberts, E.L. (2001). Do active cerebral neurons really use lactate rather than glucose? Trends in Neurosciences *24*, 573-578.

Cholet, N., Pellerin, L., Welker, E., Lacombe, P., Seylaz, J., Magistretti, P., and Bonvento, G. (2001). Local injection of antisense oligonucleotides targeted to the glial glutamate transporter GLAST decreases the metabolic response to somatosensory activation. Journal of cerebral blood flow and metabolism : official journal of the International Society of Cerebral Blood Flow and Metabolism *21*, 404-412.

Chowdhury, G.M., Gupta, M., Gibson, K.M., Patel, A.B., and Behar, K.L. (2007). Altered cerebral glucose and acetate metabolism in succinic semialdehyde dehydrogenase-deficient mice: evidence for glial dysfunction and reduced glutamate/glutamine cycling. Journal of neurochemistry *103*, 2077-2091.

Cortez, M.A., Wu, Y., Gibson, K.M., and Snead, O.C., 3rd (2004). Absence seizures in succinic semialdehyde dehydrogenase deficient mice: a model of juvenile absence epilepsy. Pharmacology, biochemistry, and behavior *79*, 547-553.

Cullingford, T. (2008). Peroxisome proliferator-activated receptor alpha and the ketogenic diet. Epilepsia *49 Suppl 8*, 70-72.

Cullingford, T.E., Dolphin, C.T., and Sato, H. (2002a). The peroxisome proliferator-activated receptor alpha-selective activator ciprofibrate upregulates expression of genes encoding fatty acid oxidation and ketogenesis enzymes in rat brain. Neuropharmacology *42*, 724-730.

Cullingford, T.E., Eagles, D.A., and Sato, H. (2002b). The ketogenic diet upregulates expression of the gene encoding the key ketogenic enzyme mitochondrial 3-hydroxy-3-methylglutaryl-CoA synthase in rat brain. Epilepsy Res *49*, 99-107.

Czabotar, P.E., Lessene, G., Strasser, A., and Adams, J.M. (2014). Control of apoptosis by the BCL-2 protein family: implications for physiology and therapy. Nature reviews. Molecular cell biology *15*, 49-63.

Danial, N.N. (2008). BAD: undertaker by night, candyman by day. Oncogene *27 Suppl 1*, S53-70.

Danial, N.N., Gramm, C.F., Scorrano, L., Zhang, C.Y., Krauss, S., Ranger, A.M., Datta, S.R., Greenberg, M.E., Licklider, L.J., Lowell, B.B., et al. (2003). BAD and glucokinase reside in a mitochondrial complex that integrates glycolysis and apoptosis. Nature *424*, 952-956.

Danial, N.N., and Korsmeyer, S.J. (2004). Cell death: critical control points. Cell *116*, 205-219.

Danial, N.N., Walensky, L.D., Zhang, C.Y., Choi, C.S., Fisher, J.K., Molina, A.J., Datta, S.R., Pitter, K.L., Bird, G.H., Wikstrom, J.D., et al. (2008). Dual role of proapoptotic BAD in insulin secretion and beta cell survival. Nature medicine *14*, 144-153.

Deng, H., Yu, F., Chen, J., Zhao, Y., Xiang, J., and Lin, A. (2008). Phosphorylation of Bad at Thr-201 by JNK1 promotes glycolysis through activation of phosphofructokinase-1. The Journal of biological chemistry *283*, 20754-20760.

DeNicola, G.M., Chen, P.H., Mullarky, E., Sudderth, J.A., Hu, Z., Wu, D., Tang, H., Xie, Y., Asara, J.M., Huffman, K.E., et al. (2015). NRF2 regulates serine biosynthesis in non-small cell lung cancer. Nat Genet *47*, 1475-1481.

DeVivo, D.C., Leckie, M.P., Ferrendelli, J.S., and McDougal, D.B., Jr. (1978). Chronic ketosis and cerebral metabolism. Ann Neurol *3*, 331-337.

Dienel, G.A. (2012). Fueling and imaging brain activation. ASN Neuro *4*.

DiNuzzo, M., Mangia, S., Maraviglia, B., and Giove, F. (2010). Changes in glucose uptake rather than lactate shuttle take center stage in subserving neuroenergetics: evidence from mathematical modeling. Journal of cerebral blood flow and metabolism : official journal of the International Society of Cerebral Blood Flow and Metabolism *30*, 586-602.

Duarte, J.M., Girault, F.M., and Gruetter, R. (2015). Brain energy metabolism measured by (13)C magnetic resonance spectroscopy in vivo upon infusion of [3-(13)C]lactate. Journal of neuroscience research *93*, 1009-1018.

Dunn-Meynell, A.A., Rawson, N.E., and Levin, B.E. (1998). Distribution and phenotype of neurons containing the ATP-sensitive K+ channel in rat brain. Brain Res *814*, 41-54.

Ebert, D., Haller, R.G., and Walton, M.E. (2003). Energy contribution of octanoate to intact rat brain metabolism measured by 13C nuclear magnetic resonance spectroscopy. The Journal of neuroscience : the official journal of the Society for Neuroscience *23*, 5928-5935.

Elias, J.E., and Gygi, S.P. (2007). Target-decoy search strategy for increased confidence in large-scale protein identifications by mass spectrometry. Nature methods *4*, 207-214.

Eng, J.K., McCormack, A.L., and Yates, J.R. (1994). An approach to correlate tandem mass spectral data of peptides with amino acid sequences in a protein database. Journal of the American Society for Mass Spectrometry *5*, 976-989.

Erecinska, M., Nelson, D., Daikhin, Y., and Yudkoff, M. (1996). Regulation of GABA level in rat brain synaptosomes: fluxes through enzymes of the GABA shunt and effects of glutamate, calcium, and ketone bodies. Journal of neurochemistry *67*, 2325-2334.

Faubert, B., Vincent, E.E., Griss, T., Samborska, B., Izreig, S., Svensson, R.U., Mamer, O.A., Avizonis, D., Shackelford, D.B., Shaw, R.J., et al. (2014). Loss of the tumor suppressor LKB1 promotes metabolic reprogramming of cancer cells via HIF-1alpha. Proceedings of the National Academy of Sciences of the United States of America *111*, 2554-2559.

Fenton, R.A., Brond, L., Nielsen, S., and Praetorius, J. (2007). Cellular and subcellular distribution of the type-2 vasopressin receptor in the kidney. Am J Physiol Renal Physiol *293*, F748-760.

Furukawa, N., Ongusaha, P., Jahng, W.J., Araki, K., Choi, C.S., Kim, H.J., Lee, Y.H., Kaibuchi, K., Kahn, B.B., Masuzaki, H., et al. (2005). Role of Rho-kinase in regulation of insulin action and glucose homeostasis. Cell metabolism *2*, 119-129.

Gandhi, G.K., Cruz, N.F., Ball, K.K., and Dienel, G.A. (2009). Astrocytes are poised for lactate trafficking and release from activated brain and for supply of glucose to neurons. Journal of neurochemistry *111*, 522-536.

Garriga-Canut, M., Schoenike, B., Qazi, R., Bergendahl, K., Daley, T.J., Pfender, R.M., Morrison, J.F., Ockuly, J., Stafstrom, C., Sutula, T., et al. (2006). 2-Deoxy-D-glucose reduces epilepsy progression by NRSF-CtBP-dependent metabolic regulation of chromatin structure. Nature neuroscience *9*, 1382-1387.

Genda, E.N., Jackson, J.G., Sheldon, A.L., Locke, S.F., Greco, T.M., O'Donnell, J.C., Spruce, L.A., Xiao, R., Guo, W., Putt, M., et al. (2011). Co-compartmentalization of the astroglial glutamate transporter, GLT-1, with glycolytic enzymes and mitochondria. The Journal of neuroscience : the official journal of the Society for Neuroscience *31*, 18275-18288.

Gimenez-Cassina, A., and Danial, N.N. (2015). Regulation of mitochondrial nutrient and energy metabolism by BCL-2 family proteins. Trends in endocrinology and metabolism: TEM *26*, 165-175.

Gimenez-Cassina, A., Garcia-Haro, L., Choi, C.S., Osundiji, M.A., Lane, E.A., Huang, H., Yildirim, M.A., Szlyk, B., Fisher, J.K., Polak, K., et al. (2014). Regulation of hepatic energy metabolism and gluconeogenesis by BAD. Cell metabolism *19*, 272-284.

Gimenez-Cassina, A., Martinez-Francois, J.R., Fisher, J.K., Szlyk, B., Polak, K., Wiwczar, J., Tanner, G.R., Lutas, A., Yellen, G., and Danial, N.N. (2012). BAD-dependent regulation of fuel metabolism and K(ATP) channel activity confers resistance to epileptic seizures. Neuron *74*, 719-730.

Grinberg, M., Schwarz, M., Zaltsman, Y., Eini, T., Niv, H., Pietrokovski, S., and Gross, A. (2005). Mitochondrial carrier homolog 2 is a target of tBID in cells signaled to die by tumor necrosis factor alpha. Molecular and cellular biology *25*, 4579-4590.

Gut, P., and Verdin, E. (2013). The nexus of chromatin regulation and intermediary metabolism. Nature *502*, 489-498.

Hartman, A.L., Gasior, M., Vining, E.P., and Rogawski, M.A. (2007). The neuropharmacology of the ketogenic diet. Pediatric neurology *36*, 281-292.

Hassel, B., and Brathe, A. (2000a). Cerebral metabolism of lactate in vivo: evidence for neuronal pyruvate carboxylation. Journal of cerebral blood flow and metabolism : official journal of the International Society of Cerebral Blood Flow and Metabolism *20*, 327-336.

Hassel, B., and Brathe, A. (2000b). Neuronal pyruvate carboxylation supports formation of transmitter glutamate. The Journal of neuroscience : the official journal of the Society for Neuroscience *20*, 1342-1347.

Heidenrich, K.A., Gilmore, P.R., and Garvey, W.T. (1989). Glucose transport in primary cultured neurons. Journal of neuroscience research *22*, 397-407.

Herard, A.S., Dubois, A., Escartin, C., Tanaka, K., Delzescaux, T., Hantraye, P., and Bonvento, G. (2005). Decreased metabolic response to visual stimulation in the superior colliculus of mice lacking the glial glutamate transporter GLT-1. The European journal of neuroscience *22*, 1807-1811.

Hertz, L., Chen, Y., and Waagepetersen, H.S. (2015). Effects of ketone bodies in Alzheimer's disease in relation to neural hypometabolism, beta-amyloid toxicity, and astrocyte function. Journal of neurochemistry *134*, 7-20.

Hertz, L., and Hertz, E. (2003). Cataplerotic TCA cycle flux determined as glutamate-sustained oxygen consumption in primary cultures of astrocytes. Neurochemistry international *43*, 355-361.

Hertz, L., and Rodrigues, T.B. (2014). Astrocytic-Neuronal-Astrocytic Pathway Selection for Formation and Degradation of Glutamate/GABA. Frontiers in endocrinology *5*, 42.

Holding, A.N. (2015). XL-MS: Protein cross-linking coupled with mass spectrometry. Methods *89*, 54-63.

Hue, L., and Taegtmeyer, H. (2009). The Randle cycle revisited: a new head for an old hat. Am J Physiol Endocrinol Metab *297*, E578-591.

Jarrett, S.G., Milder, J.B., Liang, L.P., and Patel, M. (2008). The ketogenic diet increases mitochondrial glutathione levels. Journal of neurochemistry *106*, 1044-1051.

Juge, N., Gray, J.A., Omote, H., Miyaji, T., Inoue, T., Hara, C., Uneyama, H., Edwards, R.H., Nicoll, R.A., and Moriyama, Y. (2010). Metabolic control of vesicular glutamate transport and release. Neuron *68*, 99-112.

Kaelin, W.G., Jr., and McKnight, S.L. (2013). Influence of metabolism on epigenetics and disease. Cell *153*, 56-69.

Karschin, C., Ecke, C., Ashcroft, F.M., and Karschin, A. (1997). Overlapping distribution of K(ATP) channel-forming Kir6.2 subunit and the sulfonylurea receptor SUR1 in rodent brain. FEBS letters *401*, 59-64.

Katada, S., Imhof, A., and Sassone-Corsi, P. (2012). Connecting threads: epigenetics and metabolism. Cell *148*, 24-28.

Kim, D.Y., Davis, L.M., Sullivan, P.G., Maalouf, M., Simeone, T.A., van Brederode, J., and Rho, J.M. (2007). Ketone bodies are protective against oxidative stress in neocortical neurons. Journal of neurochemistry *101*, 1316-1326.

Kramer, M.A., and Cash, S.S. (2012). Epilepsy as a disorder of cortical network organization. Neuroscientist *18*, 360-372.

Kreft, M., Bak, L.K., Waagepetersen, H.S., and Schousboe, A. (2012). Aspects of astrocyte energy metabolism, amino acid neurotransmitter homoeostasis and metabolic compartmentation. ASN Neuro *4*, 187-199.

Lewis, C.A., Parker, S.J., Fiske, B.P., McCloskey, D., Gui, D.Y., Green, C.R., Vokes, N.I., Feist, A.M., Vander Heiden, M.G., and Metallo, C.M. (2014). Tracing compartmentalized NADPH metabolism in the cytosol and mitochondria of mammalian cells. Molecular cell *55*, 253-263.

Ljubicic, S., Polak, K., Fu, A., Wiwczar, J., Szlyk, B., Chang, Y., Alvarez-Perez, J.C., Bird, G.H., Walensky, L.D., Garcia-Ocana, A., et al. (2015). Phospho-BAD BH3 mimicry protects beta cells and restores functional beta cell mass in diabetes. Cell Rep *10*, 497-504.

Lund, T.M., Risa, O., Sonnewald, U., Schousboe, A., and Waagepetersen, H.S. (2009). Availability of neurotransmitter glutamate is diminished when beta-hydroxybutyrate replaces glucose in cultured neurons. Journal of neurochemistry *110*, 80-91.

Lundgaard, I., Li, B., Xie, L., Kang, H., Sanggaard, S., Haswell, J.D., Sun, W., Goldman, S., Blekot, S., Nielsen, M., et al. (2015). Direct neuronal glucose uptake heralds activity-dependent increases in cerebral metabolism. Nat Commun *6*, 6807.

Lunt, S.Y., and Vander Heiden, M.G. (2011). Aerobic glycolysis: meeting the metabolic requirements of cell proliferation. Annual review of cell and developmental biology *27*, 441-464.

Lutas, A., Birnbaumer, L., and Yellen, G. (2014). Metabolism regulates the spontaneous firing of substantia nigra pars reticulata neurons via KATP and nonselective cation channels. The Journal of neuroscience : the official journal of the Society for Neuroscience *34*, 16336-16347.

Lutas, A., and Yellen, G. (2013). The ketogenic diet: metabolic influences on brain excitability and epilepsy. Trends Neurosci *36*, 32-40.

Ma, W., Berg, J., and Yellen, G. (2007). Ketogenic diet metabolites reduce firing in central neurons by opening K(ATP) channels. The Journal of neuroscience : the official journal of the Society for Neuroscience *27*, 3618-3625.

Maalouf, M., Sullivan, P.G., Davis, L., Kim, D.Y., and Rho, J.M. (2007). Ketones inhibit mitochondrial production of reactive oxygen species production following glutamate excitotoxicity by increasing NADH oxidation. Neuroscience *145*, 256-264.

Magistretti, P.J., and Pellerin, L. (1999). Cellular mechanisms of brain energy metabolism and their relevance to functional brain imaging. Philos Trans R Soc Lond B Biol Sci *354*, 1155-1163.

Maher, F., Davies-Hill, T.M., and Simpson, I.A. (1996). Substrate specificity and kinetic parameters of GLUT3 in rat cerebellar granule neurons. The Biochemical journal *315 (Pt 3)*, 827-831.

Mamer, O., Gravel, S.P., Choiniere, L., Chenard, V., St-Pierre, J., and Avizonis, D. (2013). The complete targeted profile of the organic acid intermediates of the citric acid cycle using a single stable isotope dilution analysis, sodium borodeuteride reduction and selected ion monitoring GC/MS. Metabolomics *9*, 1019-1030.

Mangia, S., Simpson, I.A., Vannucci, S.J., and Carruthers, A. (2009). The in vivo neuron-to-astrocyte lactate shuttle in human brain: evidence from modeling of measured lactate levels during visual stimulation. Journal of neurochemistry *109 Suppl 1*, 55-62.

Marcondes, M.C., Sola-Penna, M., Torres Rda, S., and Zancan, P. (2011). Muscle-type 6-phosphofructo-1-kinase and aldolase associate conferring catalytic advantages for both enzymes. IUBMB life *63*, 435-445.

Maroon, J.C., Seyfried, T.N., Donohue, J.P., and Bost, J. (2015). The role of metabolic therapy in treating glioblastoma multiforme. Surg Neurol Int *6*, 61.

Masino, S.A., Li, T., Theofilas, P., Sandau, U.S., Ruskin, D.N., Fredholm, B.B., Geiger, J.D., Aronica, E., and Boison, D. (2011). A ketogenic diet suppresses seizures in mice through adenosine A(1) receptors. The Journal of clinical investigation *121*, 2679-2683.

Mason, G.F., Gruetter, R., Rothman, D.L., Behar, K.L., Shulman, R.G., and Novotny, E.J. (1995). Simultaneous determination of the rates of the TCA cycle, glucose utilization, alpha-ketoglutarate/glutamate exchange, and glutamine synthesis in human brain by NMR. Journal of cerebral blood flow and metabolism : official journal of the International Society of Cerebral Blood Flow and Metabolism *15*, 12-25.

Matschinsky, F.M. (2009). Assessing the potential of glucokinase activators in diabetes therapy. Nat Rev Drug Discov *8*, 399-416.

Matsumoto, H., and Ito, M. (1985). Aspartate metabolism in rats during aging. Experimental gerontology *20*, 187-191.

McAlister, G.C., Nusinow, D.P., Jedrychowski, M.P., Wuhr, M., Huttlin, E.L., Erickson, B.K., Rad, R., Haas, W., and Gygi, S.P. (2014). MultiNotch MS3 enables accurate, sensitive, and multiplexed detection of differential expression across cancer cell line proteomes. Anal Chem *86*, 7150-7158.

McGuirk, S., Gravel, S.P., Deblois, G., Papadopoli, D.J., Faubert, B., Wegner, A., Hiller, K., Avizonis, D., Akavia, U.D., Jones, R.G., et al. (2013). PGC-1alpha supports glutamine metabolism in breast cancer. Cancer Metab *1*, 22.

McKenna, M.C. (2012). Substrate competition studies demonstrate oxidative metabolism of glucose, glutamate, glutamine, lactate and 3-hydroxybutyrate in cortical astrocytes from rat brain. Neurochemical research *37*, 2613-2626.

McKenna, M.C. (2013). Glutamate pays its own way in astrocytes. Frontiers in endocrinology *4*, 191.

McKenna, M.C., Waagepetersen, H.S., Schousboe, A., and Sonnewald, U. (2006). Neuronal and astrocytic shuttle mechanisms for cytosolic-mitochondrial transfer of reducing equivalents: current evidence and pharmacological tools. Biochem Pharmacol *71*, 399-407.

Melo, T.M., Nehlig, A., and Sonnewald, U. (2006). Neuronal-glial interactions in rats fed a ketogenic diet. Neurochemistry international *48*, 498-507.

Menard, L., Maughan, D., and Vigoreaux, J. (2014). The structural and functional coordination of glycolytic enzymes in muscle: evidence of a metabolon? Biology *3*, 623-644.

Mergenthaler, P., Lindauer, U., Dienel, G.A., and Meisel, A. (2013). Sugar for the brain: the role of glucose in physiological and pathological brain function. Trends Neurosci *36*, 587-597.

Merkley, E.D., Metz, T.O., Smith, R.D., Baynes, J.W., and Frizzell, N. (2014). The succinated proteome. Mass spectrometry reviews *33*, 98-109.

Metallo, C.M., Gameiro, P.A., Bell, E.L., Mattaini, K.R., Yang, J., Hiller, K., Jewell, C.M., Johnson, Z.R., Irvine, D.J., Guarente, L., et al. (2012). Reductive glutamine metabolism by IDH1 mediates lipogenesis under hypoxia. Nature *481*, 380-384.

Moldoveanu, T., Follis, A.V., Kriwacki, R.W., and Green, D.R. (2014). Many players in BCL-2 family affairs. Trends in biochemical sciences *39*, 101-111.

Montal, E.D., Dewi, R., Bhalla, K., Ou, L., Hwang, B.J., Ropell, A.E., Gordon, C., Liu, W.J., DeBerardinis, R.J., Sudderth, J., et al. (2015). PEPCK Coordinates the Regulation of Central Carbon Metabolism to Promote Cancer Cell Growth. Molecular cell *60*, 571-583.

Morken, T.S., Brekke, E., Haberg, A., Wideroe, M., Brubakk, A.M., and Sonnewald, U. (2014). Neuron-astrocyte interactions, pyruvate carboxylation and the pentose phosphate pathway in the neonatal rat brain. Neurochemical research *39*, 556-569.

Muzykewicz, D.A., Lyczkowski, D.A., Memon, N., Conant, K.D., Pfeifer, H.H., and Thiele, E.A. (2009). Efficacy, safety, and tolerability of the low glycemic index treatment in pediatric epilepsy. Epilepsia *50*, 1118-1126.

Nanchen, A., Fuhrer, T., and Sauer, U. (2007). Determination of metabolic flux ratios from 13C-experiments and gas chromatography-mass spectrometry data: protocol and principles. Methods in molecular biology *358*, 177-197.

Neal, E.G., Chaffe, H., Schwartz, R.H., Lawson, M.S., Edwards, N., Fitzsimmons, G., Whitney, A., and Cross, J.H. (2009). A randomized trial of classical and medium-chain triglyceride ketogenic diets in the treatment of childhood epilepsy. Epilepsia *50*, 1109-1117.

Newman, J.C., and Verdin, E. (2014a). beta-hydroxybutyrate: much more than a metabolite. Diabetes Res Clin Pract *106*, 173-181.

Newman, J.C., and Verdin, E. (2014b). Ketone bodies as signaling metabolites. Trends in endocrinology and metabolism: TEM *25*, 42-52.

Okada, Y., and Lipton, P. (2007). 1.2 Glucose, Oxidative Energy Metabolism, and Neural Function in Brain Slices—Glycolysis Plays a Key Role in Neural Activity. In Handbook of Neurochemistry and Molecular Neurobiology: Brain Energetics. Integration of Molecular and Cellular Processes. A. Lajtha, G.E. Gibson, and G.A. Dienel, eds. (Boston, MA: Springer US), pp. 17-39.

Owen, O.E., Kalhan, S.C., and Hanson, R.W. (2002). The key role of anaplerosis and cataplerosis for citric acid cycle function. The Journal of biological chemistry *277*, 30409-30412.

Owen, O.E., Morgan, A.P., Kemp, H.G., Sullivan, J.M., Herrera, M.G., and Cahill, G.F., Jr. (1967). Brain metabolism during fasting. The Journal of clinical investigation *46*, 1589-1595.

Pacold, M.E., Brimacombe, K.R., Chan, S.H., Rohde, J.M., Lewis, C.A., Swier, L.J., Possemato, R., Chen, W.W., Sullivan, L.B., Fiske, B.P., et al. (2016). A PHGDH inhibitor reveals coordination of serine synthesis and one-carbon unit fate. Nature chemical biology *12*, 452-458.

Pan, J.W., Bebin, E.M., Chu, W.J., and Hetherington, H.P. (1999). Ketosis and epilepsy: 31P spectroscopic imaging at 4.1 T. Epilepsia *40*, 703-707.

Patel, A.B., Lai, J.C., Chowdhury, G.M., Hyder, F., Rothman, D.L., Shulman, R.G., and Behar, K.L. (2014). Direct evidence for activity-dependent glucose phosphorylation in neurons with implications for the astrocyte-to-neuron lactate shuttle. Proceedings of the National Academy of Sciences of the United States of America *111*, 5385-5390.

Pekkurnaz, G., Trinidad, J.C., Wang, X., Kong, D., and Schwarz, T.L. (2014). Glucose regulates mitochondrial motility via Milton modification by O-GlcNAc transferase. Cell *158*, 54-68.

Pellerin, L., and Magistretti, P.J. (2004). Neuroenergetics: calling upon astrocytes to satisfy hungry neurons. Neuroscientist *10*, 53-62.

Perkins, J.R., Diboun, I., Dessailly, B.H., Lees, J.G., and Orengo, C. (2010). Transient protein-protein interactions: structural, functional, and network properties. Structure *18*, 1233-1243.

Pfeifer, H.H., and Thiele, E.A. (2005). Low-glycemic-index treatment: a liberalized ketogenic diet for treatment of intractable epilepsy. Neurology *65*, 1810-1812.

Possemato, R., Marks, K.M., Shaul, Y.D., Pacold, M.E., Kim, D., Birsoy, K., Sethumadhavan, S., Woo, H.K., Jang, H.G., Jha, A.K., et al. (2011). Functional genomics reveal that the serine synthesis pathway is essential in breast cancer. Nature *476*, 346-350.

Quaegebeur, A., Segura, I., Schmieder, R., Verdegem, D., Decimo, I., Bifari, F., Dresselaers, T., Eelen, G., Ghosh, D., Davidson, S.M., et al. (2016). Deletion or Inhibition of the Oxygen Sensor PHD1 Protects against Ischemic Stroke via Reprogramming of Neuronal Metabolism. Cell metabolism *23*, 280-291.

Rafalski, V.A., and Brunet, A. (2011). Energy metabolism in adult neural stem cell fate. Progress in neurobiology *93*, 182-203.

Randle, P.J. (1981). Phosphorylation-dephosphorylation cycles and the regulation of fuel selection in mammals. Current topics in cellular regulation *18*, 107-129.

Ranger, A.M., Zha, J., Harada, H., Datta, S.R., Danial, N.N., Gilmore, A.P., Kutok, J.L., Le Beau, M.M., Greenberg, M.E., and Korsmeyer, S.J. (2003). Bad-deficient mice develop diffuse large B cell lymphoma. Proceedings of the National Academy of Sciences of the United States of America *100*, 9324-9329.

Rappsilber, J. (2011). The beginning of a beautiful friendship: cross-linking/mass spectrometry and modelling of proteins and multi-protein complexes. Journal of structural biology *173*, 530-540.

Rappsilber, J., Mann, M., and Ishihama, Y. (2007). Protocol for micro-purification, enrichment, pre-fractionation and storage of peptides for proteomics using StageTips. Nature protocols *2*, 1896-1906.

Reed, L.J. (1981). Regulation of mammalian pyruvate dehydrogenase complex by a phosphorylation-dephosphorylation cycle. Current topics in cellular regulation *18*, 95-106.

Roberts, E.L. (2007). 2.1 The Support of Energy Metabolism in the Central Nervous System with Substrates Other than Glucose. In Handbook of Neurochemistry and Molecular Neurobiology: Brain Energetics. Integration of Molecular and Cellular Processes. A. Lajtha, G.E. Gibson, and G.A. Dienel, eds. (Boston, MA: Springer US), pp. 137-179.

Rowley, N.M., Madsen, K.K., Schousboe, A., and Steve White, H. (2012). Glutamate and GABA synthesis, release, transport and metabolism as targets for seizure control. Neurochemistry international *61*, 546-558.

Schousboe, A., Bak, L.K., and Waagepetersen, H.S. (2013). Astrocytic Control of Biosynthesis and Turnover of the Neurotransmitters Glutamate and GABA. Frontiers in endocrinology *4*, 102.

Seibenhener, M.L., and Wooten, M.W. (2012). Isolation and culture of hippocampal neurons from prenatal mice. J Vis Exp.

Serres, S., Raffard, G., Franconi, J.M., and Merle, M. (2008). Close coupling between astrocytic and neuronal metabolisms to fulfill anaplerotic and energy needs in the rat brain. Journal of cerebral blood flow and metabolism : official journal of the International Society of Cerebral Blood Flow and Metabolism *28*, 712-724.

Seyfried, T.N., Kiebish, M., Mukherjee, P., and Marsh, J. (2008). Targeting energy metabolism in brain cancer with calorically restricted ketogenic diets. Epilepsia *49 Suppl 8*, 114-116.

Shimazu, T., Hirschey, M.D., Hua, L., Dittenhafer-Reed, K.E., Schwer, B., Lombard, D.B., Li, Y., Bunkenborg, J., Alt, F.W., Denu, J.M., et al. (2010). SIRT3 deacetylates mitochondrial 3-hydroxy-3-methylglutaryl CoA synthase 2 and regulates ketone body production. Cell metabolism *12*, 654-661.

Simpson, I.A., Carruthers, A., and Vannucci, S.J. (2007). Supply and demand in cerebral energy metabolism: the role of nutrient transporters. Journal of cerebral blood flow and metabolism : official journal of the International Society of Cerebral Blood Flow and Metabolism *27*, 1766-1791.

Smart, S.L., Lopantsev, V., Zhang, C.L., Robbins, C.A., Wang, H., Chiu, S.Y., Schwartzkroin, P.A., Messing, A., and Tempel, B.L. (1998). Deletion of the K(V)1.1 potassium channel causes epilepsy in mice. Neuron *20*, 809-819.

Sonnewald, U. (2014). Glutamate synthesis has to be matched by its degradation - where do all the carbons go? Journal of neurochemistry *131*, 399-406.

Sonnewald, U., Westergaard, N., Petersen, S.B., Unsgard, G., and Schousboe, A. (1993). Metabolism of [U-13C]glutamate in astrocytes studied by 13C NMR spectroscopy: incorporation of more label into lactate than into glutamine demonstrates the importance of the tricarboxylic acid cycle. Journal of neurochemistry *61*, 1179-1182.

Stanley, I.A., Ribeiro, S.M., Gimenez-Cassina, A., Norberg, E., and Danial, N.N. (2014). Changing appetites: the adaptive advantages of fuel choice. Trends Cell Biol *24*, 118-127.

Szlyk, B., Braun, C.R., Ljubicic, S., Patton, E., Bird, G.H., Osundiji, M.A., Matschinsky, F.M., Walensky, L.D., and Danial, N.N. (2014). A phospho-BAD BH3 helix activates glucokinase by a mechanism distinct from that of allosteric activators. Nat Struct Mol Biol *21*, 36-42.

Tanner, G.R., Lutas, A., Martinez-Francois, J.R., and Yellen, G. (2011). Single K ATP channel opening in response to action potential firing in mouse dentate granule neurons. The Journal of neuroscience : the official journal of the Society for Neuroscience *31*, 8689-8696.

Valente-Silva, P., Lemos, C., Kofalvi, A., Cunha, R.A., and Jones, J.G. (2015). Ketone bodies effectively compete with glucose for neuronal acetyl-CoA generation in rat hippocampal slices. NMR in biomedicine *28*, 1111-1116.

Vanitallie, T.B., Nonas, C., Di Rocco, A., Boyar, K., Hyams, K., and Heymsfield, S.B. (2005). Treatment of Parkinson disease with diet-induced hyperketonemia: a feasibility study. Neurology *64*, 728-730.

Vincent, E.E., Sergushichev, A., Griss, T., Gingras, M.C., Samborska, B., Ntimbane, T., Coelho, P.P., Blagih, J., Raissi, T.C., Choiniere, L., et al. (2015). Mitochondrial Phosphoenolpyruvate Carboxykinase Regulates Metabolic Adaptation and Enables Glucose-Independent Tumor Growth. Molecular cell *60*, 195-207.

Voutsinos-Porche, B., Bonvento, G., Tanaka, K., Steiner, P., Welker, E., Chatton, J.Y., Magistretti, P.J., and Pellerin, L. (2003). Glial glutamate transporters mediate a functional metabolic crosstalk between neurons and astrocytes in the mouse developing cortex. Neuron *37*, 275-286.

Waagepetersen, H.S., Qu, H., Hertz, L., Sonnewald, U., and Schousboe, A. (2002). Demonstration of pyruvate recycling in primary cultures of neocortical astrocytes but not in neurons. Neurochemical research *27*, 1431-1437.

Waagepetersen, H.S., Qu, H., Schousboe, A., and Sonnewald, U. (2001). Elucidation of the quantitative significance of pyruvate carboxylation in cultured cerebellar neurons and astrocytes. Journal of neuroscience research *66*, 763-770.

Walls, A.B., Waagepetersen, H.S., Bak, L.K., Schousboe, A., and Sonnewald, U. (2015). The glutamine-glutamate/GABA cycle: function, regional differences in glutamate and GABA production and effects of interference with GABA metabolism. Neurochemical research *40*, 402-409.

White, A.R., Zheng, H., Galatis, D., Maher, F., Hesse, L., Multhaup, G., Beyreuther, K., Masters, C.L., and Cappai, R. (1998). Survival of cultured neurons from amyloid precursor protein knock-out mice against Alzheimer's amyloid-beta toxicity and oxidative stress. The Journal of neuroscience : the official journal of the Society for Neuroscience *18*, 6207-6217.

Yang, C., Ko, B., Hensley, C.T., Jiang, L., Wasti, A.T., Kim, J., Sudderth, J., Calvaruso, M.A., Lumata, L., Mitsche, M., et al. (2014). Glutamine oxidation maintains the TCA cycle and cell survival during impaired mitochondrial pyruvate transport. Molecular cell *56*, 414-424.

Yang, E., Zha, J., Jockel, J., Boise, L.H., Thompson, C.B., and Korsmeyer, S.J. (1995). Bad, a heterodimeric partner for Bcl-XL and Bcl-2, displaces Bax and promotes cell death. Cell *80*, 285-291.

Yellen, G. (2008). Ketone bodies, glycolysis, and KATP channels in the mechanism of the ketogenic diet. Epilepsia *49 Suppl 8*, 80-82.

Yu, A.C., Drejer, J., Hertz, L., and Schousboe, A. (1983). Pyruvate carboxylase activity in primary cultures of astrocytes and neurons. Journal of neurochemistry *41*, 1484-1487.

Yudkoff, M., Daikhin, Y., Horyn, O., Nissim, I., and Nissim, I. (2008). Ketosis and brain handling of glutamate, glutamine, and GABA. Epilepsia *49 Suppl 8*, 73-75.

Yudkoff, M., Daikhin, Y., Melo, T.M., Nissim, I., Sonnewald, U., and Nissim, I. (2007). The ketogenic diet and brain metabolism of amino acids: relationship to the anticonvulsant effect. Annual review of nutrition *27*, 415-430.

Yudkoff, M., Daikhin, Y., Nissim, I., Grunstein, R., and Nissim, I. (1997). Effects of ketone bodies on astrocyte amino acid metabolism. Journal of neurochemistry *69*, 682-692.

Yudkoff, M., Daikhin, Y., Nissim, I., Horyn, O., Lazarow, A., Luhovyy, B., Wehrli, S., and Nissim, I. (2005). Response of brain amino acid metabolism to ketosis. Neurochemistry international *47*, 119-128.

Yudkoff, M., Daikhin, Y., Nissim, I., Lazarow, A., and Nissim, I. (2001). Brain amino acid metabolism and ketosis. Journal of neuroscience research *66*, 272-281.

Yudkoff, M., Nelson, D., Daikhin, Y., and Erecinska, M. (1994). Tricarboxylic acid cycle in rat brain synaptosomes. Fluxes and interactions with aspartate aminotransferase and malate/aspartate shuttle. The Journal of biological chemistry *269*, 27414-27420.

Zala, D., Hinckelmann, M.V., Yu, H., Lyra da Cunha, M.M., Liot, G., Cordelieres, F.P., Marco, S., and Saudou, F. (2013). Vesicular glycolysis provides on-board energy for fast axonal transport. Cell *152*, 479-491.

Zarling, D.A., Watson, A., and Bach, F.H. (1980). Mapping of lymphocyte surface polypeptide antigens by chemical cross-linking with BSOCOES. Journal of immunology *124*, 913-920.

Zawar, C., Plant, T.D., Schirra, C., Konnerth, A., and Neumcke, B. (1999). Cell-type specific expression of ATP-sensitive potassium channels in the rat hippocampus. The Journal of physiology *514 (Pt 2)*, 327-341.

Zhou, W., Mukherjee, P., Kiebish, M.A., Markis, W.T., Mantis, J.G., and Seyfried, T.N. (2007). The calorically restricted ketogenic diet, an effective alternative therapy for malignant brain cancer. Nutrition & metabolism *4*, 5.

Zielke, H.R., Zielke, C.L., and Baab, P.J. (2007). Oxidation of (14)C-labeled compounds perfused by microdialysis in the brains of free-moving rats. Journal of neuroscience research *85*, 3145-3149.

Zielke, H.R., Zielke, C.L., and Baab, P.J. (2009). Direct measurement of oxidative metabolism in the living brain by microdialysis: a review. Journal of neurochemistry *109 Suppl 1*, 24-29.

Zuccoli, G., Marcello, N., Pisanello, A., Servadei, F., Vaccaro, S., Mukherjee, P., and Seyfried, T.N. (2010). Metabolic management of glioblastoma multiforme using standard therapy together with a restricted ketogenic diet: Case Report. Nutrition & metabolism *7*, 33.